MONASH University

Tropical SST Impact on the Southern Hemisphere Eddy-driven Jet and Antarctic Sea Ice Variation

Dongxia Yang

A thesis submitted for the degree of

Doctor of Philosophy

at Monash University in 2021

School of Earth, Atmosphere and Environment

Melbourne, Australia

Copyright notice

Abstract

The Southern Hemisphere eddy-driven jet plays an important role in weather and climate both locally and on a global scale, influencing Southern Hemisphere rainfall distributions, the frequency of extreme weather events, Antarctic sea ice extent and ocean circulations. The objective of this thesis is to examine the drivers of decadal changes in the eddy-driven jet and its associated Antarctic sea ice variations, with a focus on the role of internal variability from tropical sea surface temperatures (SSTs). To achieve this, a range of climate model experiments were utilised, including fully-coupled, partially-coupled (pacemaker simulations where SSTs were nudged to observed anomalies in different regions), and atmosphere-only configurations of the Community Earth System Model Version 1 (CESM1). The main conclusions gained from this thesis include:

a) Both external forcing and observed internal tropical Pacific SST variability were found to be important in driving a positive Southern Annular Mode phase and poleward migration of the eddy-driven jet in austral summer from the late 20th Century to the early 21st Century. Tropical Pacific SST variability acted to shift the jet poleward over the South Indian and Southwest Pacific and intensify the jet in the Southeast Pacific basin, while external forcing drove a significant poleward jet shift in the South Atlantic basin. In comparison, the tropical & North Atlantic SST and Indian Ocean SST made a weak and sometimes offsetting contribution.

b) Comparing coupled and uncoupled experiments, we found that the tropical Pacific SST impacts the South Pacific jet mainly via direct atmospheric teleconnections, but that air-sea coupling is essential in driving the teleconnections between tropical Pacific SST anomalies and South Atlantic-Indian jet variations. Experiments that extended the nudging region to include the South Pacific Convergence Zone produced similar results.

c) Tropical Indian/western Pacific pacemaker experiments were found to best reproduce the pattern of observed Antarctic sea ice expansion especially in the western Ross Sea region during 1980-2013. In both the observations and model analysis, the western Ross Sea displayed a substantial surface cooling and freshening with subsurface warming and salinity increasing, suppressing the heat content and brine released to deeper layers, producing a fresh and cool environment at the surface, further conducive to the sea ice increase. The identification that surface and subsurface temperature and salinity trends that closely resemble observations can be simulated in a global coupled climate model driven by remote tropical forcing was one of the key findings of our study.

Overall, this thesis has stressed the importance of tropical SST internal decadal variability in driving zonally asymmetric changes of the Southern Hemisphere eddy-driven jet and the regional variations of Antarctic sea ice. Some limitations of the climate model simulations employed in this study and suggestions for future work have also been identified. This work has improved our current understanding of the mechanisms of decadal changes in the Southern Hemisphere extratropical circulation and Antarctic climate, leading to better insights for constraining future projections of westerly winds, precipitation, Southern Ocean circulation, and Antarctic sea ice changes.

Publications during enrolment

1. **Yang, D**., Arblaster, J.M., Meehl, G.A., England, M.H., Lim, E.P., Bates, S. and Rosenbloom, N., 2020. Role of tropical variability in driving decadal shifts in the Southern Hemisphere summertime eddy-driven jet. *Journal of Climate*, 33(13), pp.5445-5463.

2. Meehl, G.A., **Yang, D.,** Arblaster, J.M., Bates, S.C., Rosenbloom, N., Neale, R., Bacmeister, J., Lauritzen, P.H., Bryan, F., Small, J. and Truesdale, J., 2019. Effects of model resolution, physics, and coupling on Southern Hemisphere storm tracks in CESM1. 3. *Geophysical Research Letters*, 46(21), pp.12408-12416.

3. Meehl, G.A., Arblaster, J.M., Chung, C.T., Holland, M.M., DuVivier, A., Thompson, L., **Yang, D.** and Bitz, C.M., 2019. Sustained ocean changes contributed to sudden Antarctic sea ice retreat in late 2016. *Nature Communications*, 10(1), pp.1-9.

Thesis including published works declaration

I hereby declare that this thesis contains no material which has been accepted for the award of any other degree or diploma at any university or equivalent institution and that, to the best of my knowledge and belief, this thesis contains no material previously published or written by another person, except where due reference is made in the text of the thesis.

This thesis includes one original paper published in a peer reviewed journal, one submitted manuscript and one to be submitted for publication. The core theme of the thesis is to improve our understanding of tropical SST Impact on Southern Hemisphere eddy-driven jet and Antarctic sea ice variation. The ideas, development and writing up of all the papers in the thesis were the principal responsibility of myself, the student, working within the School of Earth, Atmosphere and Environment under the supervision of Prof. Julie Arblaster.

The inclusion of co-authors reflects the fact that the work came from active collaboration between researchers and acknowledges input into team-based research.

In the case of each chapter my contribution to the work involved the following:

Thesis Chapter	**Publication Title**	**Status** *(published, in press, accepted or returned for revision, submitted)*	**Nature and % of student contribution**	**Co-author name(s) Nature and % of Co-author's contribution***	**Co-author(s), Monash student Y/N***
2	Role of tropical variability in driving decadal shifts in the Southern Hemisphere summertime eddy-driven jet	published	70% Concept, data analysis and writing first draft	Julie Arblaster (10%), Gerald Meehl (5%), Matthew England (5%), Eun-Pa Lim (5%), Susan Bates (3%), Nan Rosenbloom (2%)	N, N, N, N, N, N
3	The role of coupled feedbacks in the decadal variability of the Southern Hemisphere eddy-driven jet	returned for revision	80% Concept, data analysis and writing first draft	Julie Arblaster (10%), Gerald Meehl (5%), Matthew England (5%)	N, N, N
4	Impact of tropical Indian SST on the sea ice trend over the western Ross Sea	to be submitted	80% Concept, data analysis and writing first draft	Julie Arblaster (10%), Ariaan Purich (10%)	N, N

I have renumbered sections of submitted or published papers in order to generate a consistent presentation within the thesis.

Student name: Dongxia Yang

Student signature: **Date:**

I hereby certify that the above declaration correctly reflects the nature and extent of the student's and co-authors' contributions to this work. In instances where I am not the responsible author I have consulted with the responsible author to agree on the respective contributions of the authors.

Main Supervisor name: Prof. Julie Arblaster

Main Supervisor signature: **Date:**

Acknowledgements

This research was funded by the Monash International Postgraduate Research Scholarship (MIPRS), the Monash Graduate Scholarship (MGS), and the Australian Research Council Centre of Excellence for Climate Extremes (Grant CE170100023).

This thesis could not have been completed without the support and assistance of so many people which I am very grateful for. First, I must thank my supervisor Prof. Julie Arblaster, who offered me a great opportunity to study in Melbourne, where I decided to settle down for the next few decades. I appreciate all the time, efforts and patience she put into mentoring me throughout my PhD projects. Julie sets me a great model for us women in science with her hard work and enormous achievements. Also, I am truly grateful for all her kind support in my life especially during the hard time of COVID lockdown.

My grateful thanks are extended to Shayne McGregor, Eunpa Lim, Harry Hendon, Matthew England, Gerald Meehl, Nan Rosenbloom, and Adam Phillips, who offered constructive ideas and comments for my research.

A huge thanks to my climate colleagues at Monash, Ailie Gallant, David Hoffmann, Roseanna McKay, Zoe Gillett, Pia Freisen, Peter van Rensch, Ariaan Purich, Mustapha Adamu, Rajashree Naha, Christian Stassen, Sonja Neske, Mathias Zeller and Joshua Soderholm; and my Chinese fellows Chen Li, Chang Xu, Fang Wen, Aya Wen, Gan Duan, Qiushi Guan, Wenhui Zhao, Zhiang Xie, for all your support and friendship during the course of the PhD.

A big thank you to my family and friends back in China. All the phone calls and video chats are important for me to finish my PhD during this COVID-19 pandemic.

My heartfelt thanks go to my partner Minzheng and our baby girl Luna. Thank you so much for your love and company along the way.

Table of Contents

List of Figures

List of Tables

Chapter 1

Introduction

1 Introduction

The strong influence of tropical sea surface temperature (SST) anomalies on the Southern Hemisphere extratropical and polar climate variability have been widely recognised. These tropical-extratropical teleconnections show large regional differences and are developed at various time ranges. For example, previous studies have emphasized the impact of tropical Pacific SST variability on the large-scale changes in the Southern Hemisphere extratropical atmospheric circulation (Karoly 1989; L'Heureux and Thompson 2006a; Ding et al. 2011) and on Southern Ocean SST anomalies (Ciasto and Thompson 2008; Ciasto and England 2011). The majority of tropical Pacific-extratropical studies have focused on interannual timescales, showing an association between the El Niño Southern Oscillation (ENSO) and a Southern Annular Mode (SAM) phase shift in late spring / early summer (Fogt et al. 2011; Gong et al. 2013; Yu et al. 2015). During La Niña events, a positive SAM phase occurs more frequently while the opposite is found for El Niño years. Chen et al. (2008) suggest that the mid-latitude jet could be expected to undergo a poleward migration during La Niña years due to the poleward displacement of transient eddy momentum flux divergence and convergence zones. Despite this well-established interannual ENSO– SAM relationship, less is known about the influence of tropical Pacific SST decadal variability on the midlatitude jet. Furthermore, the impact of tropical Atlantic and Indian SST variations on the extratropical atmospheric circulation are less understood and the relative roles of individual tropical basin variability on the recent decadal changes in the Southern Hemisphere mid-latitude circulation have not been quantified.

Links between each tropical basin SST variations and Antarctic surface temperature and sea ice changes have also been established. At both interannual (e.g., ENSO) and interdecadal timescales (e.g., Interdecadal Pacific Oscillation, IPO), tropical Pacific SST variability has been identified to drive sea ice variations over the Amundsen-Bellingshausen Sea and Weddell Sea (Yuan 2004; Stammerjohn et al. 2008; Simpkins et al. 2012; Meehl et al. 2016; Clem et al. 2017a; Schneider and Deser 2017; Stuecker et al. 2017; Meehl et al. 2019b). For example, the negative phase of the IPO has been linked to Antarctic sea ice expansion via a positive phase of the SAM combined with a deepened Amundsen Sea Low (ASL), which alters the wind patterns over the Antarctic sea ice zone (Meehl et al. 2016; Purich et al. 2016a; Clem et al. 2019; Holland et al. 2019; Meehl et al. 2019b). Some studies have also highlighted the role of Atlantic SSTs on Antarctic climate. For instance, Li et al. (2015) suggested tropical Atlantic SSTs could force a positive response in the SAM and a strengthened ASL via stationary Rossby wave activities in Southern Hemisphere winter. By contrast, very few studies have investigated the impact of tropical Indian Ocean SST variability on Antarctic

sea ice changes (Nuncio and Yuan 2015) until recently when it was linked to the drastic sea ice retreat event during austral spring 2016 (Meehl et al. 2019b; Purich and England 2019; Wang et al. 2019). However, the details of how tropical Indian SSTs impact Antarctic sea ice remain unclear, especially at multidecadal timescales. The response of Antarctic sea ice to tropical variability is strongest in western Antarctica, especially over the Amundsen-Bellingshausen Sea and the Weddell Sea, where has been a focus in previous studies. In comparison, our knowledge about the tropical SST impact on the eastern Antarctic is rather limited.

The interactions and teleconnections between the tropical and midlatitude regions are an important modulator of extratropical circulation anomalies and their associated weather patterns. The westerly wind changes have been linked to rainfall redistributions, frequency of extreme weather events such as droughts and wildfires, as well as changes in sea ice extent and ocean circulations. Therefore, the aim of this thesis is to examine the impact of decadal variability in tropical SSTs on observed Southern Hemisphere eddy-driven jet changes and Antarctic sea ice variations, and to gain a better understanding of the atmosphere-ocean-ice dynamics behind these teleconnections.

In this chapter, the climatological state and the recent trend in the Southern Hemisphere westerly winds and Antarctic sea ice are first reviewed, to provide some background information about the extratropical and polar climate changes. The dominant drivers of these trends discussed in previous work are summarised as well. The climate model simulations used throughout this thesis are then introduced. The detailed structure of this thesis is outlined at the end of this chapter.

1.1 The Southern Hemisphere jet streams

The Southern Hemisphere westerly winds are the strongest surface winds on the planet, with the maximum wind speed up to 20 m/s at the near-surface level, forming one of the most remarkable features of atmosphere circulation on our planet. In the absence of large landmasses, it shapes into an almost-annular zonal ring over the Southern Ocean. As a dominant climate mode of the midlatitude atmospheric circulation, it plays an important role in weather and climate both locally and on a global scale.

There are two different types of westerly jets based on the dynamical causes and geographic locations: the subtropical jet at around 30°S and the eddy-driven jet (or the mid-latitude jet) at 50-60°S. The subtropical jet is induced by the angular momentum transport via the thermally direct Hadley circulation, i.e., the imbalance between tropical and polar atmospheric heating by solar radiation

produces the large-scale Hadley, Ferrell, and Polar circulation cells (Kuo 1956). The westerly wind at around 30°S is accelerated due to the poleward moving air in the upper branch of the tropical Hadley circulation, thus the subtropical jet forms at the poleward edge of the Hadley cell. The eddy-driven jet is developed due to the eddy momentum flux convergence. In particular, in the mid-latitude baroclinic region, the stirring would induce the transient Rossby waves to develop, and as the transient eddies propagate away, there would be an eddy momentum flux convergence (EMFC) in the stirred region (since the sign of eddy momentum flux and the transient wave group velocity is reversed), leading to a westward flow as a result of absolute vorticity conservation. And those waves would stop to propagate and break down when it approaches its critical latitude (where wave phase speed equals zonal wind), resulting in an eddy momentum flux divergence (EMFD) and an eastward flow. Therefore, the midlatitude transient eddy–mean flow interactions are critical for the development, maintenance and variation of eddy-driven jet (Vallis et al. 2004; Hendon et al. 2014).

These two jets are well distinguished in spatial locations except during the summertime when the subtropical jet sometimes drifts poleward and merges with the eddy-driven jet (Ceppi and Hartmann 2013, also Figure 1.1). The vertical structure of the two jets also shows large differences. The subtropical jet is relatively shallow and confined to the upper troposphere, with maximum wind speed around 50 m/s in winter and 30 m/s in summer. It is strongly baroclinic with intensive vertical wind shear below and above the jet axis (Gillett et al. 2021). In contrast, the eddy-driven jet is equivalent barotropic, which means the wind characteristics remain similar from the near surface to the top of the troposphere and lower stratosphere (Figure 1.1).

To effectively separate the eddy-driven jet from the upper level subtropical jet, the maximum zonal wind at lower levels (typically 850 hPa) is often taken as a simple metric to define the eddy-driven jet (Schneider et al. 2015; Simpson and Polvani 2016; Waugh et al. 2020). There are many other indices that have been employed to depict characteristics of the Southern Hemisphere eddy-driven jet variations. For example, Koch et al. (2006) defined a climatological jet position based on the occurrence of a jet event at a given location and integrating the spatial frequency distribution of such events, to better illustrate the impacts of jet changes on synoptic scale weather activities. Swart et al. (2015) defined the jet strength, position and width as the maximum of the zonal mean zonal wind at 10m, the latitude of the jet maximum, and the latitude range of contiguous westerlies over 20-70° S, respectively.

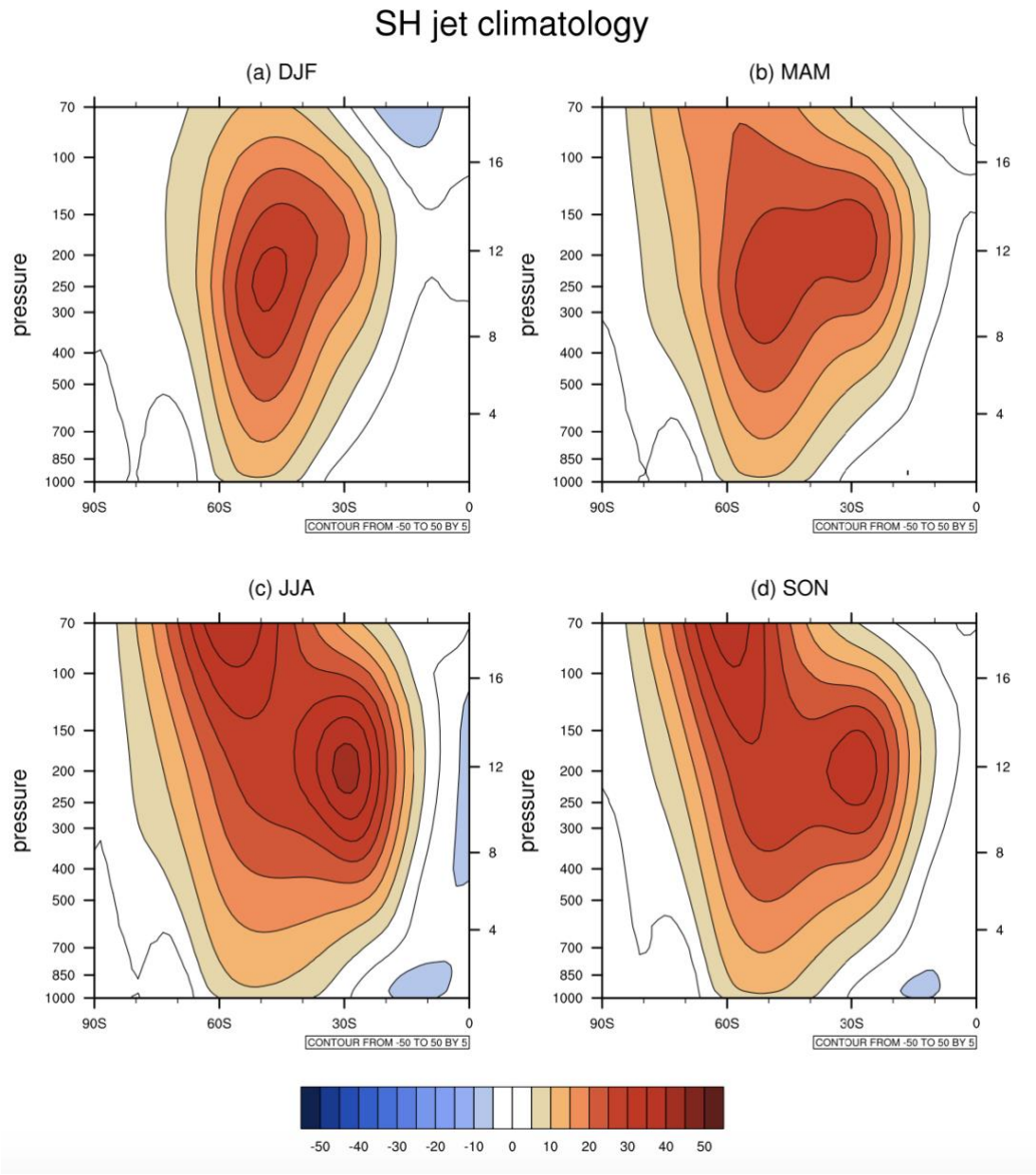

Figure 1.1 Climatology of Southern Hemisphere zonal-mean zonal wind (m/s) in four seasons using the ERA-Interim reanalysis data (1980–2013). It is used to show the latitudinal positions changes of two jet axes in four seasons and the vertical differences between the two jets.

The zonal mean eddy-driven jet position and strength changes are closely associated with SAM, the leading mode of atmospheric variability in the Southern Hemisphere extratropics. The climatological distribution of the Southern Hemisphere eddy-driven jet at 850 hPa (contours in Figure 1.2) shows a circumpolar pattern all year long, with the jet axis mainly located in the South Atlantic-Indian basin and the maximum near-surface wind is around 20 m/s. The largest seasonal variation is observed in the South Pacific basin, where in March–May (MAM) and June-August (JJA) seasons the jet is relative weak but gets stronger in DJF (December-February) and September–November (SON).

Over the recent past, the Southern Hemisphere zonal-mean eddy-driven jet generally increased in speed and shifted poleward in austral summer, along with SAM shifting to its positive phase. However these changes also exhibited large zonal and seasonal asymmetries (Schneider et al. 2015; Waugh et al. 2020). The largest poleward movement is found in the South Atlantic-Indian basin in the austral summertime (Figure 1.2a), while for the South Pacific basin, an equatorward shift in JJA-SON and jet strengthening in DJF-MAM is observed. Many studies have documented and examined those historical trends using various reanalysis data and in the Coupled Model Intercomparison Project 5 (CMIP5) and CMIP6 models (Barnes and Polvani 2013; Swart et al. 2015; Goyal et al. 2021). For instance, Swart et al. (2015) compared the zonal-mean jet trends over 1951–2011 between the Twentieth Century Reanalysis (20CR) and the CMIP5 simulations, and they found both 20CR and CMIP5 show an increase in jet strength in all seasons, but differ in the jet latitudinal position with CMIP5 models simulating a poleward shift all year round yet 20CR varying in different seasons. Simpson et al. (2020) suggested that the substantial equatorward bias found in CMIP5 still remains in CMIP6 even though there are some improvements. Some CMIP6 models place the Southern Hemisphere westerlies about 1.6° too far equatorward in JJA seasons in particular. However, using another jet metric (maximum surface westerly winds at 10m elevation), Goyal et al. (2021) found that compared to CMIP5, the CMIP6 ensemble shows a significant reduction in the zonal mean jet equatorward bias with respect to ERA5, with the multi-model mean bias declining from 1.3° in CMIP5 to 0.3° in CMIP6.

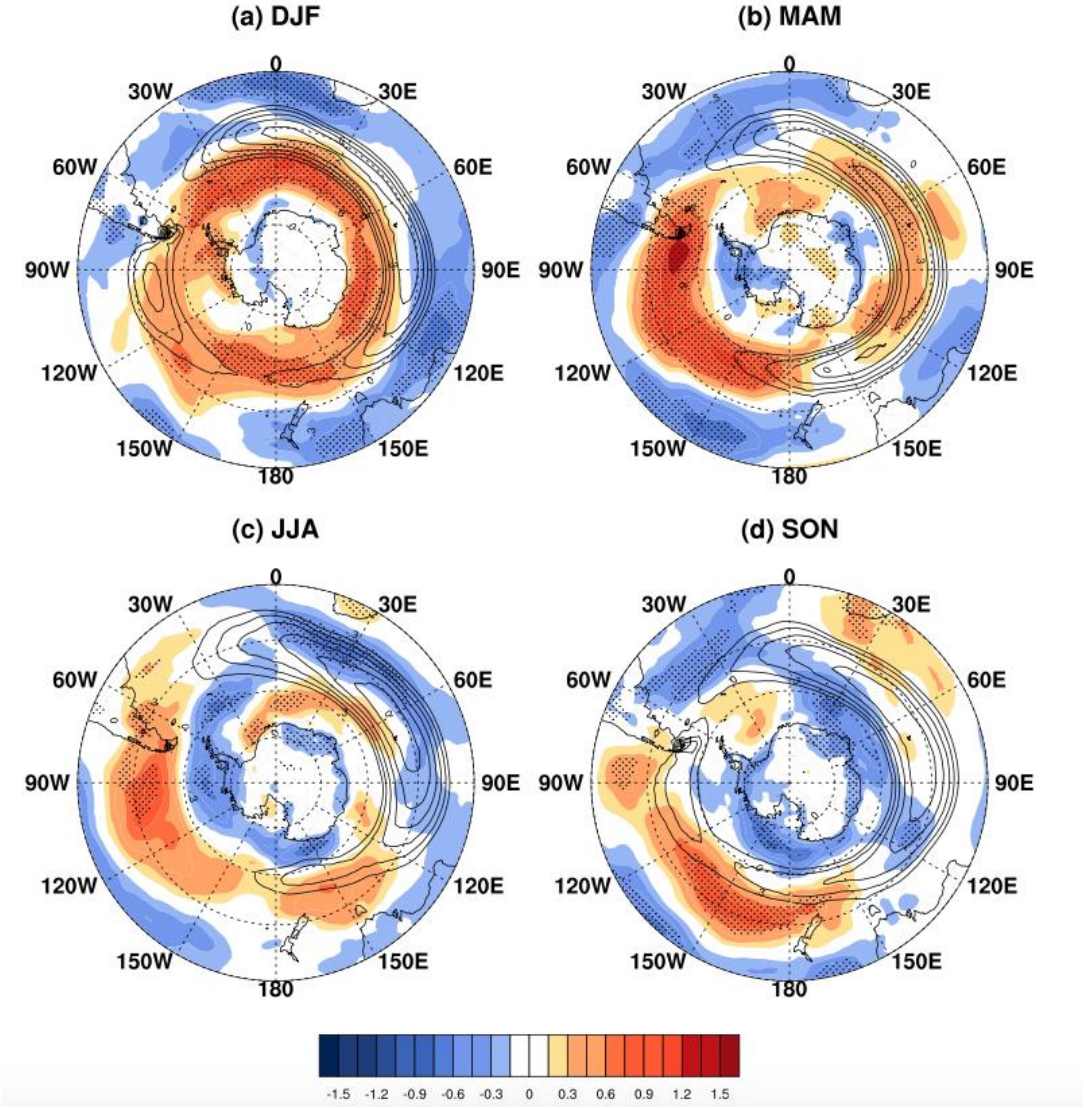

Figure 1.2 Climatology (in contours, unit: m/s, ranges from 10 m/s to 20 m/s) and trend (in shading, unit: m/s) of Southern Hemisphere eddy-driven jet (850 hPa zonal wind) over 1980-2013 in four seasons using ERA-Interim data.

The impact of increasing greenhouse gases (GHGs) and stratospheric ozone depletion on recent trends in the SH extratropical circulation has been emphasized in earlier studies. Arblaster and Meehl (2006) classified different sources of external forcings and their contributions to the SAM trend using a global coupled model and indicated that the ozone changes in the upper troposphere and stratosphere dominated the observed positive SAM trend over 1950-1999. Similar results were obtained by Polvani et al. (2011) who established that the impact of ozone depletion was 2–3 times larger than GHGs on the summertime poleward displacement of the eddy-driven jet and the expansion of the Hadley cell over the second half of the twentieth century. However, for future scenarios, it is expected that the effects of GHGs and ozone will oppose each other as ozone recovers (Banerjee et al. 2020), with GHGs playing a dominant role once the ozone level is stabilised. Under a high emission scenario

in CMIP6, Goyal et al. (2021) found that at the end of 21st Century, the annual mean jet would increase ~10% in intensity and shift ~0.8° poleward in latitude.

In contrast to above studies examining the influence of external forcing, there has been very little discussion of the contributions of internally-driven tropical decadal variability on the SH eddy-driven jet. By design, these studies using coupled models do generate their own internal variabilities through multiple ensemble members / multiple models, however they will not capture the influence of tropical decadal variability that has been observed. Therefore, to examine the separate roles of internally driven tropical SSTs and external forcing, the CESM1 coupled model large ensemble (Kay et al. 2015) and pacemaker experiments (see details at section 1.3) are employed in this thesis.

1.2 State of Antarctic sea ice

Many previous studies have revealed the close relationship between the eddy-driven jet and Antarctic sea ice changes (Lefebvre et al. 2004; Ferreira et al. 2015; Purich et al. 2016a). In this section, we start with an overview of the current state of Antarctic sea ice, widely used sea ice indices and recent trends followed with a discussion of the impact of the jet on the sea ice. Unlike the geography of the Arctic, which is an ocean basin surrounded by land, the Antarctic is a large continent surrounded by the Southern Ocean. This allows the Antarctic sea ice to stretch into lower latitudes, resulting in a relatively larger amplitude of expansion in winter and melting in summer. The extent normally peaks in September and reaches a minimum in February. Since direct on-site observations of Antarctic sea ice cover are rather difficult to obtain, reliable observational sea ice data is only available from 1979 when the regular satellite passive microwave observations became available.

A number of metrics have been used to describe the sea ice cover, here we list the definition and difference amongst the most commonly used ones. Sea ice concentration (SIC) is defined as the fraction of area covered by sea ice in an ocean pixel and is derived from satellite passive microwave data. Most sea ice indices are developed based on the SIC, for example, sea ice extent (SIE), where SIE is Σ A (x,y), with A = the area of each grid cell containing SIC > 15%. Similarly, sea ice area (SIA) is defined as the total area of ice coverage for a given domain i.e., Σ SIC(x,y) × A (x,y). Sea ice thickness (SIT) has also been used especially when its impact on the Southern Ocean water column is considered, though both in situ measurements of SIT and derivation from satellite altimeter measurement are difficult in practice (Hobbs et al. 2016).

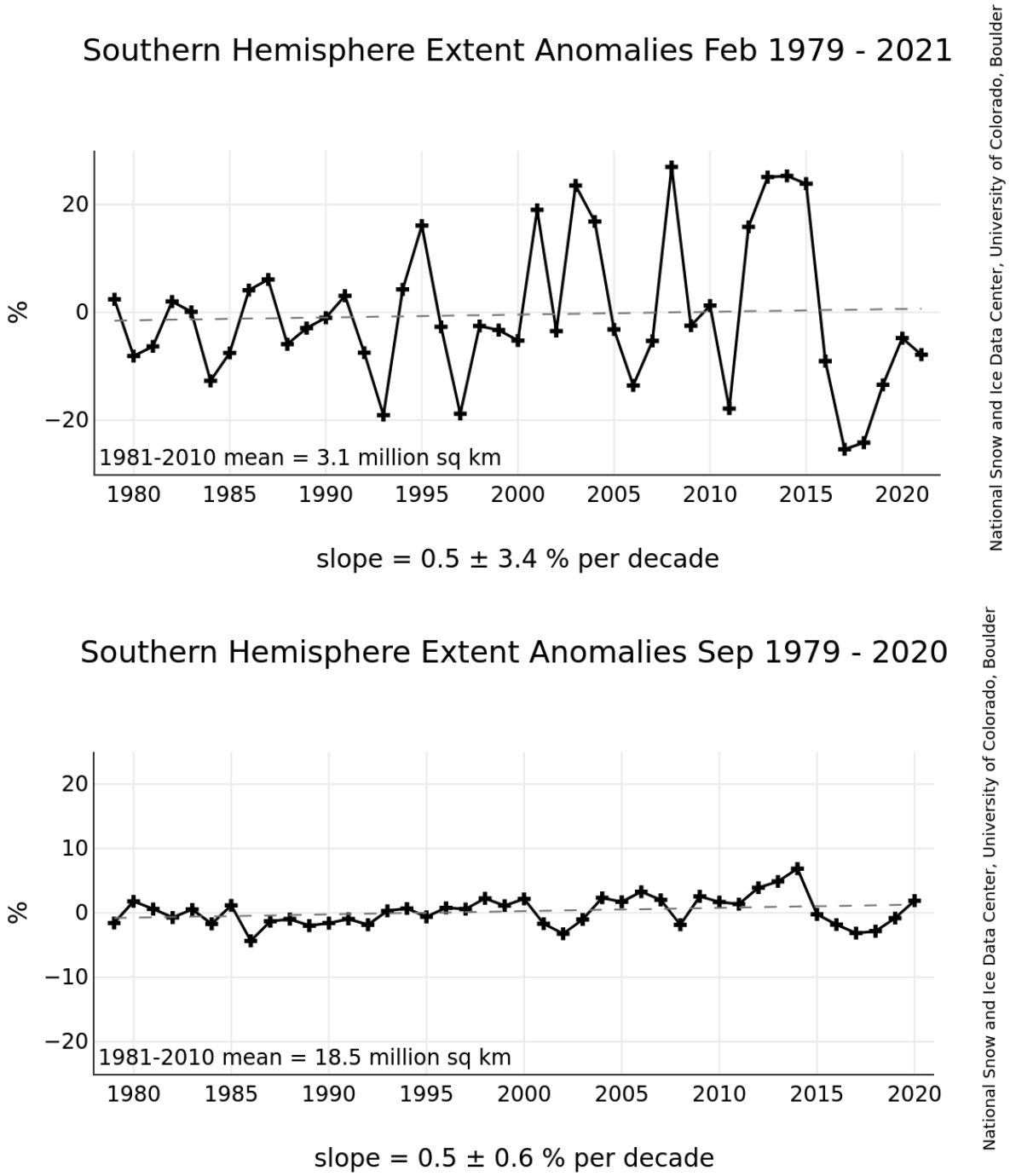

Figure 1.3 Antarctic Sea Ice Extent anomalies for February (minimum SIE month) and September (maximum SIE month) during 1979-2021. From: https://nsidc.org/data/seaice_index

The Antarctic SIE experienced a slight increase in both expansion and retreat months since the satellite era (1979-2021, shown in Figure 1.3, also discussed in Ludescher et al. 2019; Blanchard-Wrigglesworth et al. 2021), In particular, it is outstanding that during 1979-2013, the Antarctic SIE shows a significant increasing trend under the global warming background (Parkinson and Cavalieri 2012; Simmonds 2015). In fact, the annual mean of Antarctic sea ice over this period is almost one-third of the magnitude of the Arctic annual mean decrease (Simmonds 2015). However, this large

expansion trend is suspended during 2016-2018 due to a drastic decrease (Turner et al. 2017; Kusahara et al. 2018; Wang et al. 2019), which is followed by a prompt recovery around 2019-2020.

Despite the multidecadal expansion of annual-mean Antarctic sea ice, it also shows large regional and seasonal variations. To better discuss regional changes and to follow Turner et al. (2016) and Lecomte et al. (2017), we divide the Antarctic into five sectors in this thesis, as indicated in Figure 1.4: the Weddell Sea, the South Indian sector, the Adélie, the Ross Sea, and the Amundsen and Bellingshausen Seas. The regional trends are strongly seasonal in character (Holland 2014), for example, during the austral summer and autumn (Figure 1.4a and b), the largest decreasing trend is in the Amundsen and Bellingshausen Seas and the increasing trend is found in the Weddell Sea; In winter and spring (Figure 1.4c and d), the sign is reversed but in a much smaller magnitude, ie. the Amundsen and Bellingshausen region shows a weak expansion while Weddell Sea exhibits a slight retreat. In the South Indian basin, substantial increases are observed in autumn and winter seasons. Overall, only the western Ross Sea sea ice shows statistically significant expansion in all seasons, which makes the largest contribution to the total multidecadal sea ice expansion around Antarctica.

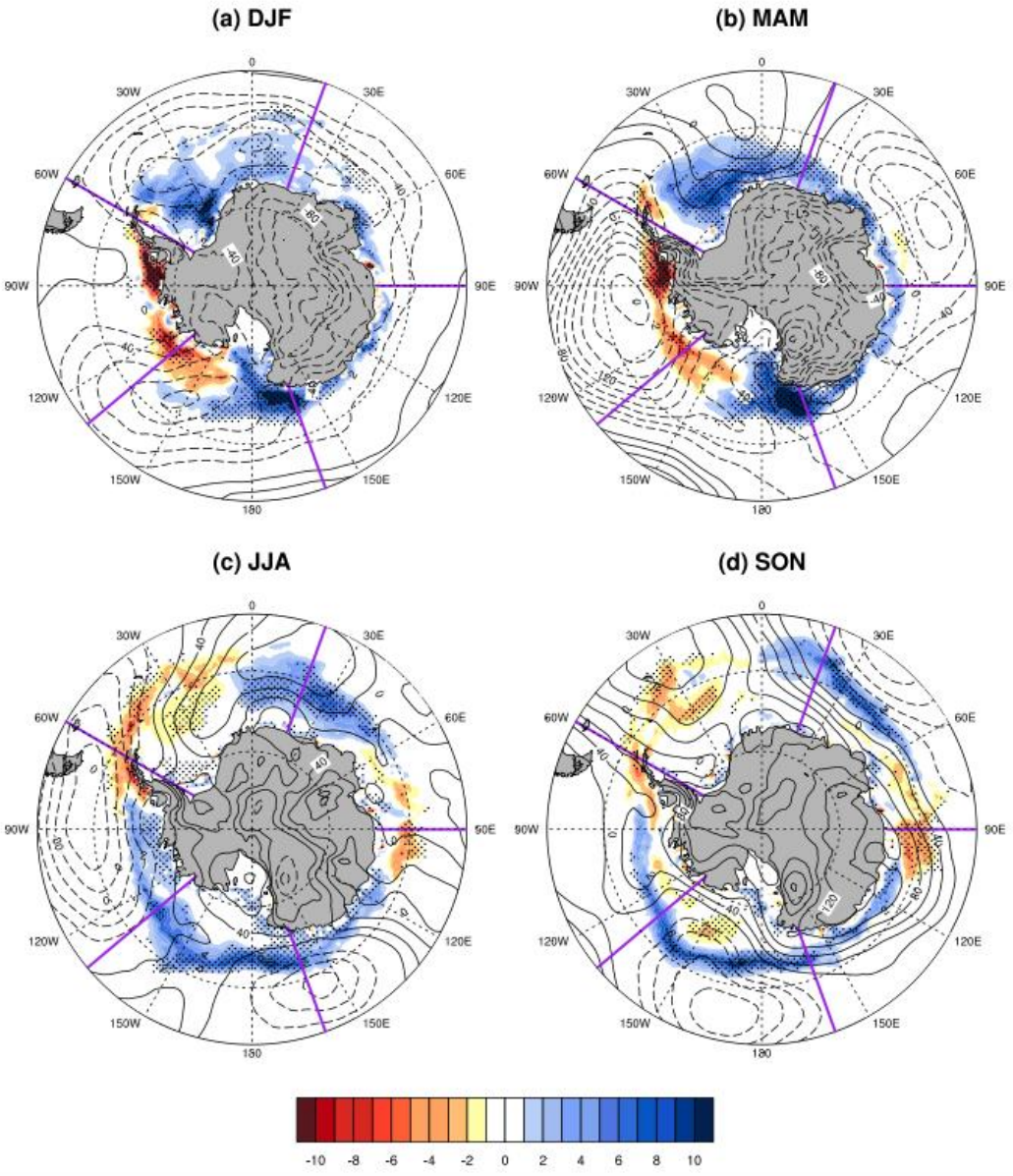

Figure 1.4 Seasonal trends in sea ice concentration (shading, unit: fraction/decade) and SLP (contours, unit: hPa/decade) for 1980-2013 based on the National Sea and Ice Data Centre (NSIDC) sea ice data (Cavalieri et al. 1996) and ERA-Interim reanalysis.

Some studies have revealed the impact of the eddy-driven jet on the Antarctic sea ice changes (Hobbs et al. 2016). In response to the jet variation, Southern Ocean and Antarctic sea ice variations consist of both annular and non-annular components. The annular expansion is primarily described by SAM, which exhibited a positive trend over 1979-2013 (Swart et al. 2015), though recently Banerjee et al. (2020) argued that this widely documented positive SAM trend has paused from around the year 2000, ascribing this to the emergence of ozone recovery as a consequence of the successful implementation of the Montreal Protocol. On interannual timescales the positive SAM phase is associated with a surface northward Ekman drift, leading to cool SST anomalies and sea ice expansion

around Antarctica (Lefebvre et al. 2004). However, at longer timescales, sustained positive SAM and enhanced westerly winds cause upward Ekman pumping of deep warm water from below the mixed layer, inducing a warm SST anomaly and sea ice decline (Ferreira et al. 2015; Kostov et al. 2017). Most CMIP5 models generally capture this two-time scale Southern Ocean SST and sea ice response to the SAM in their pre-industrial control runs, though with broad distributions about when the sea ice transitions from an initial expansion to a decline (Holland et al. 2017b). The uncertainties of the transitioning time from the initial fast cooling response to the slow warming response in different models explain a significant fraction of the large spread in the simulated historical sea ice extent trends across the CMIP models (Figure 4 of Holland et al. 2017b), which limits confidence in the models' predictions of future Antarctic sea ice trends.

Other studies indicate the importance of the jet's non-annular component on simulating the Southern Ocean heat and carbon uptake, ventilation, and Antarctic sea ice distributions. For example, Raphael (2007) identified that the atmospheric zonal wave three (ZW3) could force an equatorward and cold flow and sea ice growth with northerly meridional winds, and vice versa for poleward warm flow and sea ice retreat. Similarly, Kimura (2004) related northward ice drifts in the Weddell, Ross and Cosmonaut Seas to local meridional wind fluctuations. Keppler and Landschützer (2019) suggested that the net effect of the SAM on the Southern Ocean carbon sink variability is approximately zero, instead, regional surface winds shifts, such as ZW3, substantially contribute to multi-scale variability of the carbon sink. Therefore, a better understanding of the drivers of eddy-driven jet variations as well as the jet-sea ice relations on decadal timescales is needed.

1.3 Methodology and tools

Climate variations are caused by a combination of external radiative forcing and internal variability. The latter arises from the internal processes of each climate component (atmosphere, ocean, land, cryosphere etc.), as well as their coupled interactions. Both coupled and uncoupled climate models have been used to study the eddy-driven jet variations in previous work. However, there are limitations in both. By design the coupled models could generate a large spread of internal variabilities with multiple ensemble members / multiple models, nonetheless these natural variabilities are unlikely to follow the exact observed trajectory. On the other hand, those atmosphere-only experiments lack the interactions with the underlying ocean and sea ice, which could be important for tropical–extratropical teleconnections. Therefore, to distinguish the relative influence of external forcing and observed tropical SST decadal variability, partially-coupled experiments (CESM pacemaker simulations) have been used in this thesis.

The CESM1.1 is a coupled Earth system model consisting of atmosphere, ocean, land and sea-ice components with a nominal horizontal resolution of 1º (Hurrell et al. 2013; Kay et al. 2015) and contributed to CMIP5. The CESM1 Large Ensemble (LENS) includes 40 individual members (Kay et al. 2015) forced with historical forcing during 1920-2005 and a high emission forcing scenario of the Representative Concentration Pathway (RCP) 8.5 (Moss et al. 2010) from 2006 to 2080 following the CMIP5 design protocol, which allows us to assess the past and near-future climate change.

To disentangle the role of observed internal variabilities on the Southern Hemisphere and the Antarctic climate, especially the impact of the tropical SSTs, a pacemaker framework (Kosaka and Xie 2013; Schneider and Deser 2017; Meehl et al. 2019a) is employed, wherein SST anomalies are nudged to observed values within a specific ocean region, while the rest of the model evolves freely. The word "pacemaker" is used to describe the aim of those partially-coupled experiments - to find the key SST variation region that could impact the globe climate system. In this way, the pacemaker ensemble mean combines the responses to external forcing and to observed tropical SSTs. Thus, removing the ensemble-mean of the LENS gives an estimate of the climate system response to the observed time-varying internally-driven tropical SSTs. Three sets of pacemaker experiments are utilized in this thesis, with fully-restored observational SST anomalies applied in the tropical Pacific (15°S-15°N, 180°W to the American coast), tropical Indian (15°S-15°N, African coast to 180°W), as well as tropical and North Atlantic basin (0°-60°N, Atlantic basin), which is indicated in Figure 1.5. More details about these experiments are given in Chapter 2.

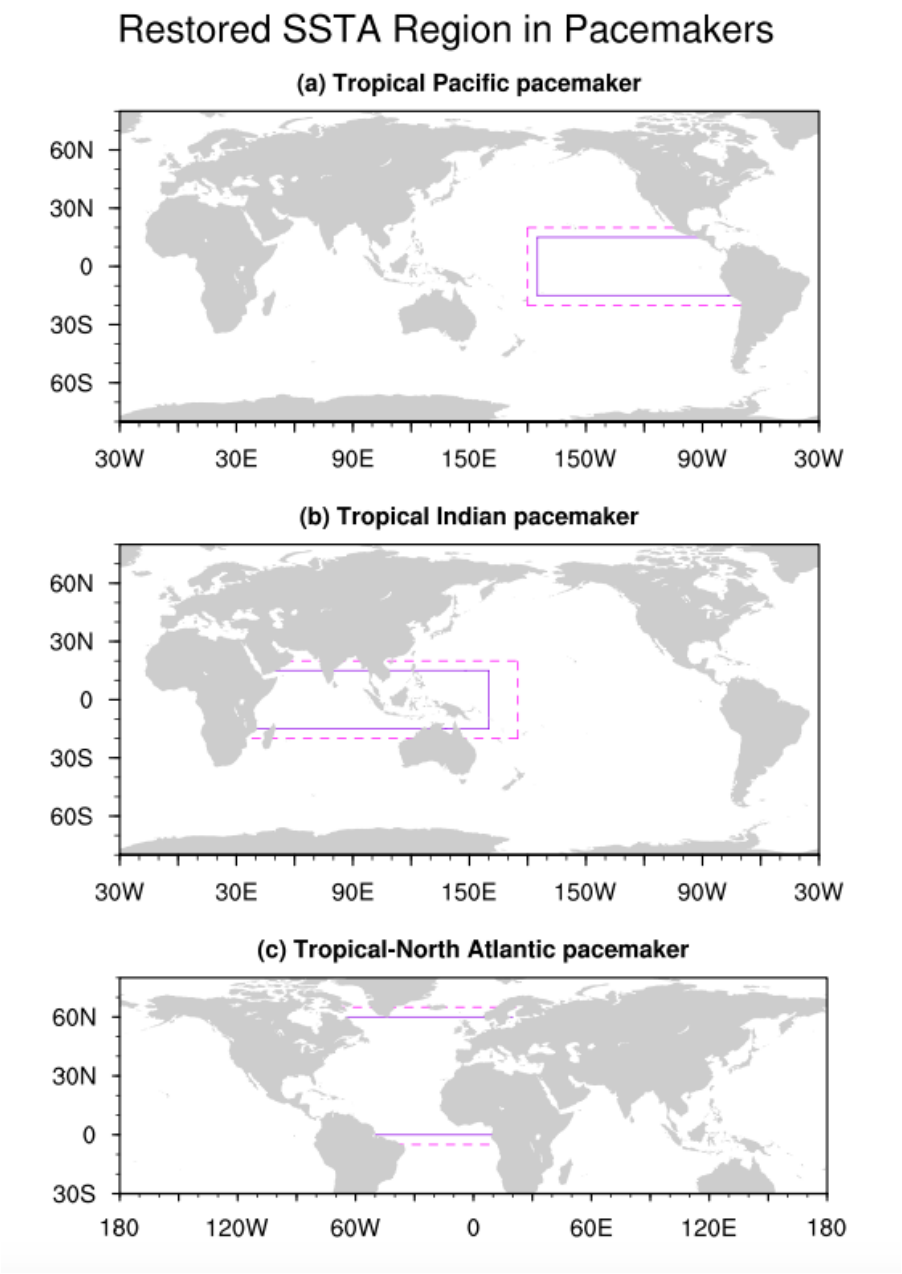

Figure 1.5 Schematic diagram showing the nudged SSTA region for (a) tropical Pacific pacemaker; (b) tropical Indian pacemaker; (c) tropical-North Atlantic pacemaker experiments. Within the solid purple lines, the SSTs are nudged to the model climatology plus observed anomalies; between the solid and the dashed lines are the buffer belts where the observed SST anomalies are linearly tapered to zero; in the blank ocean region, the SSTs are free to evolve.

1.4 Thesis aims and outline

The overall aim of this thesis is to gain a better understanding of the internally-driven tropical SST impact on recent decadal variability in the observed Southern Hemisphere eddy-driven jet and Antarctic sea ice variations. In particular, the following research questions will be addressed in this thesis:

1) What are the relative roles of external forcing versus internally driven SST variability in the tropical Pacific, tropical Indian, and tropical and North Atlantic Ocean basins in recent decadal variations of the Southern Hemisphere summertime midlatitude circulation?

2) What is the role of air-sea coupling in the teleconnection between tropical Pacific SSTs and the Southern Hemisphere eddy-driven jet?

3) What is the impact of tropical SST anomalies on observed multidecadal trends in Antarctic sea ice?

Each above research project is established as individual studies that are answered in Chapters 2, 3 and 4, with each chapter having its own Introduction, Methods, Results, Summary and Conclusion sections.

In Chapter 2, we examine the role of internal tropical SST variability in controlling the austral summer jet's poleward migration, with a focus on interdecadal time scales. The contributions of external forcing and internal variability are isolated by using a hierarchy of CESM1 simulations, including the pre-industrial control, large ensemble, and pacemaker runs.

Building on the Chapter 2, Chapter 3 further investigates the mechanism by which the Southern Hemisphere eddy-driven jet responds to tropical Pacific SSTs on decadal time scales, with a main focus on the role of air-sea coupling. To achieve this, we designed atmosphere-only Pacific SST experiments using the Community Atmosphere Model version 5 (CAM5) to compare to the fully coupled CESM1 tropical Pacific pacemaker experiments.

In Chapter 4, the relative impacts of each tropical basin's SSTs in driving the the annual-mean sea ice expansion in the South Indian sector and western Ross Sea are investigated using the CESM1

pacemaker experiments. Both atmospheric and oceanic processes are analysed to investigate the mechanisms behind the sustained sea ice increasing trends in the Ross Sea.

The thesis concludes in Chapter 5 with an overall summary and a discussion of implications and remaining uncertainties as well as some future directions for this research. This thesis, based on observational analysis and climate model experiments, aims to improve our current understanding of the drivers of decadal variabilities in the Southern Hemisphere extratropical circulation and Antarctic climate. The results of the thesis could provide insights for constraining future projections of westerly wind, its connections to Australian precipitation, Southern Ocean carbon uptake, and Antarctic sea ice, which is important for our society to adapt to climate change, especially for the agricultural and fishery industry. Furthermore, the use of a relatively new "pacemaker" technique allows us to establish the relative contributions of individual ocean basins in modulating the high latitude climate, highlighting the need for future research to focus more on the role of these various tropical ocean basins.

Chapter 2

Role of tropical variability in driving decadal shifts in the Southern Hemisphere summertime eddy-driven jet

2 Role of tropical variability in driving decadal shifts in the Southern Hemisphere summertime eddy-driven jet

Preface:

This chapter is based on the publication:

Yang, D., Arblaster, J.M., Meehl, G.A., England, M.H., Lim, E.P., Bates, S. and Rosenbloom, N., 2020. Role of tropical variability in driving decadal shifts in the Southern Hemisphere summertime eddy-driven jet. *Journal of Climate*, 33(13), pp.5445-5463.

The Southern Hemisphere summertime eddy-driven jet and storm tracks have shifted poleward over the recent few decades. In previous studies, explanations have mainly stressed the influence of external forcing in driving this trend. Based on CESM1 Large Ensemble and Pacemaker simulations, in this chapter, we examined the relative roles of external forcing and internal tropical SST variability in controlling the austral summer jet's poleward migration, with a focus on interdecadal timescales.

2.1 Introduction

As the leading mode of atmospheric variability in the Southern Hemisphere (SH) extra-tropics, the Southern Annular Mode (SAM) and its associated eddy-driven jet (or mid-latitude jet), are fundamentally important for the climate system. The SAM has been shown to have well-established connections with SH extratropical and subtropical rainfall bands (Purich et al. 2013; Hendon et al. 2014; Lim et al. 2016a). Consequently, a range of observational and model studies have sought to understand the observed poleward movement of the eddy-driven circulation in the SH over recent decades.

A poleward shift of the SH eddy-driven circulation under increasing greenhouse gases and stratospheric ozone depletion has been emphasized in early studies (Kushner et al 2001; Yin 2005). Thompson and Solomon (2002) highlighted the contribution of stratospheric ozone depletion to a positive SAM trend especially over the SH summertime since the 1960s, based on multiple observed datasets from 1969-1998. Arblaster and Meehl (2006) further classified different sources of external forcings and their contributions to the SAM trend using a global coupled model and indicated that the ozone changes in the upper troposphere and stratosphere dominated the observed positive SAM trend. Similar results were obtained by Polvani et al. (2011), who found that the impact of ozone depletion was 2-3 times larger than GHGs on the summertime poleward displacement of the eddy-driven jet and the expansion of the Hadley cell over the second half of the 20th century.

The contributions of natural intrinsic variability, particularly the influence of tropical sea surface temperatures (SSTs), have also been discussed, with a primary focus on interannual timescales. A number of previous studies have shown an association between the El Niño Southern Oscillation (ENSO) and a SAM phase shift via zonally symmetric variations in transient eddy momentum flux anomalies (L'Heureux and Thompson 2006b; Fogt et al. 2011; Gong et al. 2013; Yu et al. 2015). During La Niña events, a positive SAM phase occurs more frequently and the opposite is found for El Niño years. Chen et al. (2008) further analysed the eddy momentum flux spectrum, and found that the mid-latitude jet could be expected to undergo a poleward migration during La Niña years due to the poleward displacement of the wave-breaking critical latitude – and the associated transient eddy momentum flux divergence and convergence zones, by waves of a broad range of phase speeds.

Despite the well-established interannual ENSO-SAM relationship, less is known about the influence of internal decadal variability on the mid-latitude jet. Some research has related the Interdecadal Pacific Oscillation (IPO) transition in the late 1990s to Antarctic climate variability. For example, the negative phase of the IPO has been linked to Antarctic sea ice expansion via a positive phase of the SAM combined with a deepened Amundsen Sea Low (ASL), which alters the wind patterns over the Antarctic sea ice zone (Meehl et al. 2016; Purich et al. 2016a; Clem et al. 2019; Holland et al. 2019; Meehl et al. 2019b). Recent studies have also highlighted the role of Atlantic and Indian Ocean SSTs on Antarctic climate. For instance, Li et al. (2015) suggested tropical Atlantic SSTs could force a positive response in the SAM and a strengthened ASL via stationary Rossby wave activities in SH winter. Wang et al. (2019) and Purich and England (2019) found that tropical Indian Ocean SST likely contributed to the Antarctic sea ice decline in austral spring 2016 via SAM and zonal wave three (ZW3) teleconnections.

A few studies have further distinguished the relative roles of radiative forcing and global SST on SH mid-latitude jet variations. For example, Lee and Feldstein (2013) applied a cluster analysis based on ERA-Interim data and concluded that ozone contributed about 50% more than GHG toward the SH summertime jet shift from 1979 to 2008, with tropical convection playing an important role in the GHG-driven trend. Similar results were obtained in other studies examining simulations with time-evolving SST and external forcing prescribed in atmosphere-only models. For instance, Deser and Phillips (2009) emphasized the importance of radiative changes as the dominant driver of the poleward movement of the SH westerly jet in austral summer (December-January-February; DJF) during 1951-2000 using Community Atmosphere Model version 3 (CAM3) experiments. Schneider et al. (2015) suggested that ozone depletion could largely explain the positive SAM pattern during 1979-2011 in the austral summer season, while teleconnections from tropical SSTs also play a role, suggesting the extratropical circulation responds to a combination of both (external) radiative forcing and (internal) tropical SST variability. However, there remain issues with using atmosphere-only experiments to study the combined effects of external radiative forcing and internal SST variability. First, compared to coupled models, atmosphere-only experiments lack the interactions with the underlying ocean and sea-ice, which could be important for tropical-extratropical teleconnections. Second, the time-evolving global SSTs still implicitly contain the GHG-induced forced response, which makes it difficult to delineate between the influence of external forcing and the influence of internal variability in SST.

Here we examine the separate roles of internally-driven tropical SSTs and external forcing in the observed decadal variability of SH mid-latitude circulation using the CESM1(CAM5) coupled model

large ensemble (Kay et al. 2015) as well as various pacemaker experiments. We will address the following overarching questions:

1. What are the relative roles of external forcing versus internally-driven SST variability in the tropical Pacific, tropical Indian and tropical and north Atlantic basins in recent decadal variations of the SH summertime mid-latitude circulation?
2. By what mechanism does the SH summertime eddy-driven jet respond to tropical Pacific SST on decadal timescales?

We focus on the austral summer season since that has experienced the strongest observed latitudinal shift over the satellite-era (Swart et al. 2015; Lim et al. 2016b), for which we have the most reliable data. Furthermore, there has been much research undertaken regarding the influence of external forcings on the SH atmospheric circulation shift in this season, but very little work on the impact of internal variability on decadal timescales. The rest of this chapter is organized as follows: Section 2.2 describes the data, model simulations and the methodology employed in this study. Section 2.3 presents the main results. The physical mechanisms at play are outlined in Section 2.4 and a summary with discussion is given in Section 2.5.

2.2 Data and Methods

Our study is primarily confined to the DJF season during 1979-2013 period due to the availability of both reliable observational data and output from the CESM pacemaker simulations.

2.2.1 Reanalysis Data

Zonal (U) and meridional (V) winds and mean sea level pressure (MSLP) from January 1979 to February 2013 are taken from the European Centre for Medium-Range Weather Forecasting Interim Reanalysis (ERA-Interim, Dee et al. 2011). The observed monthly SST over the global oceans between January 1870 and December 2013 is taken from the Hadley Centre HadISST1 dataset (Rayner et al. 2003).

2.2.2 The Community Earth System Model (CESM) Simulations

Climate variations are caused by both external radiative forcing and internal variability. The latter arises from the internal processes of each climate component (atmosphere, ocean, land, cryosphere etc.), as well as their coupled interactions. In order to separate the internal variability and the influence of the external forcing, five sets of CESM1.1 experiment are analysed in this chapter (Table 2-1). The

CESM1.1 is a coupled Earth system model consisting of atmosphere, ocean, land and sea-ice components with a nominal horizontal resolution of 1º (Hurrell et al. 2013; Kay et al. 2015) and contributed to the fifth phase of the Coupled Model Intercomparison Project (CMIP5).

Table 2-1 Summary of the CESM1.1 simulations used in this research. All experiments begin in January 1920 and extend until the end of December 2013, apart from the PI control run, where years 400-2100 are selected.

Experiments	Time-evolving external forcing	Time-evolving SSTs	Members
Preindustrial Control (PI control)	1850 conditions, Year 400-2100	—	1
Large Ensemble (LENS)	Historical for 1920-2005, RCP8.5 for 2006-2013	—	40
Pacific Pacemaker	Same as LENS, except with SPARC ozone forcing	*Fully-restored SSTA for 15°S-15°N, buffer belts for 15-20°S & 15-20°N, 180° to the American coast.*	10
Indian Pacemaker	Same as LENS, except with SPARC ozone forcing	*Fully-restored SSTA for 15°S-15°N, buffer belts for 15-20°S & 15-20°N, from the African coast to 180°.*	10
Atlantic Pacemaker	Same as LENS, except with SPARC ozone forcing	*Fully-restored SSTA for 5-55°N, buffer belt for 0-5°N & 55-60°N, the Atlantic Basin.*	10

The first experiment comprises monthly data from a 1000+ year preindustrial control (PI) run with a constant forcing based on 1850 levels (Kay et al. 2015). In the absence of changes in natural or anthropogenic forcing, the fluctuation range in the PI control describes internally generated variability.

The second experiment is the CESM Large Ensemble (LENS) which includes 40 individual members (Kay et al. 2015). All ensemble members of the LENS follow the same radiative forcing scenario (Taylor et al. 2012), with historical forcing during 1920-2005, followed by the high emission forcing scenario of the representative concentration pathways (RCP) 8.5 (Moss et al. 2010) from 2006 to 2080. Ensemble members of the CESM LENS are generated with a small perturbation of the initial atmospheric temperature fields. As a result of the chaotic nature of the climate system, the small initial perturbations evolve into a diverse member spread, which reflects the internally generated variability of the climate system in the presence of external forcing. The LENS 40-member ensemble

mean yields an average that removes internal variability and thus gives an estimate of the influence of external forcing on the climate system. It is noted that the LENS members have very different tropical trends (Chung et al. 2019), thus to best estimate the external forcing signal and to be comparable with previous work using LENS (Solomon and Polvani 2016; Holland et al. 2019; Zhang et al. 2019), we employed 40 members of the LENS throughout our study.

The remaining experiments use a pacemaker framework (Kosaka and Xie 2013; Schneider and Deser 2017; Meehl et al. 2019a), wherein SST anomalies (SSTA) are nudged to observed values within a specific ocean region, while the rest of the model evolves freely. In all pacemaker experiments (Table 2-1), the identical coupled model and external forcing used in the LENS is employed, aside from ozone forcing, wherein the LENS employs the Whole Atmosphere Community Climate Model (WACCM, (Marsh et al. 2013)) ozone dataset, while the pacemaker runs are forced with the Stratosphere-Troposphere Processes and their Role in Climate (SPARC) stratospheric ozone data (Cionni et al. 2011). In these pacemaker experiments, SSTA are nudged to the NOAA Extended Reconstruction Sea Surface Temperature, version 3b (Smith et al. 2008) observed anomalies, with a climatological period of 1920-2005. For example, in the CESM tropical Pacific Ocean pacemaker run (Table 2-1), a fully-restored observational SSTA was applied over the region 15°S-15°N, 180°W to the American coast, with two buffer belts along 15°S-20°S and 15°N-20°N. In these buffer zones, the fully-nudged SSTA (at 15°S and 15°N) are gradually damped to zero (at 20°S and 20°N) via a sine function of the latitude change (Schneider and Deser 2017). The rest of the model is fully coupled and free to evolve, and able to capture the response to both external forcing and the observed SST changes in this specified region. Following the method of Schneider and Deser (2017) and Holland et al. (2019), the ensemble mean of the Pacific pacemaker combines the response to external forcing and the response to observed tropical Pacific SSTs, and thus removing the ensemble-mean of the LENS gives an estimate of the response of the global climate system to observed time-varying internally-driven Pacific SSTs. Note that while the ozone forcing differs slightly between the LENS and the pacemaker experiments, Schneider and Deser (2017) concluded that the ozone forcing differences had statistically indistinguishable impacts on the trends in the SH eddy-driven jet over the satellite era. Given the LENS stratospheric ozone forcing (WACCM) has stronger ozone depletion over that period than the SPARC ozone forcing (Cionni et al. 2011) used in the pacemaker experiments (Eyring et al. 2013), if anything, our methodology for subtracting the externally forced signal would weaken the determined impact of tropical internally-generated SSTAs.

A similar methodology is applied to isolate the tropical Indian (15°S-15°N, African coast to 180°W) and tropical and North Atlantic SST (0°-60°N, Atlantic basin) impact in the other pacemaker

experiments (Table 2-1). By subtracting the LENS ensemble-mean from the respective pacemaker ensemble means, we obtained the climate response to the internal variability originating from tropical Pacific SST, tropical Indian SST, as well as the north and tropical Atlantic SST, respectively. The sum of these four components (i.e. LENS, plus the three pacemakers with external forcing removed) reflects the estimated response of the climate system to both external forcing and the internally-generated observed variability in the three tropical basin SSTs. However, this linear summation does not take into account tropical basin interactions (Cai et al. 2019) and may result in some 'double counting' of the influence of tropical SSTs on the extratropical circulation. Finally, note that daily U and V winds are not available for the Indian and Atlantic pacemaker experiments, which limits our exploration of physical mechanisms to the Pacific pacemaker experiment and LENS only.

2.2.3 Definitions

Eddy-driven jet

The eddy-driven jet is located in the mid-latitudes and maintained by an eddy momentum flux convergence (Vallis 2006). Different from the baroclinic thermal-driven subtropical jet, the eddy-driven jet is equivalent barotropic, and the transient eddy-mean flow interaction is important for its development and variation (Hendon et al. 2014). In this chapter, the eddy-driven jet is defined as the maximum zonal wind at 850 hPa.

Cospectra analysis of transient eddy momentum flux

Cospectra analysis of transient eddy momentum flux ($\overline{u'v'}$) has been widely used to study the changes of mid-latitude eddy characteristics (generation, propagation, and dissipation) and their impact on the background zonal flow (Randel and Held 1991; Chen and Held 2007; Chen et al. 2008; Hendon et al. 2014).

Here we calculated the transient eddy momentum flux as a function of eddy phase speed and latitude following Randel and Held (1991). Specifically we 1) obtained the DJF (90-day) daily transient u', v' data from ERA-Interim, CESM LENS and Pacific pacemaker; 2) at each latitude, we computed the cospectra (real part of the complex cross power spectra) of $\overline{u'v'}$ by Fourier transforming u', v' (longitude, time) to u', v'(wavenumber, frequency), with four passes of Gaussian spectral smoothing (following equation 2 in Randel and Held 1991) operating on the frequency dimension; 3) the wavenumber-frequency cospectra is transferred to wavenumber-phase speed cospectra (following equation 3a and 3b in Randel and Held 1991); 4) we took the summation of zonal wavenumbers 1–10 for plotting the cospectra of $\overline{u'v'}$ as a function of phase speed and latitude. There is some sensitivity to the choice of smoothing method and using monthly versus seasonal length of data,

which primarily impacts the low latitude regions but minimal impacts the mid-latitudes where the eddy activity is vigorous.

Southern Annular Mode (SAM)

SAM is the leading mode of atmospheric variability in the SH extratropics, characterized by a "see-saw"-like behaviour of mass distribution between the mid- and high latitudes. In this study, the SAM index is defined as the normalized zonal-mean sea level pressure (SLP) difference between 40°S and 65°S, following Gong and Wang (1999). Positive SAM phase means higher normalized pressure anomalies over 40°S than over 65°S. This quasi-stationary pattern can be considered as the eddy-driven circulation (Vallis 2006). The SAM phase is associated with the latitudinal location of the eddy-driven jet as well as variations in the jet intensity (Swart and Fyfe 2012; Swart et al. 2015).

Interdecadal Pacific Oscillation (IPO)

The IPO is a representation of internal decadal climate variability in the Pacific Ocean. There are several IPO definitions, and here we use the second principal component (PC2) of the low pass filtered (13-year cut-off) near-global SST as in Meehl et al. (2016). A positive IPO phase reflects an eastern Pacific Ocean warming flanked by cooling in the subtropical western Pacific. The negative IPO phase sees SST anomalies of opposite sign to the positive IPO phase.

2.3 Results

Figure 2.1 shows the observed SAM variation (Figure 2.1a), the leading principal component of the eddy-driven jet (Figure 2.1b) and the regression of westerly zonal wind anomalies onto the PC1 time series (Figure 2.1c). The peak magnitude of the climatological jet is located in the southern Atlantic and Indian Oceans with maximum wind speeds of around 18 m/s. The 11-year running means (lines in Figure 2.1a and b) suggest the SAM gradually trended from a negative to positive phase during 1980-2000 and has plateaued afterwards, associated with a poleward shift of the eddy-driven jet (the dipole structure of anomalies cantered on the climatological jet axis in Figure 2.1c). As noted above, external forcing is believed to be the dominant driver of the poleward shift in the austral summer eddy-driven jet over the second half of the 20th Century, with ozone depletion being the dominant driver (Karpechko et al., 2018). After 2000, Antarctic ozone depletion plateaued (Chipperfield et al. 2017), while the IPO transitioned from a positive to negative phase around 1999, as discussed in previous study (Meehl et al. 2016) and as shown in Figure 2.2. How did the SH mid-latitude atmospheric circulation respond to these observed variations in forcing and tropical SSTs?

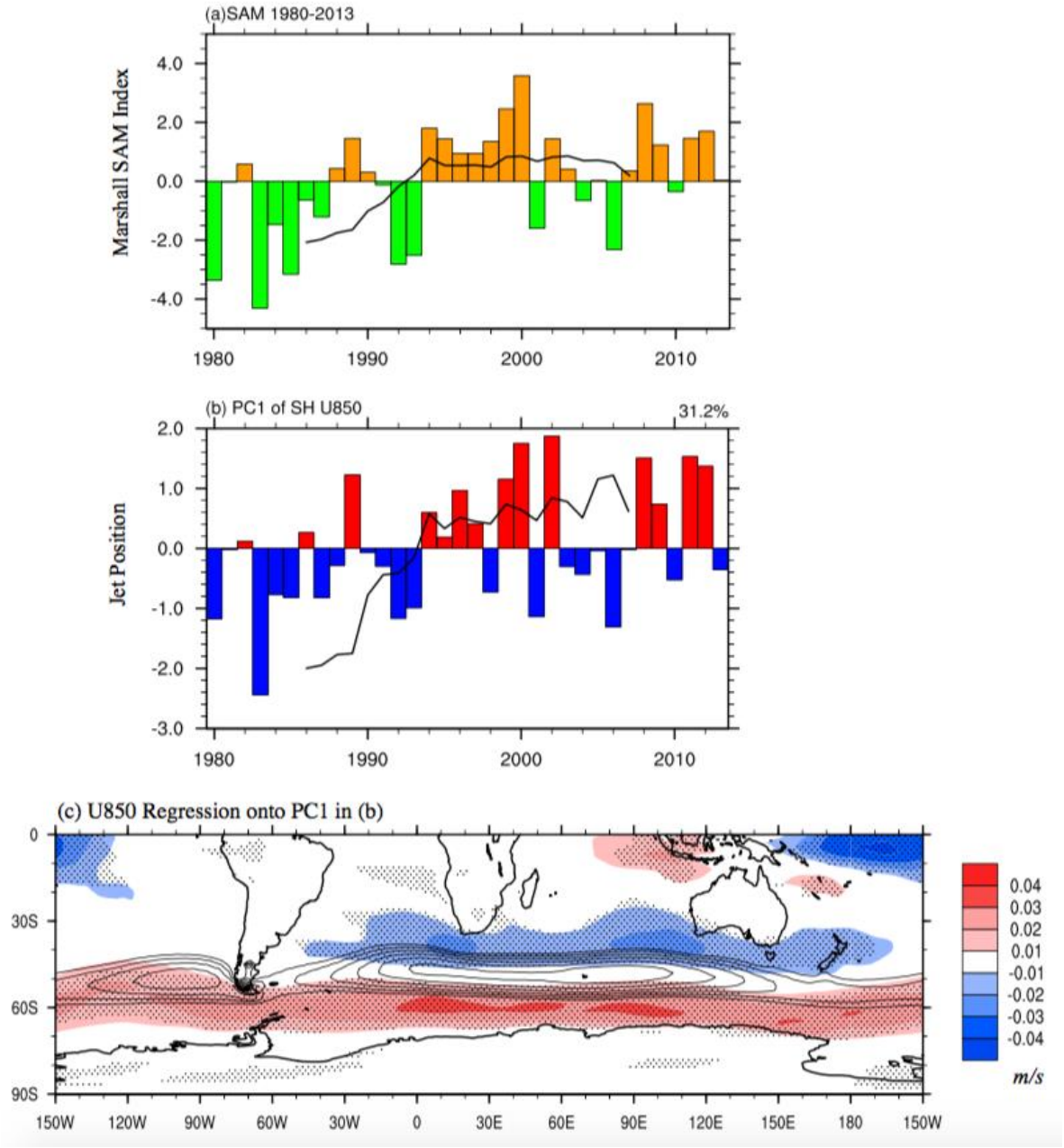

Figure 2.1 (a) Marshall SAM time series (bar) for DJF from 1980-2013, the black line is 11-year running mean; (b) PC1 time series (bar) of 850 hPa U-wind of 1980-2013 over 20-90°S, the black line is 11-year running mean; (c) Contours show the climatological mid-latitude jet from 1980-2013 with an interval of 1m/s, colours are the regression of 850 hPa zonal wind onto the PC1 in (b), with dashed areas significant at the 95% level based on a two-sided Student t-test.

2.3.1 Decadal difference between 1999-2013 and 1979-1998

To address this question the observed period is divided into two separate periods P1 (1979-1998) and P2 (1999-2013) based on the IPO time series in Figure 2.2, targeting a comparison between the influence of positive and negative IPO phases, respectively. The significance test of the decadal difference is based on a two-sample t-test for observation and model ensemble-mean. During the positive IPO period (P1), the SAM was primarily in the negative phase, with an equatorward movement (negative PC value in Figure 2.1b) of the jet, while in the negative IPO period (P2), the SAM was primarily in its positive phase with a poleward displacement of the jet. As discussed earlier, the decadal change of the SAM and the eddy-driven jet cannot be simply inferred as a response to IPO variations, because strong ozone and GHG forcings were also present at this time, along with other tropical ocean SST changes.

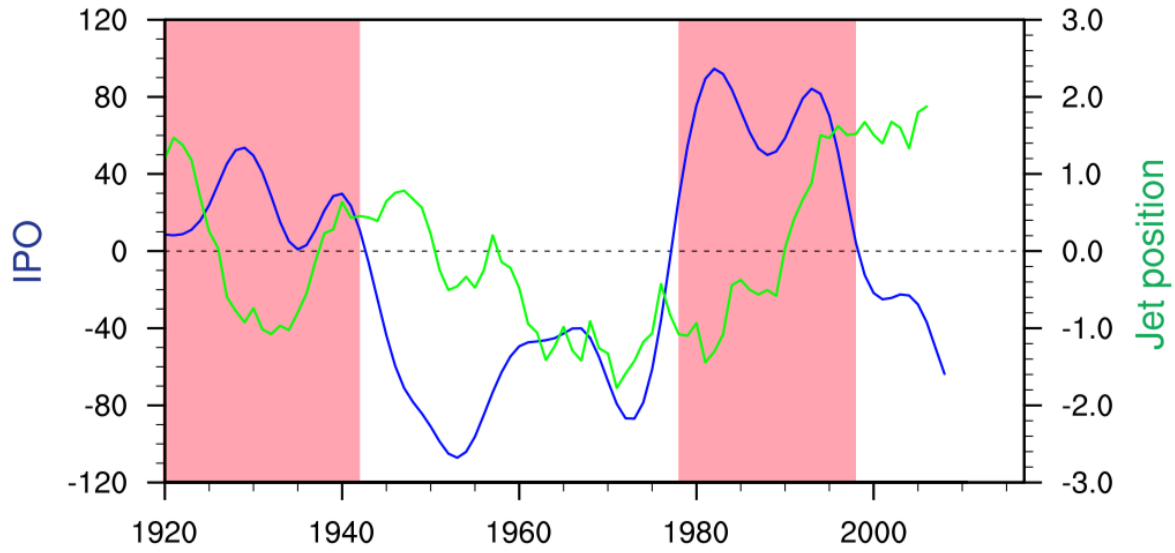

Figure 2.2 The smooth blue line is the IPO time series from 1920-2013 in DJF calculated as the 2nd EOF of low-pass filtered (13-year cut-off) near-global HadISST. Pink bars indicate the positive IPO phase and white bars show the negative phase. The green line is the the 11-year running mean for PC1 time series of 850 hPa zonal wind for 1920-2013 using 20th Century Reanalysis (V2) datasets.

Figure 2.3 shows the decadal difference of sea surface temperature between 1999-2013 and 1979-1998 for DJF in observations (Figure 2.3a), under the influence of external forcing (Figure 2.3c) and from the pacemaker experiments (Figure 2.3d-f). To distinguish the influence of external radiative changes from the intrinsic variability due to tropical ocean SSTA, the LENS ensemble mean is subtracted from the CESM pacemaker experiments. In accordance with the IPO time series in Figure 2.2, the observed SSTs display a typical negative IPO phase pattern within the Pacific basin, with

significant cooling over the central and eastern tropical Pacific, and notable warming over the subtropics. This pattern is only captured in Pacific pacemaker minus LENS (Figure 2.3d), which suggests the primary role of internal decadal variability in the observed SST difference, supporting previous work (e.g. England et al. 2014). Meanwhile the impact of external forcing across these two periods warms up the Earth surface almost globally (Figure 2.3c). The decadal SST difference due to internally-driven tropical and North Atlantic SST and tropical Indian SST are shown in Figure 2.3e and Figure 2.3f, respectively. There is an observed significant warming trend in the North Atlantic, resulting largely from the external forcing and partly from internal variations. However, there are less significant values in the Indian and Atlantic pacemaker experiments than in the tropical Pacific and from external forcing.

The sum (Figure 2.3b) of the external and internal factors yields a similar pattern to the observations in most locations except the SH high latitudes, showing that our methodology using the CESM experiments is generally able to separate the different influences and reproduce the observations to a large degree. However, there is too much warming over the Southern Ocean, especially in the Southern Atlantic basin and around New Zealand. This could be related to the systematic warm bias of coupled climate models in CMIP5 (Wang et al. 2014), with Kay et al. (2016) identifying insufficient cloud brightness and excessive absorbed shortwave radiation (ASR) biases over the Southern Ocean in CESM1. Secondly, the equatorial central Pacific SST in Figure 2.3b is not cooling enough compared with Figure 2.3a, suggesting that the model has problems reproducing the strength of the Pacific trade wind acceleration across this time period. This issue also seems to affect all coupled models and has been touched upon in several past studies, for example (England et al. 2014; McGregor et al. 2014; Luo et al. 2018; McGregor et al. 2018). Furthermore, the North Atlantic pacemaker warming induces a positive IPO-like pattern in the Pacific basin (Figure 2.3e), which is opposite to the result obtained by McGregor et al. (2018) and Meehl et al. (2019a). While noting these caveats, the pacemaker experiments remain a useful tool to test and understand the influence of each basin in driving SH circulation changes.

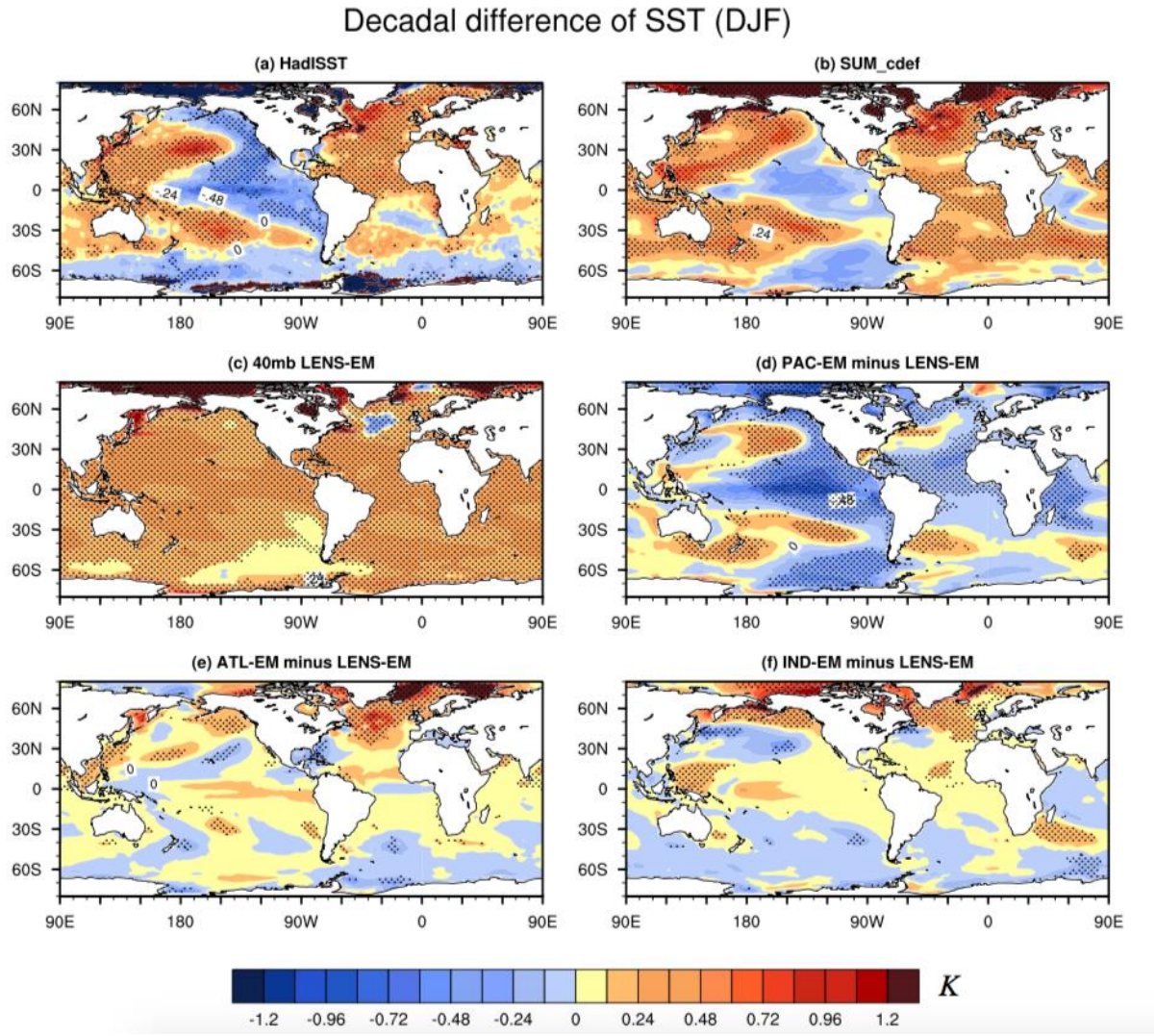

Figure 2.3 The decadal difference between averaged P2 (1999-2013) and P1 (1979-1998) for sea surface temperature. (a) HadISST; (b) Sum of (c), (d), (e) and (f); (c) CESM Large Ensemble mean (LENS-EM), indicative of external forcing; (d) Pacific pacemaker ensemble-mean (PAC-EM) minus LENS-EM, highlighting the internally-driven tropical Pacific SST impact; (e) Atlantic pacemaker ensemble-mean (ATL-EM) minus LENS-EM; (f) Indian pacemaker ensemble-mean (IND-EM) minus LENS-EM. Stippling in (a) and (c)-(f) indicates differences between the two periods are significant at the 95% level based on a t-test.

The decadal difference analysis is shown for the austral summer 850 hPa zonal wind in Figure 2.4. With easterly wind anomalies in the mid-latitudes (north of 45°S) and westerly wind anomalies in the high latitudes (south of 45°S), the dipole structure shows that the observed eddy-driven jet has migrated poleward by ~ 1° of latitude during 1999-2013 relative to 1979-1998 (refer to contours in Figure 2.4a). Significant values are found over the South Atlantic and parts of the Indian basin.

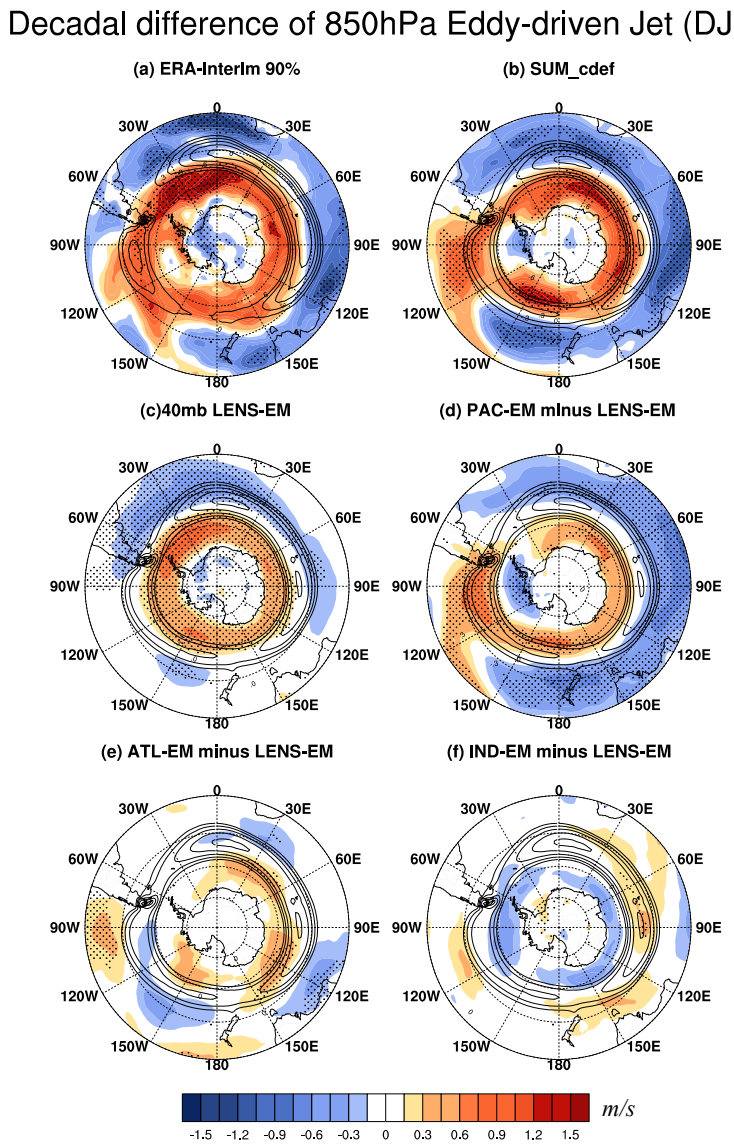

Figure 2.4 The decadal difference between averaged P2 (1999-2013) and P1 (1979-1998) for 850 hPa zonal wind. (a) Era-interim; (b) Sum of (c), (d), (e) and (f); (c) LENS-EM. (d) Pacific pacemaker ensemble-mean (PAC-EM) minus LENS-EM; (e) Atlantic pacemaker ensemble-mean (ATL-EM) minus LENS-EM; (f) Indian pacemaker ensemble-mean (IND-EM) minus LENS-EM. Contours are the 850 hPa zonal wind averaged over P1 using ERA-Interim in (a) and the LENS ensemble mean in (b)-(f). Stippling in (a) and (c)-(f) indicates differences are significant at the 90% and 95% level based on a t-test, respectively.

More quantitative features of the jet shift for the zonal-mean and each basin average are shown in Figure 2.5. The jet position is identified as the latitude of the maximum zonal wind at 850 hPa, which is obtained using a quadratic fit to the grid point with the maximum zonal wind and the eight adjacent to it (Simpson et al. 2018). The 5-95% confidence intervals (shaded boxes) in Figure 2.5 are determined from the spread across the 40 or 10-member ensembles, following the equation (8) of

Swart et al (2015). The LENS with its larger ensemble size therefore has a narrower confidence interval.

From the zonal-mean perspective, the observed jet movement (triangles in Figure 2.5) from 1979-1998 to 1999-2013 is ~0.8°S (0.23° per decade), which is significantly driven by both the external forcings (0.5°S +/-0.18°) and the Pacific SST (0.4°S +/-0.34°) based on our model simulations. This magnitude of the jet movement is consistent with the ~2° (0.3° per decade) latitudinal shift found by Swart et al. (2015) for DJF over the longer 1951-2011 period, with some difference due to a different mix of forcing and internal variability between the two periods expected. The largest observed jet shift is found in the South Atlantic basin, with ~1.3°S poleward displacement, where external forcing contributed ~0.8°S (+/-0.21°) and the influence of Pacific SST is ~0.3°S (+/-0.44°). In the South Indian basin, the observed magnitude of the jet shift is around 0.6°S, which is mainly induced by Pacific SST internal variability (~0.4°S +/-0.31°) as well as the external forcing (~0.3°S +/-0.17°). The smallest jet movement in the observations is detected in the South Pacific basin of ~0.3°S, with 1 m/s acceleration of the maximum wind mainly driven by Pacific SST (see Figure 2.4). This is consistent with Schneider et al. (2015) who found that the zonal wind in the South Pacific experienced an intensification with a slight poleward shift (their Figure 8a) during 1979-2011. It is also clear that the North and tropical Atlantic SST (Figure 2.4e and blue bars in Figure 2.5), as well as the tropical Indian SST (Figure 2.4f and magenta bars in Figure 2.5), appear to force a much weaker response, which can partly offset the poleward trend caused by external forcing and Pacific SST. If we simply add up the externally forced response and the internally generated responses from all three tropical ocean basins (Figure 2.4b), all these combined factors are able to reproduce the observed poleward jet migration over the Atlantic and Indian Oceans, as well as the jet strengthening over the southeast Pacific to some degree, but there are mismatches with some locations of the statistically significant regions.

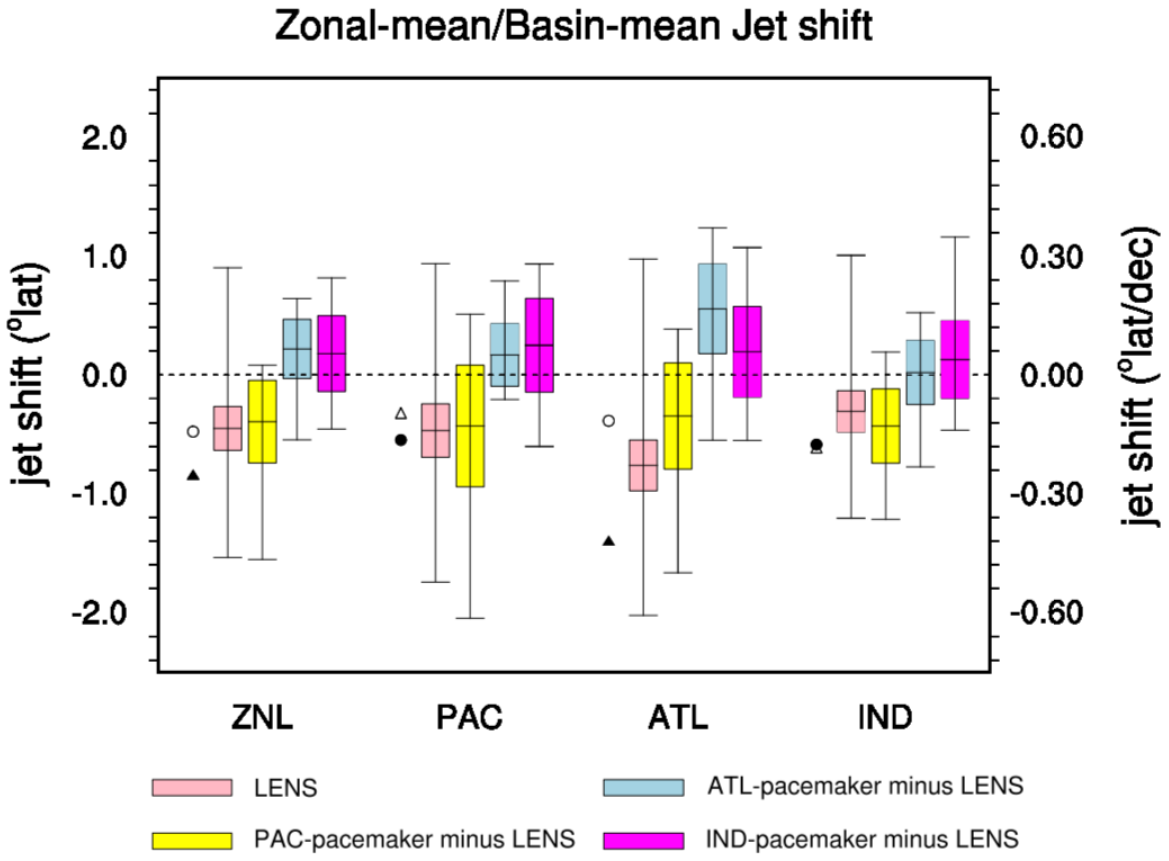

Figure 2.5 The decadal difference between averaged P2 (1999-2013) and P1 (1979-1998) of 850 hPa zonal wind for zonal-mean and basin averages. Negative values indicate the poleward shift. For each model experiment, the ensemble-mean jet shift is given by the middle horizontal line, the 95% confidence interval is shown as the vertical coloured bars, and the minimum and maximum shifts (equivalent to the 2.5th-97.5th percentile) across the ensemble are displayed as the upper and lower whiskers. The model summation of the external forcing and internal variabilities is given by small circles. The jet shift in ERA-Interim is shown as the small triangles. Solid triangles and circles indicate the decadal difference are significant at the 90% level based on the same t-test as in Figure 2.4. The longitude range for each basin is defined as 150°E-70°W for South Pacific, 70°W-20°E for the South Atlantic, and 20°E-150°E for the South Indian basin.

In summary, it is evident that the two dominant drivers of the decadal shift in the SH mid-latitude jet are external forcing and tropical Pacific SSTAs, with external forcing significantly contributing to the observed poleward jet shift over the South Atlantic basin and jet intensification over the polar region, while internal tropical Pacific SST variability drives the poleward jet migration in the South Indian basin and Pacific basin. This result is consistent with Lee and Feldstein (2013) and Schneider et al. (2015) who found that ozone depletion and teleconnections from tropic-wide SSTs act together to explain the mid-latitude poleward jet migration during 1979-2011 in SH summer. Here we further identify that the tropical SST impact is mainly from internally driven variability originating in the tropical Pacific basin.

Consistent results are obtained for the sea level pressure decadal difference, where observations (Figure 2.6a) show a zonally symmetric positive SAM phase (negative SLP anomalies at high latitudes, positive SLP anomalies at mid-latitudes), with significant changes found mainly in the South Atlantic basin. This significant pattern is largely captured by the LENS ensemble mean (Figure 2.6c), indicating a substantial role for external forcing in driving the positive SAM pattern. However, consistent with the jet variations seen in Figure 2.4d, the forcing from the tropical Pacific SST also contributes to the positive SAM pattern and better captures some of the details in the observed SLP changes, for example the observed increase in SLP to the south of New Zealand and the deepened Amundsen Sea Low in the southeast Pacific (Figure 2.6d). The summation of the experiments (Figure 2.6b) reproduces the observed positive SAM pattern reasonably well, with major contributions from external forcing and internal Pacific SST variability, but similar to Figure 2.4b, there are mismatches with some locations of the statistically significant regions.

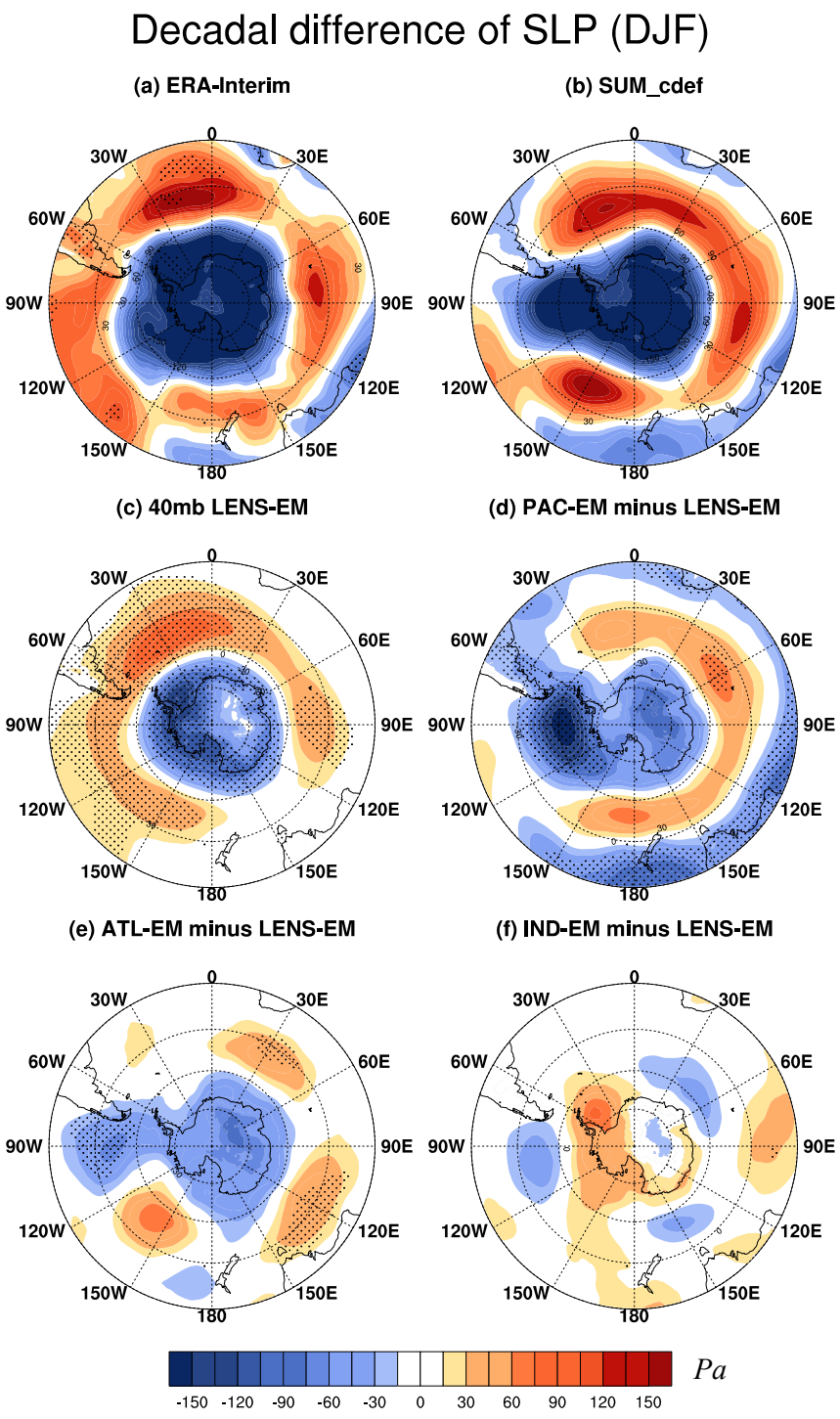

Figure 2.6 The decadal difference between averaged P2 (1999-2013) and P1 (1979-1998) for SLP. (a) Era-interim; (b) Sum of (c), (d), (e) and (f); (c) LENS-EM. (d) Pacific pacemaker ensemble-mean (PAC-EM) minus LENS-EM; (e) Atlantic pacemaker ensemble-mean (ATL-EM) minus LENS-EM; (f) Indian pacemaker ensemble-mean (IND-EM) minus LENS-EM. Stippling indicates differences are significant at the 95% level based on a t-test.

2.3.2 Preindustrial control

The results in Section 2.3.1 suggest that during the satellite-era, on top of the external forcing influence, internally-driven variability from tropical Pacific SSTs also contributed to driving the SH mid-latitude atmospheric circulation variability on decadal timescales. Since the impact of the external forcing has been widely documented, here we further investigate the influence of intrinsic variability originating from tropical Pacific SSTs by analyzing the CESM1 PI control simulations.

The leading EOF of the low-pass filtered near-global (40°S-60°N) SST from years 400-2200 of the PI control shows a typical negative IPO phase, indicating the IPO is a dominant feature of the intrinsic variability in the climate system in the absence of external forcing (Figure 2.7a). Regression of the 850 hPa zonal wind (Figure 2.7b) onto the IPO time series (related PC1 of Figure 2.7a, not shown) shows a zonally symmetric poleward migration of the eddy-driven jet in the South Atlantic and the Indian Ocean, as well as a strengthening in southeast Pacific basin, which resembles our pacemaker results (Figure 2.4d) and the uncoupled simulation results in Schneider et al. (2015) over the satellite-era. The SLP regression (Figure 2.7c) displays a positive SAM-like pattern (negative values at high latitudes) in the South Atlantic and Indian basins, combined with a deepened Amundsen Sea Low (ASL), consistent with the decadal difference result for the observations and pacemaker experiments shown in Figure 2.6, as well as previous research suggesting an impact of the IPO on Antarctic climate variability in this region (Meehl et al. 2016). This confirms the links among the IPO, SAM and the SH eddy-driven jet when examined over multiple samples and without the presence of external forcing.

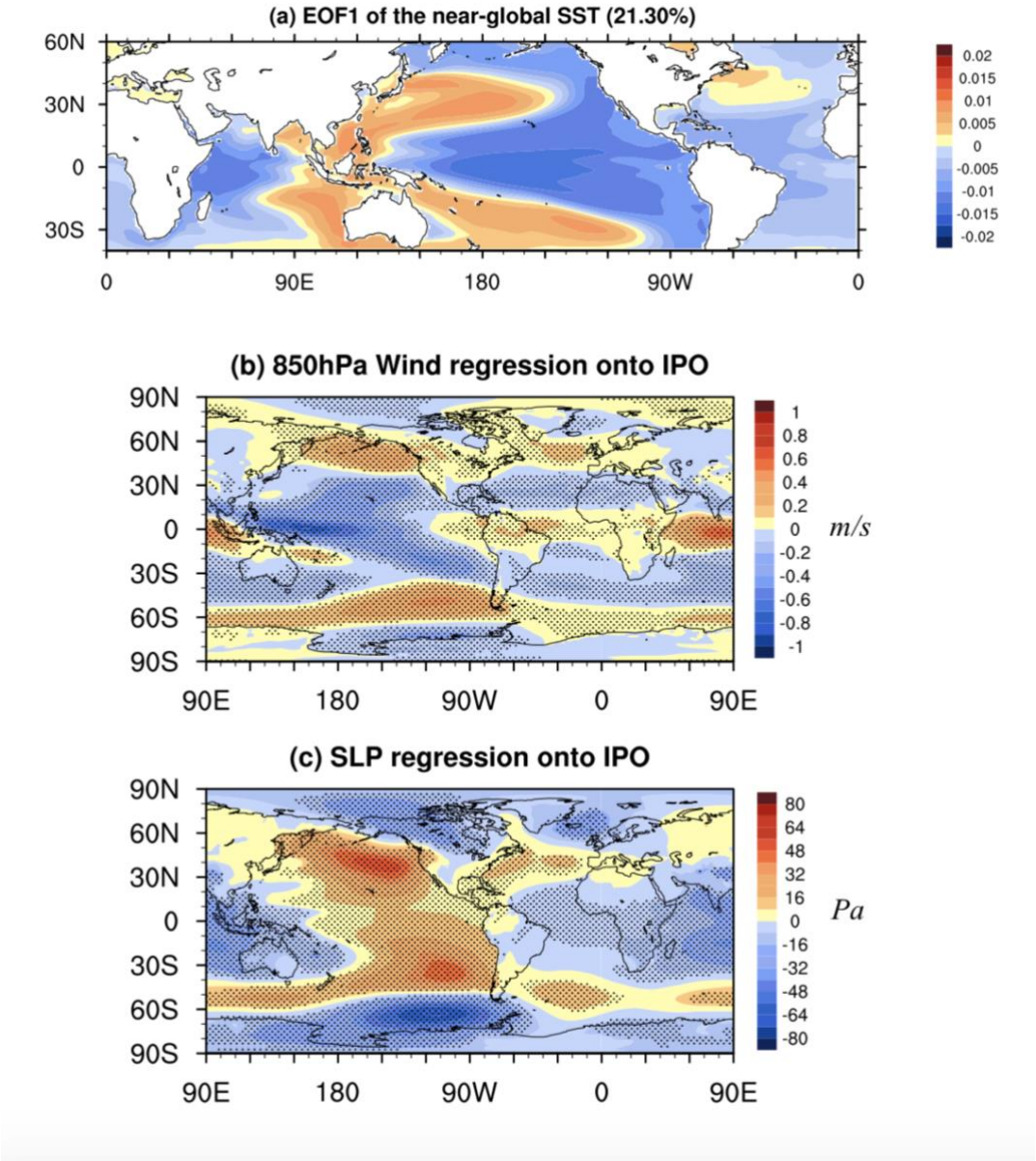

Figure 2.7 (a) First EOF pattern calculated from low-pass filtered (13-year cut-off) near-global (40°S-60N) SST from the Preindustrial-Control for years 400-2200; (b) Regression of 850 hPa U-wind onto (a); (c) Regression of SLP onto (a). Stippling indicates the regressions are significant at the 95% level based on a t-test.

2.3.3 Extended IPO composite analysis

To further examine the connections between IPO and SH extratropical circulation change, an extended IPO composite analysis (negative periods 1944-1977 and 1999-2012, minus positive periods 1920-1943 and 1978-1998) is conducted for the length of the Pacific pacemaker simulations. Averaging over these two IPO cycles, this longer period IPO composite shows a significant poleward jet shift of around 1° latitude over the Indian basin and a strengthening of the jet in the southeast Pacific (Figure 2.8a), along with a positive SAM-like pattern and a deepened ASL (Figure 2.8b),

though with a weaker magnitude compared to Figure 2.4d. Furthermore, in the extended IPO composite, the jet shift also occurs at a much higher latitude (around 55°S) compared to the reanalysis and recent decadal differences (about 50°S), as seen in Figure 2.4d.

In summary, the results from this more extended multi-decadal IPO composite analysis lend support to the previous analyses of the IPO teleconnection to the eddy-driven jet; namely, that the IPO is a key contributor to decadal variability of the SH extratropical atmospheric circulation.

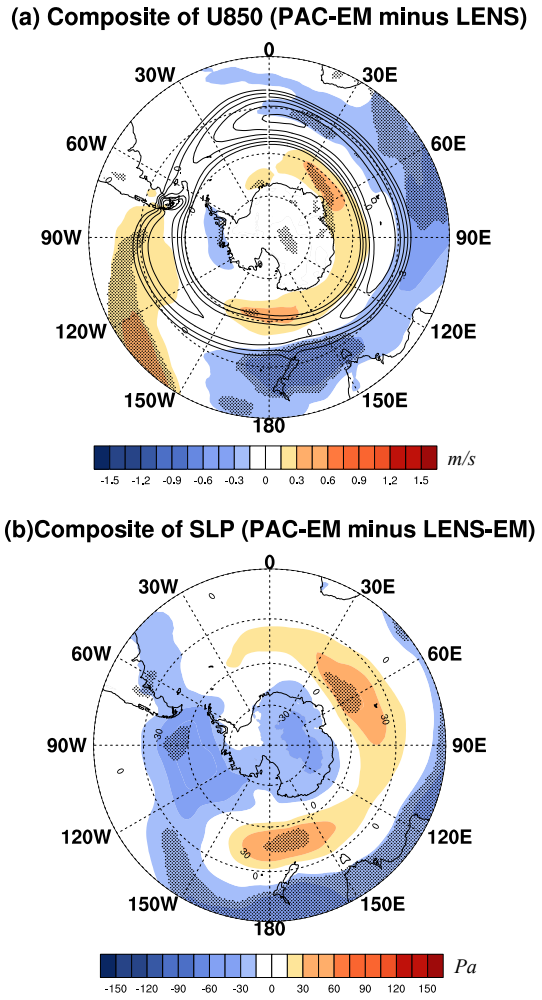

Figure 2.8 The composite (colours) of (a) 850hPa zonal wind and (b) SLP between negative IPO (1944-1977,1999-2012) and positive IPO (1921-1943,1978-1998), from the Pacific pacemaker ensemble-mean (PAC-EM) minus LENS-EM. Contours in (a) show the climatological mid-latitude jet from 1921-2013 with an interval of 1m/s, stippling indicates differences are significant at the 95% level based on a t-test.

2.4 Physical Mechanism

Now, we turn to the question of how external forcing and tropical Pacific decadal variability affect the mid-latitude jet displacement. Since the transient eddy-mean flow interactions are essential in eddy-driven jet development and maintenance, previous studies have used this approach to explain the mid-latitude atmospheric circulation change under global warming, ozone depletion, and its response to ENSO forcing (Lu et al. 2008; Hendon et al. 2014). For instance, according to Lu et al. (2008), the intensified upper-level meridional temperature gradient caused by increased GHGs can accelerate the phase speed of the transient eddies in the high latitudes. Then, the equatorward propagating faster transient eddies break at a higher latitude around the equatorward side of the eddy-driven jet when they encounter the critical latitudes where the increased phase speed equals the background zonal wind speed. As a result, the eddy momentum flux convergence (EMFC) and divergence (EMFD) zones would shift poleward, and westerly winds would strengthen on the poleward flank of the climatological eddy-driven jet. In other words, global warming increases the transient eddy phase speed, which starts the eddy-mean flow feedback that leads to the poleward jet migration and the eddy-driven circulation change. Similarly, Butler et al. (2010) employed an idealized model and found that the SH polar stratospheric cooling caused by ozone depletion would induce the poleward shift of eddy momentum and heat fluxes, resulting in a poleward shift of the eddy-driven jet around 60°S. The EMFC responds to El Niño events in the opposite sense: during El Niño events, as the tropical eastern Pacific warms and the tropical-subtropical temperature gradient increases, the subtropical jet strengthens and shifts equatorward via thermal wind balance at the edge of the descending branch of the Hadley cell. The intensified subtropical jet draws the critical latitudes equatorward for waves of all speeds, which drags the whole eddy-driven meridional circulation equatorward, resulting in a negative phase of the SAM (Seager et al. 2003; Chen et al. 2008; Lu et al. 2008; Lim et al. 2019). However, few studies have investigated the response of the transient eddies and eddy-induced circulation to tropical Pacific SST variation over decadal time-scales.

First, we calculate the decadal difference of the upper-level EMFC as a function of angular phase speed (multiplied by the Earth's radius) and latitude following Chen and Held (2007) and Chen et al. (2008). The observed climatological EMFC (solid contours in Figure 2.9a) is located at mid-latitudes (40-65°S) and induces the westerly jet. The climatological eddy momentum flux divergence (EMFD, dashed contours in Figure 2.9a) belt is located in the subtropics as well as the polar region, with the subtropical EMFD terminating near the critical latitudes around 20-25°S, where the phase speed equals the background zonal mean zonal wind speed.

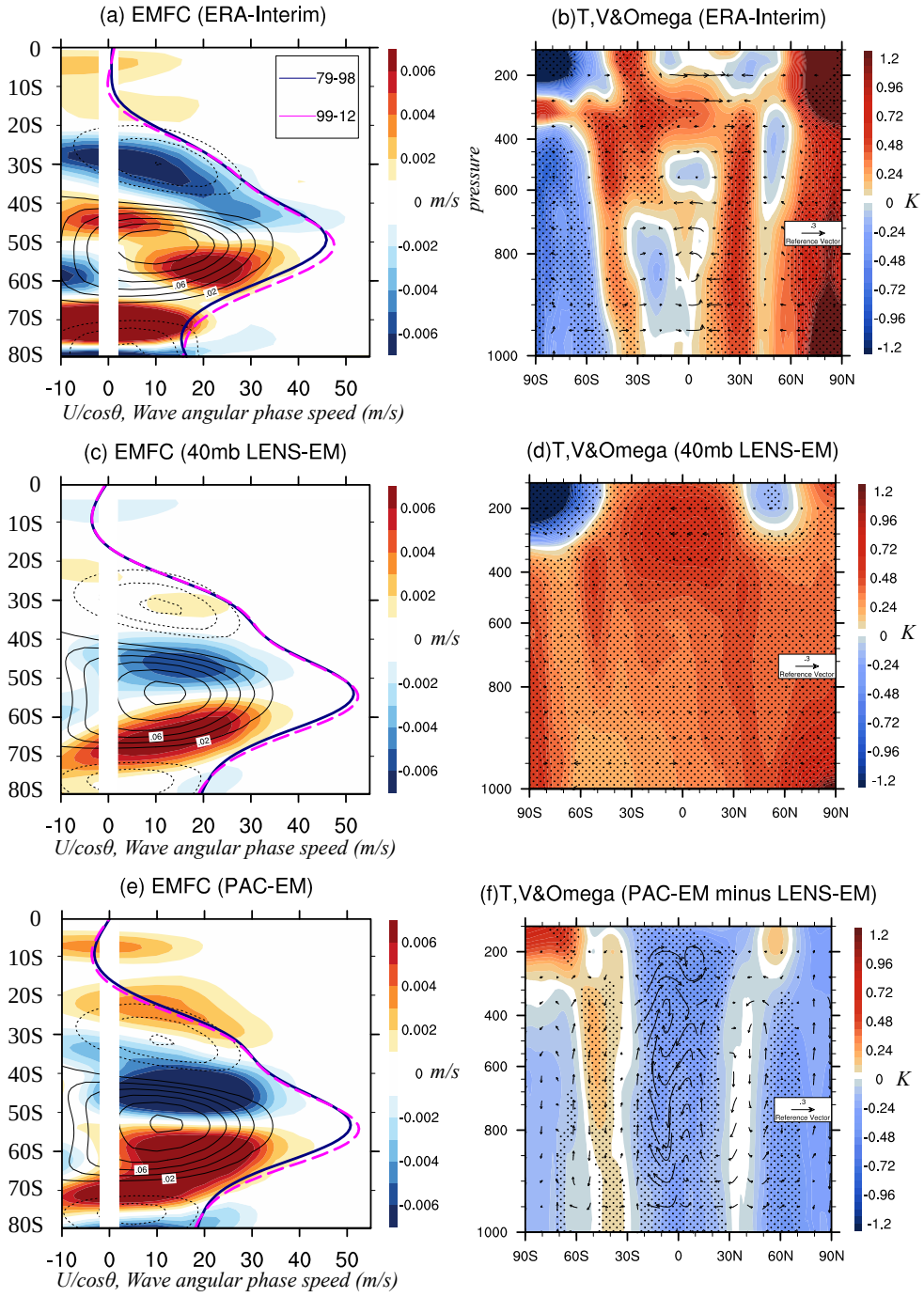

Figure 2.9 Left: Cospectra of transient eddy momentum flux convergence at 200 hPa in DJF, as a function of wave angular phase speed (multiplied by the Earth's radius) and latitude for (a) ERA-Interim; (c) LENS-EM; (f) PAC-EM (note the LENS is not removed in this case). The contours are climatological-mean values over P1 (1979-1998), with dashed/solid contour indicating the transient eddy momentum flux divergence/convergence, respectively; the coloured shading shows the decadal difference (1999-2013 minus 1979-1998). The solid navy curve is the zonal-mean zonal wind (divided by cosφ, φ is latitude) averaging over P1, the dashed magenta curve is averaged over P2. **Right:** Decadal difference (P2-P1) of temperature (shading) and meridional & vertical velocity (v and omega, vectors). (b) ERA-Interim; (d) LENS-EM; (f) PAC-EM minus LENS-EM. Stippling indicates differences are significant at the 95% level based on a t-test.

The decadal difference of the transient EMFC displays a dipole structure in the middle latitudes, with enhanced EMFC (red colours at 55-65°S) on the poleward side of the climatological convergence belt and enhanced EMFD (blue colours at 40-50°S) on its equatorward flank for eastward propagating eddies. This indicates a poleward migration of the eddy-induced momentum convergence and divergence, resulting in a poleward movement of the zonal mean zonal wind (the thick magenta compared to navy lines in Figure 2.9a) by ~1° of latitude. The poleward migration of EMFC and mid-latitude jet is related to the steepened meridional temperature gradient around 50°S (Figure 2.9b), with enhanced baroclinicity providing more energy for transient eddy generations as well as westerly strengthening on the poleward flank of the climatological jet. In the subtropics, the EMFD anomaly is in the same location as the climatological EMFD, and the subtropical wave-breaking latitude has barely changed in the two periods. The EMFC anomalies (the decrease of climatological EMFD) at 0-20°S suggest that there is less eddy breaking in the deeper tropics due to the weakened zonal winds for speeds smaller than 15 m/s.

The contributions of external forcing and tropical Pacific SST are examined using LENS and Pacific pacemaker simulations. The zonal mean temperature anomaly induced by external forcing (Figure 2.9d) exhibits overall warming in the middle and low latitudes as well as a cooling in the South Pole in the upper level, leading to a sharp meridional gradient at about 45°S; the increased meridional temperature gradient is also found in the middle troposphere (800-300 hPa). These would lead to an enhanced baroclinicity and more transient waves produced at higher latitudes, as a result, the climatological EMFC experiences a significant poleward migration at 55-60°S (Figure 2.9c), leading to jet intensification on its poleward flank (similar to Figure 2.4c, polar region jet strengthening), thus inducing a poleward shift of the zonal mean zonal wind by around 1° latitude. This result is in accordance with Figure 10 of Lu et al. (2008) and Butler et al. (2010) as discussed above, suggesting the external forcing (including ozone depletion and global warming) can partly explain the observed zonal mean jet migration. In the subtropics, there is not much response in either EMFD or zonal mean zonal wind to the external forcing, suggesting there are other factors beyond anthropogenic forcing that drive the slight poleward shift of the zonal wind at 20°S in observation (Figure 2.9a).

When the tropical Pacific SST is combined with the external forcing influence in the Pacific pacemaker simulation (Figure 2.9e), the decadal difference of the zonal mean zonal wind better matches the observations in the extratropics. Under this combined impact, a stronger EMFC/EMFD anomaly at 60°S/45°S is formed, with a slight increase of transient wave speed to 45m/s. This appears to be associated with the meridional temperature structure induced by external forcing and negative

IPO, with the latter warming the subtropics and increasing the meridional temperature gradient between the subtropics and the middle latitudes. With faster speed eddies generated and confined in the higher latitudes, eddies would break down at a higher latitude on the equatorward flank of the eddy driven jet, resulting in a poleward shift of the eddy-driven jet. On the other hand, comparisons between Figure 2.9e and Figure 2.9c suggest the influence of negative IPO on the zonal wind can be also found in the subtropics. The negative IPO, with reduced tropical-subtropical meridional temperature gradient and an expanded Hadley cell circulation, induces a slight deceleration of the subtropical jet around 20°S and a poleward displacement of the subtropical jet and wave-breaking critical latitude by ~0.3° of latitude through the EMFC anomaly (P2-P1, orange colour at ~25°S in Figure 2.9e) on the equatorward side of the subtropical jet and EMFD anomaly on its poleward side. The mid-latitude EMFD anomaly and the high-latitudes EMFC anomaly combined induces a positive SAM circulation (Vallis et al. 2004), which further validates the Figure 2.6d result. This subtropical EMFC anomaly and the slight shift of the wave-breaking critical latitude (at around 15°S) induced by negative IPO generally resembles the observation, though there are some mismatches in terms of the magnitude and central locations of EMFC/EMFD anomaly, indicating either there are other factors playing the opposite role as negative IPO in driving the positive SAM or the model has uncertainties reproducing the reanalysis.

On top of the negative IPO induced subtropical warming, the upper-level anomalous EMFC (dark red at ~60°S) with westerly acceleration (magenta line exceeds the black line to the right) in Figure 2.9e would induce equatorward flow (due to the Coriolis force; see Figure 2.9f), while the anomalous EMFD (dark blue at ~45°S) with easterly acceleration would induce a poleward flow (Lim and Hendon 2015). Due to mass conservation, a downward tendency and a narrow adiabatic warming anomaly around 50°S-55°S would result as seen in the middle troposphere of Figure 2.9f. This adiabatic warming would further enhance the mid-to-high latitude meridional temperature gradient, which encourages more eddy generation in the high latitudes, forming positive feedback between the barotropic (wave-breaking) and baroclinic processes (wave-generation), and leading to a more persistent “poleward shifted” eddy-driven jet and positive SAM (Barnes et al. 2010; Nie et al. 2014).

Note that here we focus on a zonal mean perspective, not only because the EMFC co-spectra calculation requires longitudinal cyclicity, but also because the jet shift is largely zonally symmetric in austral summer (Figure 2.4a). However, earlier studies demonstrated that anomalies in the activity of equivalent barotropic Rossby wave trains emanating from the tropical eastern Indian and western Pacific Ocean and propagating to the South Pacific could amplify the SAM response to tropical SST forcing (Lim et al. 2016a; Adames and Wallace 2017; Lim et al. 2019). Figure 2.4a also shows that

the mid-latitude circulation change is not entirely zonally symmetric, as in the South Pacific Ocean it is dominated by a jet intensification rather than a poleward shift. Thus, the metric using zonal mean zonal wind could underestimate the poleward displacement of the main body of the eddy-driven jet.

The poleward displacement of the critical latitude in response to negative IPO is consistent with several previous studies. For example, Tandon et al. (2013) conducted a series of idealized thermal forcing experiments and found that with idealized global warming (their Figure 2d), the mid-latitude meridional temperature gradient increases and the eddy-driven jet shifts poleward; moreover in their Figure 2g, with the subtropical warming anomaly, the Hadley Cell expands and the eddy-driven jet also moves poleward (their Figure 2h), which partly mimics the response to the negative IPO pattern in observations. Similarly, Mantsis et al. (2017) also suggested that the subtropics shifted poleward with an expansion of the Hadley Cell during the early 2000s. In contrast to other studies that focused on the GHG influence, Mantsis et al. (2017) stressed the impact of tropical Pacific SST on the widening, analogous to our arguments that in response to the negative IPO, an expansion of the Hadley cell and a poleward migration of the eddy-driven jet would be induced.

2.5 Discussion and Conclusions

A methodology using the CESM LENS and Pacemaker experiments has been applied to isolate the external forcing signals from the internal tropical SST influence on decadal shifts of the SH eddy-driven jet during austral summer. The pacemaker experiments are nudged separately to observed SSTs in three tropical basins: the tropical central and eastern Pacific, the tropical Indian and western Pacific, and the tropical and north Atlantic. Our work extends on previous studies that focused on the contribution of external forcing to trends in the SH extratropical circulation over the twentieth century, by zeroing in on the decadal differences across the shorter satellite era. In addition, the response to tropical SSTs is further examined for each tropical basin individually. The decadal difference result shows a zonally symmetric poleward shift in the eddy-driven jet, with external forcing and internal variability originating from tropical Pacific SST playing comparably dominant roles, with the tropical & North Atlantic SST and Indian Ocean SST appearing to make a weak and sometimes offsetting contribution. Consistent patterns are found for longer composites over the historical period and preindustrial control simulations.

A dynamical mechanism of external forcing and tropical Pacific SSTAs inducing eddy-driven circulation variations was examined. We found that the poleward shift of the transient eddy

momentum flux convergence could fundamentally explain the poleward migration of the eddy-driven jet from a zonal symmetric perspective. Under the external forcing influence, the mid-latitude EMFC shows a significant poleward migration around 55°S, leading to the southward migration of the eddy-driven jet by ~1° of latitude. In addition to the external forcing component, the importance of tropical Pacific SST has also been demonstrated. During negative IPO, the meridional temperature gradient between the subtropics and the middle latitudes is further increased, resulting in faster speed eddies generated in the higher latitudes, thus leading to the poleward migration of EMFC and eddy-driven jet. In addition, the subtropical EMFD and associated subtropical wave-breaking critical latitude displace poleward for slower eddies during negative IPO, pushing the mid-latitude EMFC and eddy-driven jet further poleward. On top of this tropical-extratropical association, the "poleward shifted" eddy momentum flux convergence/divergence would induce a mid-latitude warming anomaly (around 55°S, Figure 2.9d), also steepening the mid-to-high meridional SST gradient and leading to positive feedback to generate more baroclinic transient eddies, accelerating the westerlies at higher latitudes. Besides, there is also evidence suggesting the feedback of zonal wind and SAM onto the EMFC, for instance, Barnes et al. (2010) found that when the jet is at high latitudes, the wave-breaking critical latitude would move poleward and eddies would break at higher latitudes, which would in turn maintain the positive phase. Via this extratropical eddy-mean flow interaction, the poleward jet movement would be more persistent (Barnes et al. 2010; Nie et al. 2014). The mechanism of external forcing and negative IPO influence on the middle latitude circulation through the enhanced meridional temperature gradient is similar to the impact of global warming on the mid-latitude jet in some previous studies (Chen et al. 2008; Lu et al. 2008). However, there is some weak contribution from the poleward shifted subtropical critical latitude in response to negative IPO, though the subtropical EMFD barely moves, which is different from the La Niña events established by Lu et al. (2008). Here we identify the importance of EMFC analysis in understanding eddy-driven circulation changes to decadal Pacific SST variability.

However, there are some questions that remain to be addressed. First, we note that the eddy-driven jet in the South Pacific region responds somewhat differently to the South Atlantic and South Indian basins. In both the observations and response to tropical Pacific SSTs (Figure 2.4d and Figure 2.8a), the jet experiences an intensification in the South Pacific with a deepened Amundsen Sea Low (ASL), compared to the poleward movement in the South Atlantic and South Indian basins. While previous studies have suggested that the negative IPO could largely explain the deepened ASL in the austral cool seasons, through an anomalous stationary Rossby wave response, similar analysis for the austral summer season leads to a weakened ASL, opposite to that observed (Meehl et al. 2016; Clem et al.

2019). Therefore, further work is needed to understand the zonally asymmetric jet strengthening in the South Pacific basin. Second, the interdependence between the tropical basins exists that makes it difficult to isolate each basin's contribution in a linear way (Cai et al. 2019). For instance, due to the air-sea coupling and inter-basin coupling in the pacemaker runs, the tropical Pacific SSTA forcing can promote a response in other tropical basins that can then force their own teleconnection to mid-latitudes. In fact, teleconnections between three tropical basins have been widely documented (Ashok et al. 2004; Li et al. 2016). Therefore, a linear summation of each coupled component (external forcing and three tropical ocean forcings) could therefore overestimate (or underestimate) the influence of tropical SSTs on extratropical circulation change. Third, the mechanisms by which tropical Indian and Atlantic SSTs influence the SH mid-latitude circulation require further exploration but were limited by data availability and model deficiencies in simulating the inter-basin SST interactions (Cai et al. 2019) in this study. It should also be noted that the estimation of the external forcing influence on the EMFC poleward shift and eddy-driven jet migration could be somewhat member-dependent in magnitude. To best estimate the externally forced signal and to be comparable with previous work using LENS (Solomon and Polvani 2016; Chung et al. 2019; Holland et al. 2019; Zhang et al. 2019), we used all 40 LENS members. Finally, model and SST errors may also play a role. For example, there is a strong link between clouds and the eddy-driven jet (Ceppi et al. 2012; Ceppi and Hartmann 2015) and there are known errors in CMIP5 class models in simulating clouds over the Southern Ocean (Kay et al. 2016).

Our work highlights the combination of external forcing and tropical Pacific SSTs in driving the recent decadal variability of the SH summertime eddy-driven jet, and the physical processes associated with eddy-mean flow interactions through which this has occurred. These findings could have significant implications for decadal prediction of the Southern Hemisphere atmospheric circulation. For instance, the IPO appeared to transition into a positive phase around 2014-2016 (Meehl et al. 2019b), which, along with ozone recovery, might potentially offset the impact of greenhouse gases in driving a poleward shift of the eddy-driven jet over the coming decade.

Chapter 3

The role of coupled feedbacks in the decadal variability of the Southern Hemisphere eddy-driven jet

3 The role of coupled feedbacks in the decadal variability of the Southern Hemisphere eddy-driven jet

Preface:

This chapter is a reproduction of the paper "The role of coupled feedbacks in the decadal variability of the Southern Hemisphere eddy-driven jet", which is under review with *Journal of Geophysical Research - Atmospheres*, with section and figure numbers changed to fit the thesis structure.

Chapter 2 suggested that tropical Pacific decadal variability and external forcings have had a comparable influence on the observed changes in the Southern Hemisphere summertime eddy-driven jet over the satellite era. In this chapter, we examine the zonally asymmetric response of the Southern Hemisphere eddy-driven jet to tropical Pacific decadal variability by designing an atmosphere-only PAC-A experiment using the Community Atmosphere Model version 5 (CAM5) and comparing it with the partially coupled CESM1 tropical Pacific pacemaker experiments. Comparisons between these coupled/uncoupled simulations highlighted the importance of the air-sea coupling in driving the teleconnections between tropical Pacific SST anomalies and South Atlantic-Indian jet variations.

3.1 Introduction

Observational and model studies have shown that the Southern Hemisphere summertime (December-January-February, DJF) eddy-driven jet experienced a poleward shift during the last four decades, along with a positive trend in the Southern Annular Mode (SAM). Along with the dominant impact of Southern Hemisphere stratospheric ozone depletion on these trends, as discussed in previous research (Polvani et al. 2011; Lee and Feldstein 2013; Banerjee et al. 2020), the role of tropical sea surface temperature variations has also recently been emphasized in (Deser and Phillips 2009; Schneider et al. 2015) and Chapter 2. In particular, Chapter 2 examined the separate influence of internally generated decadal variability from tropical Pacific, Indian and Atlantic basin SSTs on the position and strength of the Southern Hemisphere eddy-driven jet. Using the CESM1 pacemaker experiments, in Chapter 2 we found the internally-driven decadal changes of tropical Pacific SSTs (specifically the central and eastern tropical Pacific regions within the solid lines labelled in Figure 3.1c) and external forcing played comparable and dominant roles in the poleward jet shift between the 1979-1998 and 1999-2013 periods, with the tropical and North Atlantic and Indian Ocean SST making only a weak and sometimes offsetting contribution. Therefore, the focus of this chapter is on the dynamical mechanisms regulating the jet response to tropical Pacific SSTs.

In Chapter 2 we found that in both the observations and in response to tropical Pacific SSTs, the summertime eddy-driven jet experiences an intensification in the South Pacific with a deepened Amundsen Sea Low, unlike the poleward movement in the South Atlantic and South Indian basins. These zonal asymmetric jet variations are also described by Waugh et al. (2020) for the DJFMAM seasons, i.e. the South Pacific jet underwent a strengthening in contrast to the latitudinal position change in the South Atlantic-Indian basins. The tropical Pacific - South Pacific teleconnection has been widely discussed in previous studies, for example, Irving and Simmonds (2016) suggested that the interannual to interdecadal tropical SST trends over 1979-2014 can influence the Southern Hemisphere high latitudes and regional Antarctic climate via an anomalous Pacific–South American Rossby wave pattern. Meehl et al. (2016) linked the negative phase of the Interdecadal Pacific Oscillation (IPO) during 2000-2014 to the Ross Sea and Amundsen Sea sea ice changes via a positive phase of the SAM combined with an enhanced Amundsen Sea Low.

By contrast, the tropical Pacific remote impact on the South Atlantic/Indian atmospheric circulation has been less studied and previous work mainly attributes this remote connection to the downstream effect of the Pacific–South American pattern. For instance, Rodrigues et al. (2015) found in response to La Niña events and its induced positive Pacific–South American, a northeast-southwest South

Atlantic SST dipole develops with a warming anomaly around 40°S and cooling anomaly at 20°S. Similar results are attained at the interdecadal time scales, where Lopez et al. (2016) found South Atlantic SST and sea surface height dipole variability is remotely modulated by the IPO via Pacific–South American wave trains.

The strength of using coupled Pacific pacemaker experiments in Chapter 2 is that it allows coupled feedbacks in response to regionally prescribed SSTs, however, these pacemaker simulations cannot separate out the secondary atmospheric teleconnections that arise due to interbasin interactions, particularly between the tropical Pacific and adjacent oceans (Cai et al. 2019). Hence an outstanding question arises: Does tropical Pacific SST impact the jet variation via direct atmospheric pathway or by inducing SST changes in other basins first due to the air-sea coupling?

In Chapter 2 we argue that the South Pacific jet intensification was primarily induced by internal fluctuations from tropical Pacific SST. However, other studies also suggest the South Pacific Convergence Zone (SPCZ) could potentially modulate the South Pacific mid-to-high latitude circulation response to tropical Pacific SST anomaly (Clem et al. 2019; Meehl et al., 2016; Meehl et al., 2019). For example, using atmospheric heating experiments, Meehl et al. (2016) found that for the DJF season, the eastern Pacific cooling would induce a deepened Amundsen Sea Low while the SPCZ warming would lead to a shallowed Amundsen Sea Low instead, with the latter more consistent with observed changes in that season. Consistent results are obtained by Clem et al. (2019) for the DJFMAM season where a 2°C SST anomaly was prescribed over the SPCZ using the CAM5 model. However, both studies used idealised experiments and the separate influence of tropical eastern Pacific and SPCZ SST anomalies on the Southern Hemisphere circulation using realistic SSTs over recent decades has yet to be explored.

There remain questions regarding the mechanism driving the zonal asymmetric South Pacific jet response to the tropical Pacific SST and the importance of coupled feedbacks to the jet response in general. Therefore, two main questions would be addressed in this Lefebvre:

1. What is the role of air-sea coupling in the tropical Pacific SST and Southern Hemisphere eddy-driven jet teleconnections? What is the dynamical mechanism behind the coupling impact?
2. What are the relative influences of tropical eastern Pacific and SPCZ SST anomalies on the Amundsen Sea Low and eddy-driven jet variations?

The rest of this chapter is organized as follows. The model and experimental design are described in Section 3.2. The main results are presented in Section 3.3. A brief summary and discussion are outlined in Section 3.4.

3.2 Model and Experimental Design

In this study, the observed Zonal (U) and meridional (V) winds and mean sea level pressure datasets are taken from the European Centre for Medium-Range Weather Forecasts Interim reanalysis (ERA-Interim; Dee et al. 2011). The monthly SST data is from the National Oceanic and Atmospheric Administration (NOAA) Extended Reconstruction Sea Surface Temperature, version 3b (ERSSTv3b, Smith et al. 2008).

The fully-coupled CESM1 40-member Large Ensemble (LENS) and 10-member Pacific pacemaker (PAC-C) experiments are identical to those employed in Chapter 2, with LENS used to estimate the impact of external forcing, and PAC-C (with external forcing removed, i.e., PAC-C minus LENS) reflecting the influence of internally-driven tropical Pacific SST on the jet. Another two uncoupled simulations, PAC-A and extSPCZ-A, are designed to further separate the direct atmospheric teleconnection from tropical Pacific SST to the Southern Hemisphere jet (see Table 3-1).

Table 3-1 Summary of the CESM and CAM5 experiments used in Chapter 3.

Experiments	external forcing	SST forcing	coupling	members
Large Ensemble (LENS)	Historical for 1920-2005, RCP8.5 for 2006-2013	—	√	40
Pacific Pacemaker (PAC-C)	Same as LENS, except with SPARC ozone	Fully-restored SSTA for 15°S-15°N, 175°W to the American coast.	√	10
PAC-A	Same as PAC-C	PAC-C SST for **15°S-15°N,** 165E° to the American coast; LENS SST outside eastern Pacific.	×	10
extSPCZ-A	Same as PAC-C	PAC-C SST for **35°S-15°N**, 165E° to the American coast; LENS SST outside eastern Pacific.	×	10

The CESM Large Ensemble is generated by a small perturbation to the initial atmospheric temperature field at the beginning of the simulations in 1920, which then develops into a diverse

spread and produces 40 different realizations of intrinsic climate variability. All LENS ensemble members are constrained to the same radiative forcing scenario (Taylor et al. 2012), with historical forcing during 1920-2005 and a high emission forcing scenario of the Representative Concentration Pathway (RCP) 8.5 (Moss et al. 2010) from 2006 to 2080 following the Coupled Model Intercomparison Project Phase 5 (CMIP5) design protocol. The LENS 40-member ensemble mean then averages out this random internal variability and reflects the impact of external radiative forcings on the climate system.

All the experiments listed in Table 3-1 use the same CESM1 code base and time-varying radiative forcing as the LENS, apart from a minor difference in ozone forcing. While the LENS uses the Whole Atmosphere Community Climate Model (WACCM, Marsh et al. 2013) ozone dataset (see Kay et al. 2015), the PAC-C and uncoupled runs are forced with the Stratosphere-Troposphere Processes and their Role in Climate (SPARC) stratospheric ozone data (Cionni et al. 2011). However, according to Schneider and Deser (2017), the ozone forcing differences have statistically indistinguishable impacts on the trends in the Southern Hemisphere eddy-driven jet over the satellite era.

In the coupled pacemaker experiment (PAC-C), the SSTs in the tropical eastern Pacific are restored to the model climatology plus observed SST anomalies using a nudging technique (Kosaka and Xie 2013). Specifically, the SST anomalies between 15°S-15°N, 175°W to the American coast (shown as solid black lines in Figure 3.1c), are nudged to the observed SST anomalies from NOAA ERSSTv3b. There are three buffer belts along 15°S-20°S, 15°N-20°N and 175°W-180° (dashed black lines in Figure 3.1c), where the SST anomalies are linearly tapered to zero. In this way, as described in Chapter 2, the PAC-C contains both the radiatively forced and internally-driven variability from observed tropical Pacific SSTs. Subtracting LENS from PAC-C then removes the externally forced signal and provides an estimate of the response of the global climate system to the observed time-varying internally-generated tropical Pacific SSTs.

However, in the coupled PAC-C where the SST anomalies over the eastern Pacific region are nudged to observations and the rest of the model is free to evolve (Table 3-1 and Figure 3.1c), the tropical Pacific SST forcing promotes an SST response in other regions, which can then force a secondary teleconnection and influence the mid-latitude jet. This means in the PAC-C set, the tropical Pacific SST can influence the jet in two ways, one is via a direct atmospheric impact, the other is via the Pacific inducing SST changes in adjacent ocean basins first, and then having a secondary impact on the jet.

To remove the compounding effects of Pacific coupling to other ocean basins, an atmosphere-only simulation (hereafter denoted PAC-A) is designed to compare with the PAC-C. This uncoupled PAC-A experiment is intended to match the coupled PAC-C in every way, apart from the inclusion of coupling outside of the tropical Pacific region. The PAC-A runs use the same atmospheric model (CAM5) as in the PAC-C and are subjected to identical external forcing. The PAC-A SST forcing in the tropical eastern Pacific region is prescribed using the time-evolving PAC-C SSTs (i.e., model climatology plus observed anomalies) from 165°E to the American coast. The western boundary of this prescribed region (solid box in Figure 3.1d) is extended by 20-degree west to 165°E, compared to the nudged region in the PAC-C (solid box in Figure 3.1c) experiment which stops at 175°W. This extended region better mimics the coupled PAC-C experiment which naturally extends the anomalies related to tropical eastern Pacific oscillations (such as the IPO and El Niño–Southern Oscillation (ENSO)) to the west of the nudged region due to coupled air-sea dynamics.

Outside of the tropical Pacific, the time-evolving LENS 40-member ensemble mean SST is imposed. In this way, the PAC-A 10-member ensemble mean with external forcing removed (i.e., PAC-A minus LENS) isolates the direct atmospheric influence of tropical Pacific SST on the Southern Hemisphere atmospheric circulation which is of interest here.

Another uncoupled experiment (hereafter named extSPCZ-A), with PAC-C SSTs applied over 35°S-20°N, 165°E to the American coast (Figure 3.1e), is also performed to further investigate the relative role of observed tropical eastern Pacific and SPCZ SST anomalies. Since PAC-A and extSPCZ-A are identical except for the expanded nudged region, comparisons between extSPCZ-A and PAC-A distinguishes the impact of the SPCZ SST variations on the atmospheric teleconnection patterns in the SH mid-to-high latitudes.

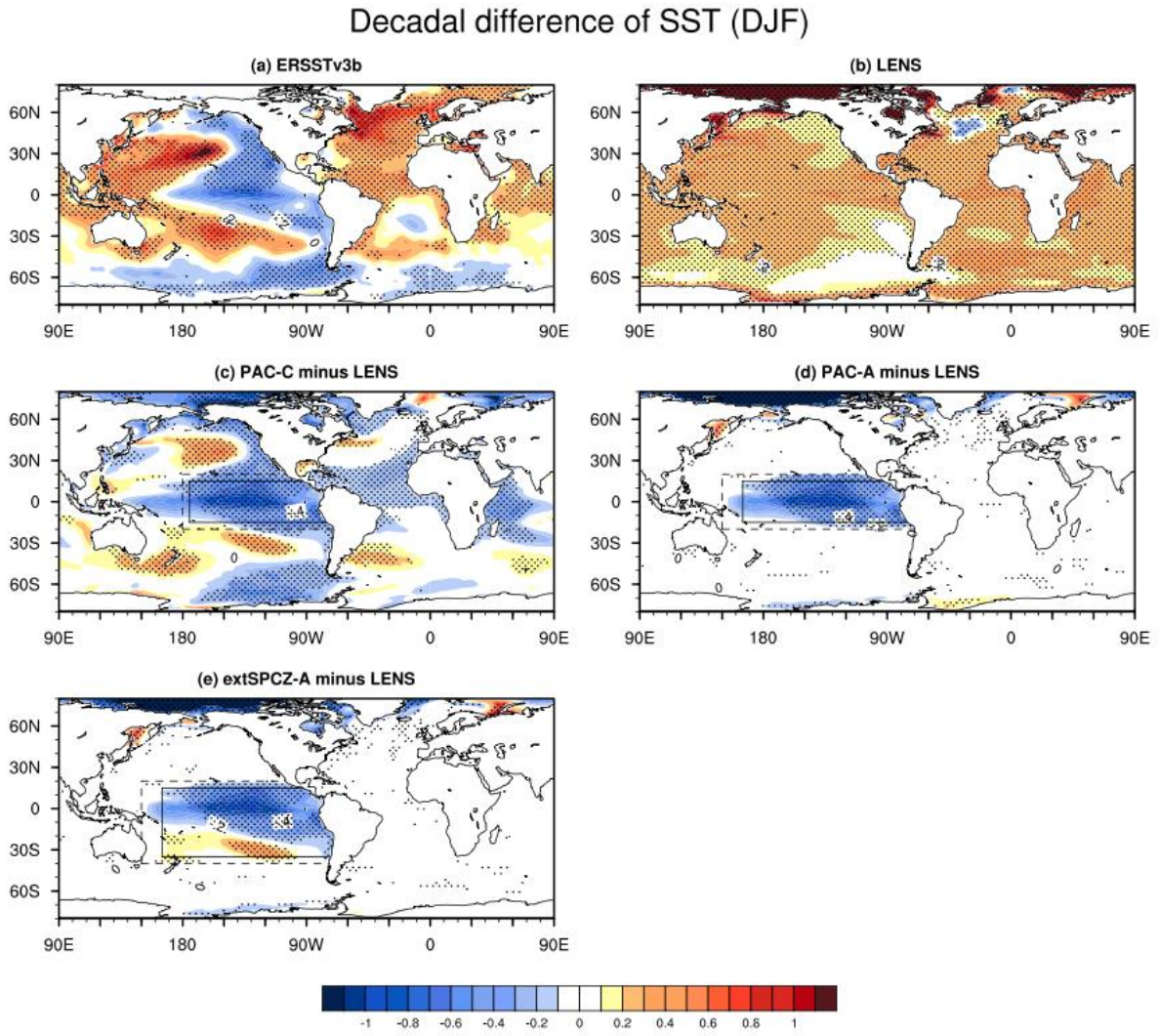

Figure 3.1 The decadal difference between averaged P2 (1999-2013) and P1 (1979-1998) for sea surface temperature (units: K) in the DJF season. (a) ERSSTv3b; (b) CESM Large Ensemble mean (LENS), indicative of external forcing; (c) Pacific pacemaker ensemble-mean (PAC-C) minus LENS; (d) PAC-A ensemble-mean minus LENS; (e) extSPCZ-A ensemble-mean minus LENS. Stippling indicates differences are significant at the 95% level based on a t-test. In panel (c) - (e), within the solid black lines, the SSTs are nudged to the model climatology plus observed anomalies; between the solid and the dashed lines are the buffer belts where the nudging is linearly tapered to zero; outside of the dashed lines, the SSTs are free to evolve in PAC-C but prescribed with LENS SST in PAC-A and extSPCZ-A.

3.3 Results

3.3.1 Tropical Pacific pacemaker and PAC-A comparison

Based on the IPO phase transition (positive to negative) around 1999, we separate the satellite era into two periods 1980-1998 (P1) and 1999-2013 (P2). Figure 3.1 shows the decadal difference (P2 average minus P1 average) of SST for observations and model simulations. In the tropical eastern

and central Pacific, the observations, PAC-C and PAC-A SST all show large cooling anomalies, which is typical of the negative phase of the IPO (Figure 3.1a/1c/1d). Outside of this region, the coupled pacemaker response is a result of (1) the atmospheric response to the nudged tropical Pacific SST and (2) the secondary impact from SST anomalies in other basins, that have evolved in response to the tropical Pacific SSTs. Specifically, in PAC-C minus LENS (Figure 3.1c), the eastern Pacific cooling promotes a warming anomaly over the SPCZ and the South Atlantic Convergence Zone. This is consistent with Clem et al. (2019) who argued that cooling in the eastern Pacific can induce a warming anomaly in the SPCZ region as part of the negative IPO pattern. The negative IPO induced South Atlantic warming anomaly in Figure 3.1c is also consistent with Lopez et al. (2016) in terms of the decadal teleconnections between the negative IPO and South Atlantic SST changes. By contrast, PAC-A isolates the direct atmospheric impact of tropical Pacific SST anomalies alone.

In terms of summertime variations, a poleward shift of the eddy-driven jet is observed in the Atlantic and Indian basins and an in-place intensification over the Pacific basin (Figure 3.2a). As discussed in Chapter 2, the external forcing (Figure 3.2b) drives an annular poleward displacement of the eddy-driven jet, with the largest impact in the South Atlantic basin. Internal variability in tropical Pacific SST, on the other hand, contributes to both the poleward shift of the South Atlantic-Indian jet as well as the strengthening of the South Pacific jet (Figure 3.2c, PAC-C with external forcing removed). The distinct zonally asymmetric jet strengthening at 45°S in the South Pacific basin is reproduced in the PAC-A experiment (Figure 3.2d, with external forcing removed). However, the PAC-A experiment fails to capture the poleward displacement of the jet over the South Atlantic-Indian basins, exhibiting non-significant weakening over the Atlantic-Indian sector. Differences between the uncoupled PAC-A and coupled PAC-C implies that the influence of tropical Pacific SST on South Pacific jet intensification is mainly via atmospheric processes. It is also clear that for the teleconnections between the tropical Pacific SST and South Atlantic-Indian jet variations, air-sea coupling is critical since the observed poleward shift of the jet in those basins is only reproduced in the coupled PAC-C experiment.

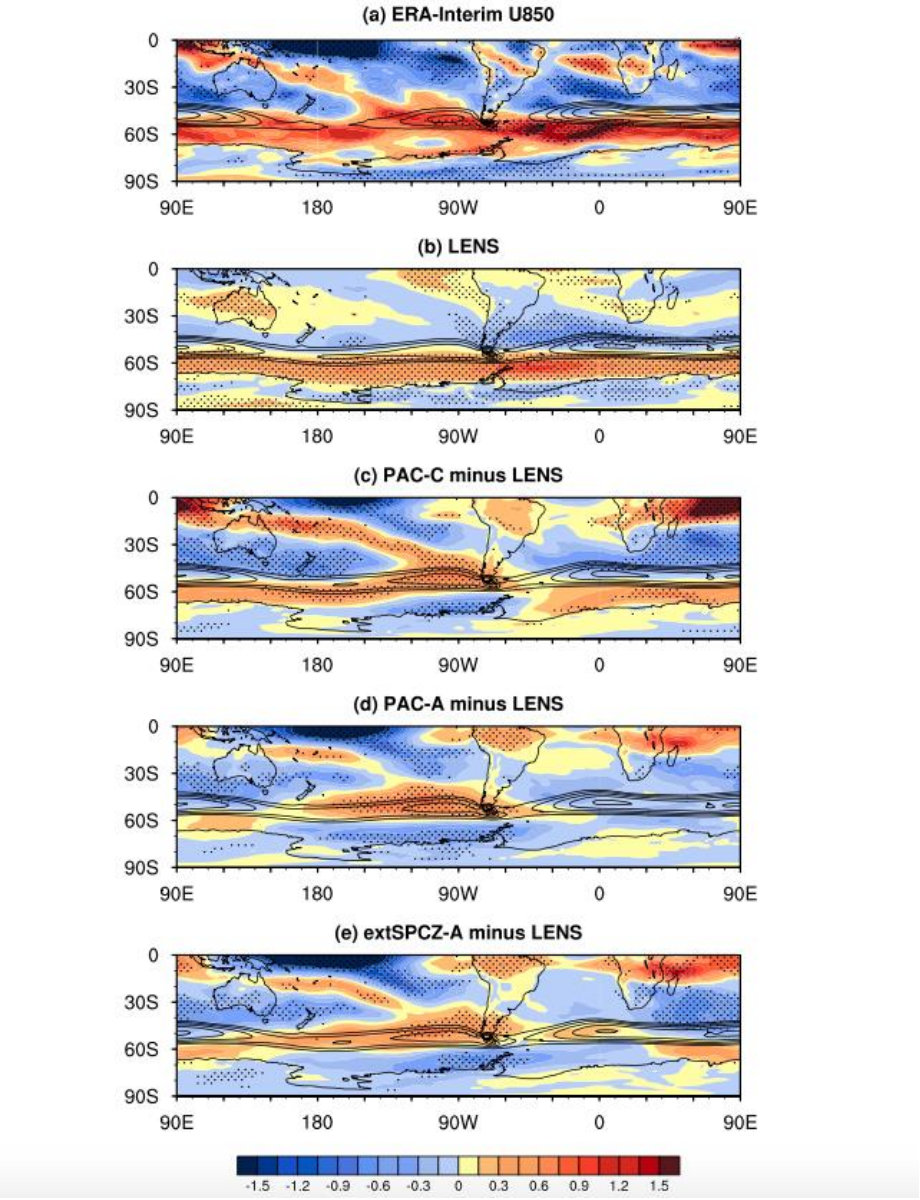

Figure 3.2 The decadal difference between averaged P2 (1999-2013) and P1 (1980-1998) for 850 hPa zonal wind (units: m/s) in the DJF season. (a/ ERA-Interim; (b) LENS; (c) PAC-C minus LENS; (d) PAC-A minus LENS; (e) extSPCZ-A minus LENS. The black contours indicate climatological jet distribution (10-20 m/s with 1 m/s intervals) averaged over 1980-2013 in observation for (a) and in each model simulation for (b)-(e). Stippling indicates differences significant at the 90% level for (a) and 95% level for all other panels, based on a t-test.

These zonally asymmetric results are also found in the sea level pressure field. In the South Atlantic-Indian sector a positive SAM phase is observed, with a high-pressure anomaly at 40°S and low-pressure anomaly along 65°S (Figure 3.3a). This pattern is simulated in the PAC-C experiment (Figure 3.3c), consistent with a poleward displacement of the jet. In contrast, PAC-A exhibits a non-significant negative SAM-like pattern with weakened jet, largely diverging from the observations, which again indicates that coupling is important to establish the teleconnections between the tropical

Pacific and the South Atlantic-Indian basin. In the South Pacific basin, the deepened Amundsen Sea Low and 30°S high-pressure anomaly is well captured in both the PAC-C and PAC-A experiments.

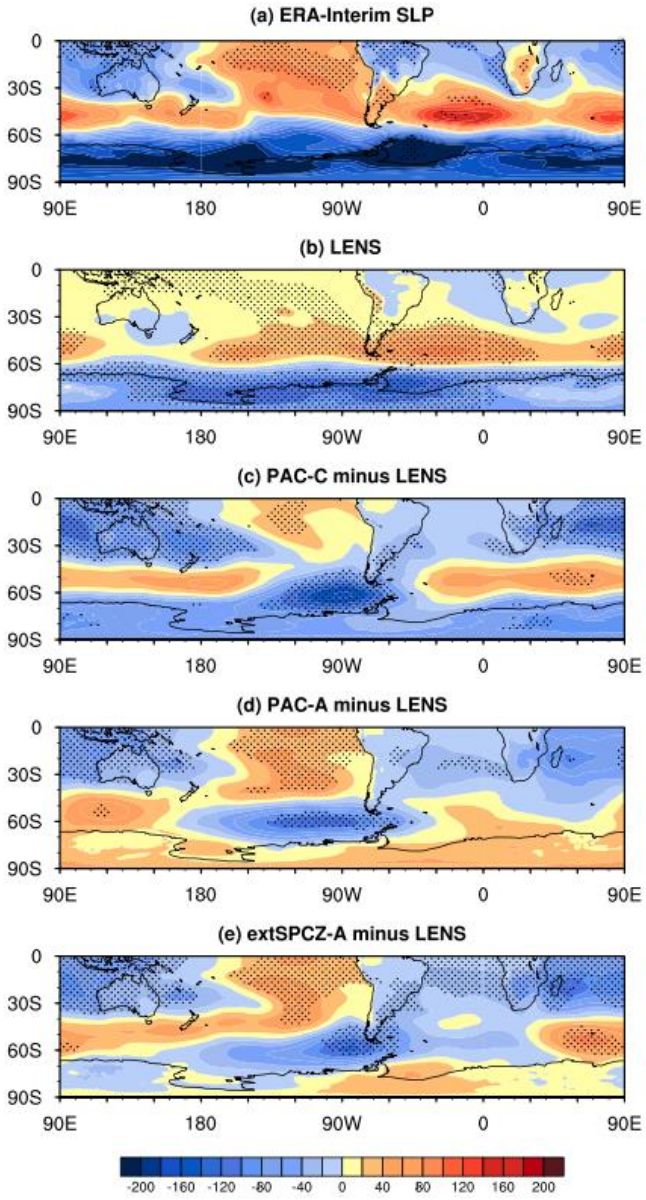

Figure 3.3 The decadal difference between averaged P2 (1999-2013) and P1 (1980-1998) for sea level pressure (units: Pa) in the DJF season. (a) ERA-Interim; (b) LENS; (c) PAC-C minus LENS; (d) PAC-A minus LENS; (e) extSPCZ-A minus LENS. Stippling indicates differences significant at the 95% level based on a t-test.

This tropical-extratropical teleconnection within the Pacific basin is also detected in the other three seasons. In the reanalysis, the largest decadal trend of the South Pacific jet has occurred during the MAM season (Schneider et al. 2015), with significant enhancement over 40-50°S, 170°E-70°W. In accordance with this strengthened South Pacific jet during austral autumn, a deepened Amundsen Sea Low has also been observed (not shown). This trend is largely reproduced by the PAC-A (with external forcing removed, Figure 3.4c), highlighting the role of the direct atmospheric pathway in this

tropical Pacific-South Pacific teleconnection (the SST differences in MAM are similar to DJF, not shown). This builds on Schneider et al (2015), who attributed the South Pacific changes in MAM to tropical SSTs using experiments with CAM4, by narrowing the attribution to tropical Pacific SSTs specifically. By contrast, the South Pacific jet strengthening in austral autumn is not well captured by the coupled PAC-C ensemble mean (with external forcing removed, Figure 3.4b), indicating that air-sea coupling might induce other secondary circulation changes that offset the Rossby wave propagation from the central equatorial Pacific to the Amundsen Sea Low.

In the austral winter-spring seasons (June-July-August, JJA, and September-October-November, SON), the observed South Pacific eddy-driven jet exhibits an equatorward shift, with the peak westerly increase centred at 40-45°S, where both the PAC-A and PAC-C ensemble mean captures this pattern. The South Pacific jet strengthening during DJF-MAM, as well as the equatorward displacement during JJA-SON, are in agreement with Waugh et al. (2020), who suggest that the westerly trends in JJA-SON are largely due to the internal variability since the reanalysis fall within the ensemble spread for historical climate model simulations. Based on our PAC-A results, we further find that the South Pacific westerly variation in all seasons is mainly induced by direct atmospheric teleconnections from tropical Pacific SST anomalies. In the non-summer seasons, the South Atlantic-Indian jet exhibits less uniform changes in both intensity and position compared to the DJF season, and neither PAC-C nor PAC-A can fully reproduce the South Atlantic-Indian jet variation, indicating there are other factors beyond tropical Pacific SST anomaly that drive the South Atlantic-Indian jet changes outside of the summertime.

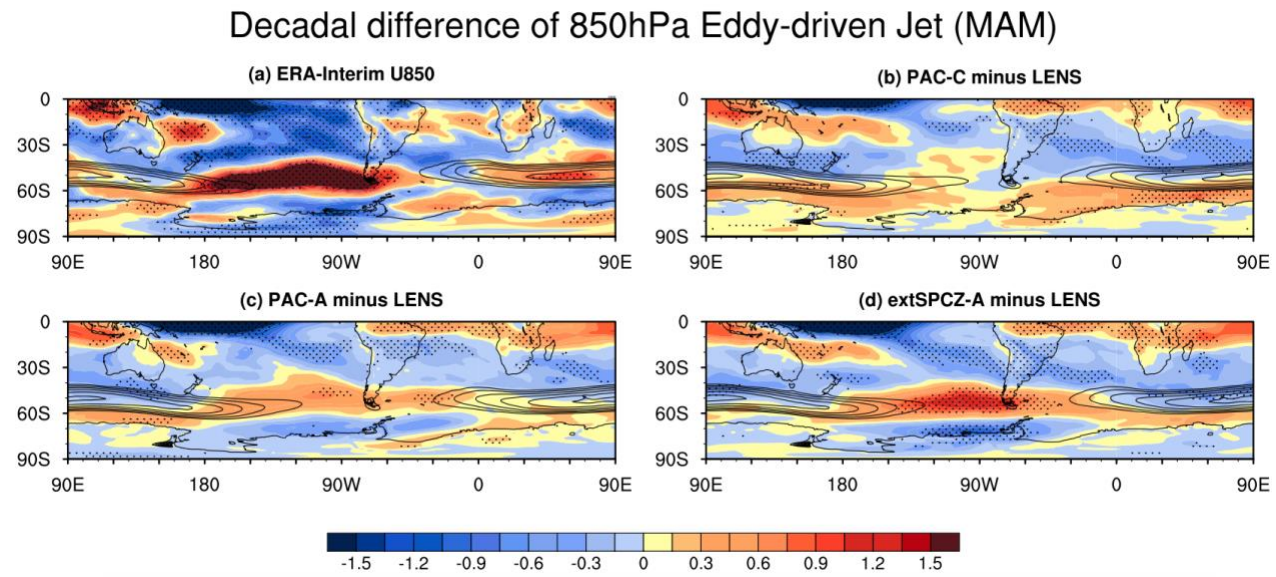

Figure 3.4 The decadal difference between averaged P2 (1999-2013) and P1 (1979-1998) for 850 hPa zonal wind (units: m/s) in **MAM** season. (a) ERA-Interim; (b) PAC-C minus LENS; (c) PAC-A minus LENS; (d) extSPCZ-A minus LENS. Stippling indicates differences are significant at the 90% level for (a) and 95% level for all other panels, based on a t-test.

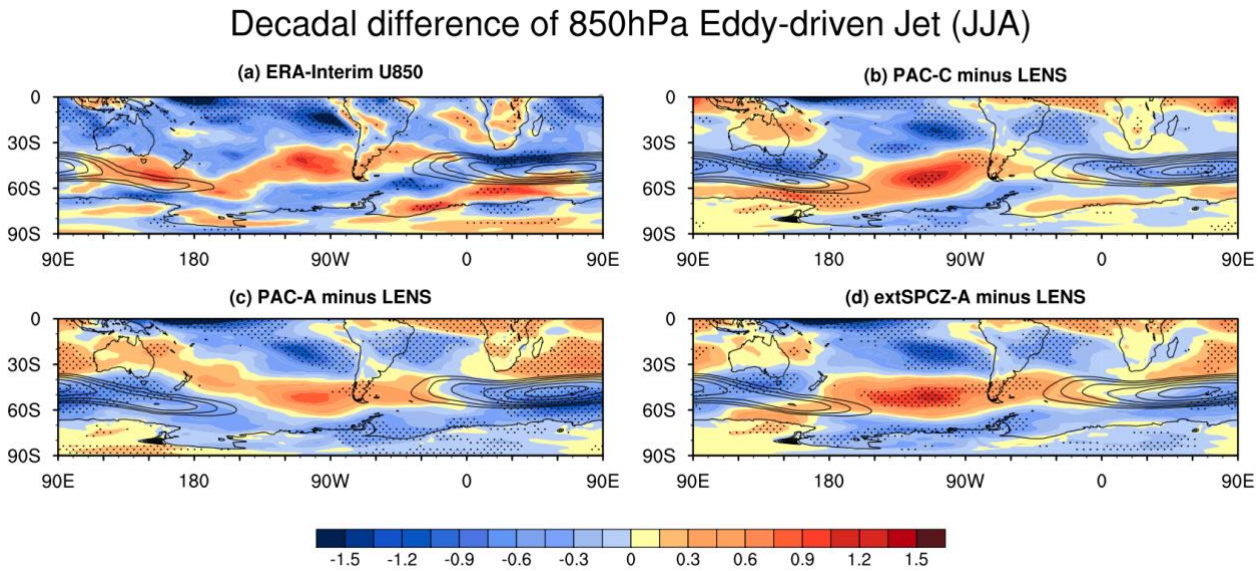

Figure 3.5 The decadal difference between averaged P2 (1999-2013) and P1 (1979-1998) for 850 hPa zonal wind (units: m/s) in **JJA** season. (a) ERA-Interim; (b) PAC-C minus LENS; (c) PAC-A minus LENS; (d) extSPCZ-A minus LENS. Stippling indicates differences are significant at the 90% level for (a) and 95% level for all other panels, based on a t-test.

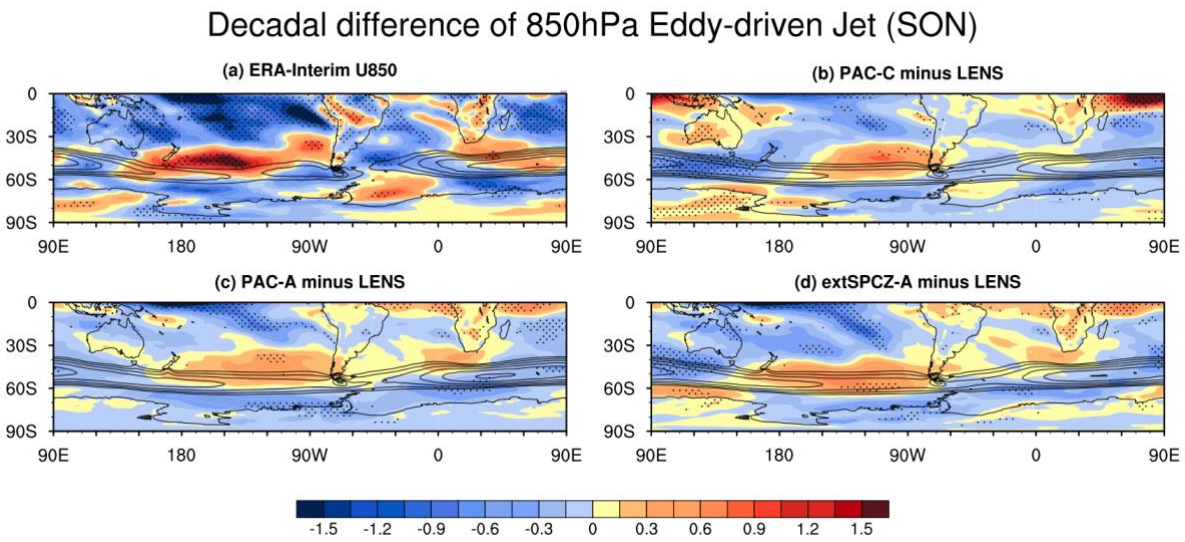

Figure 3.6 The decadal difference between averaged P2 (1999-2013) and P1 (1979-1998) for 850 hPa zonal wind (units: m/s) in **SON** season. (a) ERA-Interim; (b) PAC-C minus LENS; (c) PAC-A minus LENS; (d) extSPCZ-A minus LENS. Stippling indicates differences are significant at the 90% level for (a) and 95% level for all other panels, based on a t-test.

3.3.2 PAC-A and extSPCZ-A comparison

Differences between the PAC-A and PAC-C in the South Atlantic-Indian jet simulations indicate that tropical Pacific SSTs could influence the Southern Hemisphere jet by modifying SSTs outside this region which then induce atmospheric teleconnections. Based on Figure 3.1c, the eastern Pacific SST cooling develops a warming belt in the Southern Hemisphere subtropical area in each basin, including the SPCZ, South Atlantic and Indian convergence zones. Previous studies (Meehl et al. 2016; Clem et al. 2019) suggest that SPCZ warming shallows the Amundsen Sea Low in the DJF-MAM seasons, playing an opposite role to eastern Pacific SST cooling.

Accordingly, another experiment is conducted to further investigate the relative roles of eastern Pacific SST cooling and its provoked SPCZ warming. Comparison between extSPCZ-A and PAC-A (Figure 3.2 and Figure 3.7e) shows little difference in the South Pacific jet variations during austral summer, which suggests that the eastern Pacific cooling is the main driver of the South Pacific jet strengthening, and that contributions from the SPCZ warming are rather small. Similar relations can be found in the other three seasons (Figure 3.4 - Figure 3.6). The extSPCZ-A captures a slight poleward displacement of the South Indian jet during DJF, which is in better agreement with the PAC-C results than PAC-A, suggesting that SPCZ warming may be important to enable the tropical Pacific SST influence on the South Indian jet variations. However, in the South Atlantic basin, neither

PAC-A nor extSPCZ-A reproduce the southward movement in the jet that can be seen in observations and in the PAC-C.

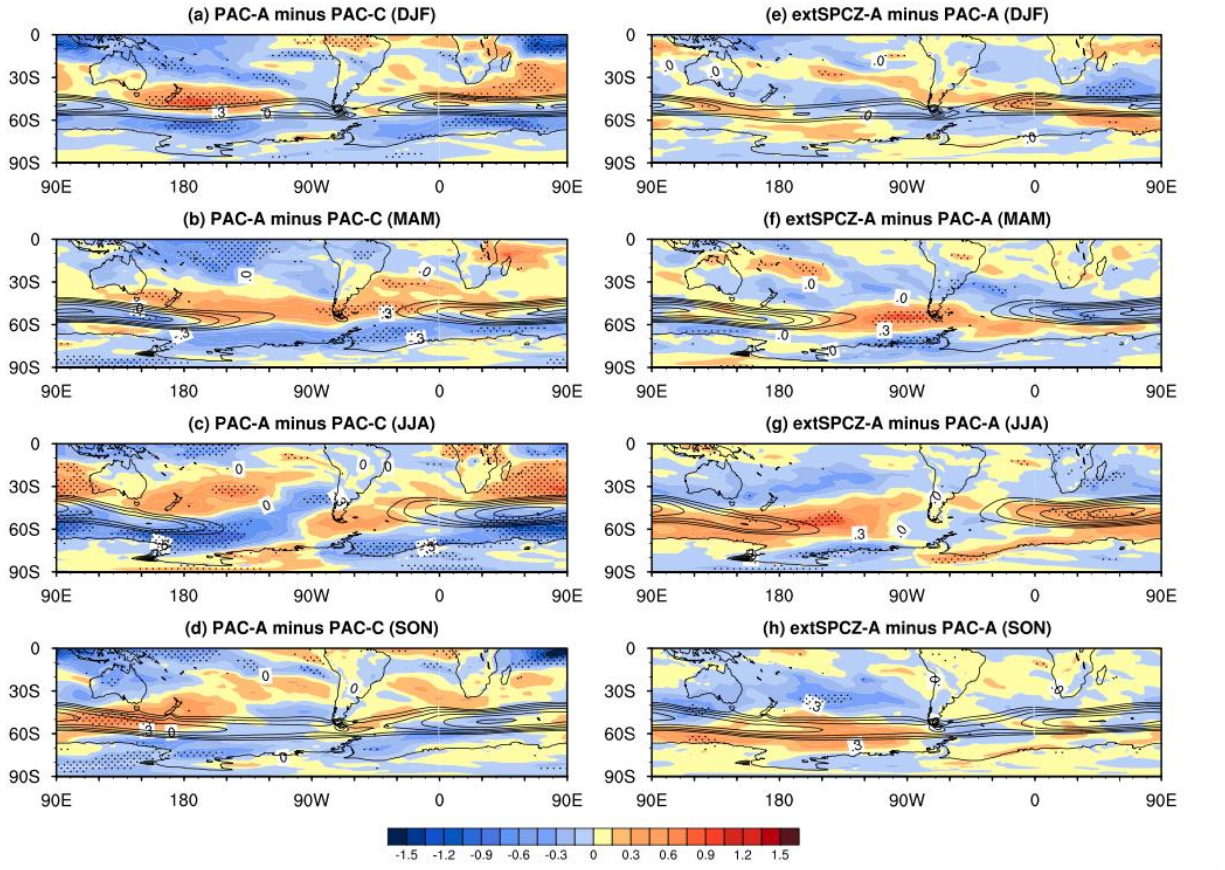

Figure 3.7 The decadal difference between averaged P2 (1999-2013) and P1 (1980-1998) for 850 hPa zonal wind (left, unit: m/s) in (a/e) DJF, (b/f) MAM, (c/g) JJA, and (d/h) SON season. The left panel is PAC-A minus PAC-C; the right panel is extSPCZ-A minus PAC-A. Stippling indicates differences are significant at the 95% level based on a t-test.

3.4 Mechanisms

3.4.1 Poleward propagation of Rossby waves

Early studies imply that tropical Pacific SSTs can impact the extratropical circulation via the poleward propagation of stationary Rossby waves (Hoskins & Karoly, 1981), and recent work further suggests the SPCZ SST anomaly as an additional hotspot for Rossby wave sources (Lopez et al. 2016; Clem et al. 2019). Here we examine this teleconnection at the decadal timescales in the uncoupled runs and compare with the coupled PAC-C to identify the role of air-sea coupling.

For the observed SST decadal difference, there is a cooling of the central tropical Pacific SST as noted earlier (Figure 3.1a), which leads to reduced precipitation with descending air (Figure 3.8a, the largest negative values occur on and just south of the Equator, at around 150°E), and more outgoing longwave radiation (OLR) over that same area (Figure 3.8b). The positive OLR anomaly coincides with an upper troposphere horizontal convergence in the central Pacific (negative geopotential height anomaly at 200 hPa, Figure 3.8c). Mirroring the tropical Pacific cooling, there is also significant warming over the SPCZ near 30°S. This region shows opposite tendencies compared to the tropical central Pacific, with enhanced rainfall, less OLR and a positive 200 hPa geopotential height anomaly. These two centres (central Pacific cooling and SPCZ warming), both act as Rossby wave sources for the extratropics (Clem et al., 2019), driving a positive geopotential height anomaly at around 40° S and a negative tendency along 65° S at 200 hPa (Figure 3.8c). Since the mid-latitude atmospheric circulation is equivalent barotropic, at the surface level the observed Southern Hemisphere circulation response (with external forcing included) also shows positive sea level pressure anomalies over mid-latitudes and negative sea level pressure anomalies along high-latitudes, resulting in a positive SAM phase (Figure 3.3a).

The PAC-C (with external forcing removed) captures most features in the observations, with a cooling SST anomaly, associated decreased rainfall, positive OLR and upper-level convergence in the central Pacific, as well as a warming SST anomaly, enhanced rainfall, negative OLR and upper-level divergence over the SPCZ (Figure 3.8d-f). However, the Rossby wave train produced by the PAC-C (external forcing removed) is more prominent and zonally asymmetric compared to observations, with distinct low-high geopotential height fluctuations propagating from the tropical Pacific to the subtropical South Atlantic via South America, forming a clear Pacific–South American Rossby wave pattern (Figure 3.8f). This suggests a strong role for internally driven tropical Pacific SST variability in driving the asymmetric component of the observed response.

To better depict the evolution of the Pacific–South American pattern, here we examine the Rossby wave activity flux, which can be used to diagnose the propagation of stationary wave energy on a zonal background flow. Following (Wang et al. 2019), we calculate the horizontal component of the Rossby wave flux on the 200 hPa, as:

$$W = \frac{1}{2|\bar{U}|}\begin{bmatrix}\bar{u}(\psi_x'^2 - \psi'\psi_{xx}') + \bar{v}(\psi_x'\psi_y' - \psi'\psi_{xy}'^2) \\ \bar{u}(\psi_x'\psi_y' - \psi'\psi_{xy}') + \bar{v}(\psi_y'^2 - \psi'\psi_{yy}'^2)\end{bmatrix} \quad (3\text{-}1)$$

where x represents the latitudinal component and y indicates the longitudinal component. $\bar{\boldsymbol{U}} = (\bar{u}, \bar{v})$ is the background wind field; and ψ' is the streamfunction anomaly. The zonal background flow is the DJF wind climatology over 1980-2013.

In the reanalysis, the wave activity flux emanates from the central subtropical Pacific as well as to the east of Australia and propagates poleward to the South Atlantic basin. In PAC-C, in response to the tropical Pacific cooling at the Equator (i.e. negative IPO), there is an outflow of the stationary wave activity flux originating from 15-20°S, 120°W, co-located with a low-pressure anomaly (cyclonic tendency) at upper levels. This wave activity flux propagates poleward and eastward towards the Antarctic Peninsula and circulates back to the tropics in the South Atlantic basin following a great circle track, which corresponds with the Pacific–South American wave train (Fig Figure 3.8f). The wave activity flux in PAC-C is more prominent following the Pacific–South American track compared to observations, with the latter including the externally-forced response – not just the negative IPO.

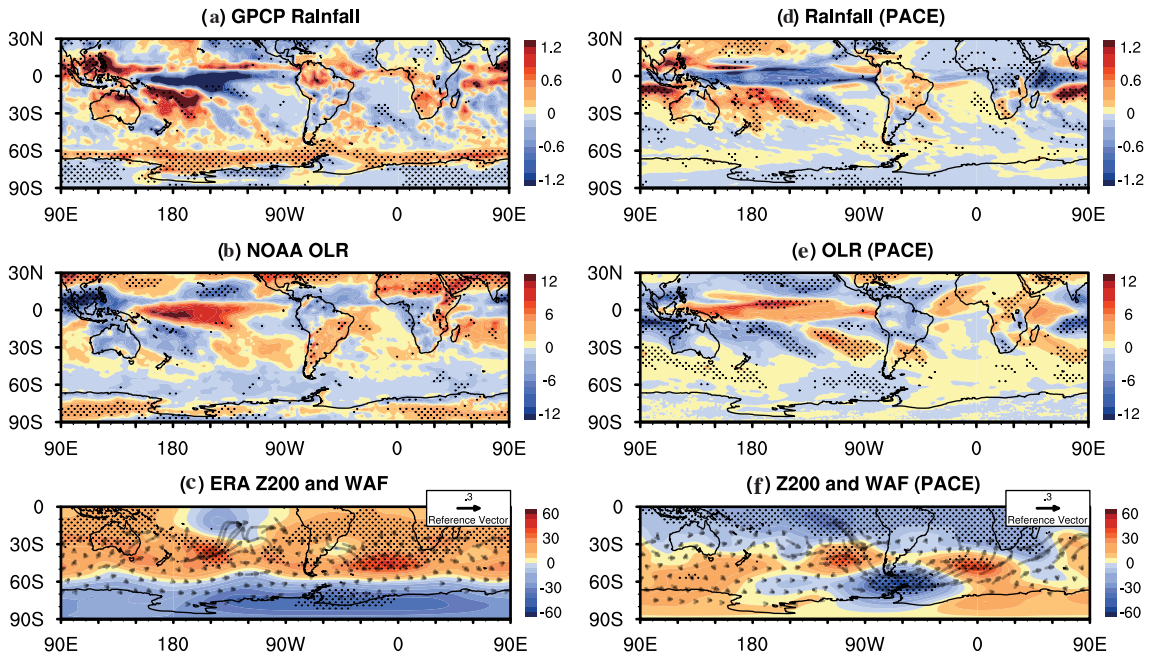

Figure 3.8 Decadal difference (P2-P1) for observations/reanalysis (left) and the PAC-C (right) in the DJF season. (a) GPCP rainfall (mm/day); (b) NOAA Outgoing Longwave Radiation (OLR, 10^{-2}W/m^2); (c) ERA-Interim 200 hPa geopotential height (m) and wave activity flux (WAF, vectors, m^{2}s^{-2}).). (d)-(f): same as in (a)-(c), but for the PAC-C minus LENS except for wave activity flux in (f) where LENS is not subtracted to study the wave propagation on a climatological zonal background flow. Stippling indicates differences are significant at the 95% level based on a t-test.

The PAC-A (external forcing removed) reproduces the observed rainfall and OLR anomalies in the tropical Pacific. The 200 hPa geopotential height field displays a mid-latitude anticyclonic anomaly and deepened Amundsen Sea Low in the South Pacific basin, aligned with the wave activity flux, which travels southeastward toward the southern tip of South America, and then dissipates after turning around the south of South America (Figure 3.9c). In other words, the Pacific–South American

turning around the south of South America (Figure 3.9c). In other words, the Pacific–South American pattern and the wave activity flux in PAC-A is well resolved within the South Pacific basin but vanishes upon entering the South Atlantic region. Comparisons between PAC-A and PAC-C thus highlight the importance of coupling in the Rossby wave propagation and in maintaining the tropical Pacific- South Atlantic-Indian teleconnections.

The combined impact of tropical Pacific cooling and SPCZ warming (Figure 3.9f) exhibits a similar Rossby wave pattern to PAC-A in the South Pacific basin, although the deepened low shifts slightly east from the Ross Sea (in PAC-A) to the Amundsen Sea (in extSPCZ-A), which is in closer agreement with the PAC-C simulations. The wave activity flux in the mid-latitude South Pacific shows similar results, with comparable southeastward flow as in the PAC-C, but the magnitude of the wave activity flux in the South Atlantic is much reduced. In the South Indian basin, the positive SAM-like pattern is better captured in extSPCZ-A, indicating SPCZ warming could be bridging the teleconnections between tropical SST anomaly and South Indian jet variations. This additive influence of tropical Pacific cooling and SPCZ warming on the Amundsen Sea Low seems to be contrary to Clem et al. (2019) suggesting that during the DJFMAM season, the SPCZ warming plays an opposite role to the eastern Pacific cooling by shallowing the Amundsen Sea Low. However, in our work, we find that the summertime Amundsen Sea Low longitudinal location is improved with SPCZ but its intensity does not vary much with/without SPCZ warming. Another potential source of this difference is that Clem et al. (2019) imposes a fixed +2°C SST anomaly over the south-west SPCZ region, instead of the observed SST anomaly across the whole basin used in this study. Aside from these differences in region, if the combined impact of SPCZ warming and tropical Pacific cooling is not linearly additive, this could cause a significant difference from the observations.

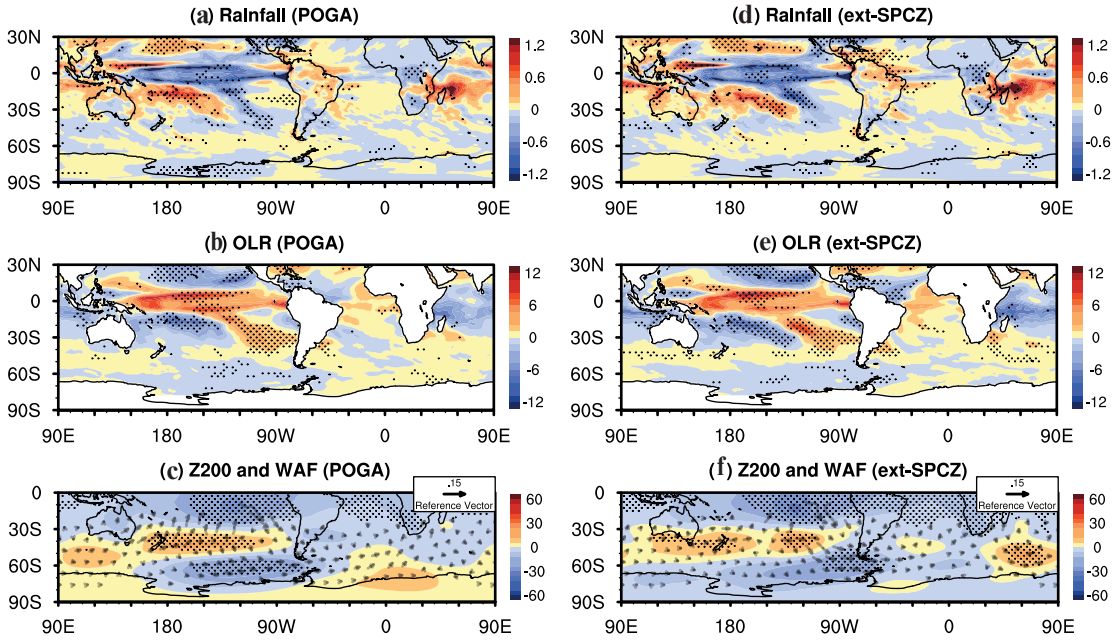

Figure 3.9 Decadal difference (P2-P1) for PAC-A minus LENS (left) and extSPCZ-A minus LENS (right) simulations in the DJF season. (a/d) rainfall(mm/day); (b/e) Outgoing Longwave Radiation (OLR, 10^{-2}W/m^2); (c/f) 200 hPa geopotential height (m) and wave activity flux (vectors, m^{2}s^{-2}). For wave activity flux in (c/f), LENS is not removed to study the wave propagation on a climatological zonal background flow. Stippling indicates differences are significant at the 95% level based on a t-test.

3.4.2 Eddy-mean flow interactions

In Chapter 2 the influence of tropical Pacific SST on the zonal-mean westerlies was explained via the meridional temperature contrast and associated transient eddy-mean flow interactions. In that study, it was found that in both observations and the coupled pacemaker, a significant air temperature warming anomaly could be found throughout the troposphere at 45°S in response to anomalously cool tropical Pacific SSTs, which then lead to an enhanced meridional temperature gradient, increased near-surface baroclinity, more transient eddy generation at high latitudes and a poleward shifted eddy-driven jet.

We also examine the air temperature distribution in the uncoupled experiments (Figure 3.10), but instead of zonal mean metrics as analysed in Chapter 2, here we examine the South Pacific and Atlantic-Indian basins separately, given our focus on the jet's zonally-asymmetric variations. In the South Pacific basin, both PAC-A and extSPCZ-A reproduce a significant warming anomaly throughout the troposphere as in the PAC-C, although with a diminished magnitude (Figure 3.10c-d). As a consequence of the enhanced meridional temperature contrast at around 50°S, more transient

eddies would be generated at high latitudes, which could be potentially related to the substantial jet intensification in the South Pacific basin in both observations and all model simulations.

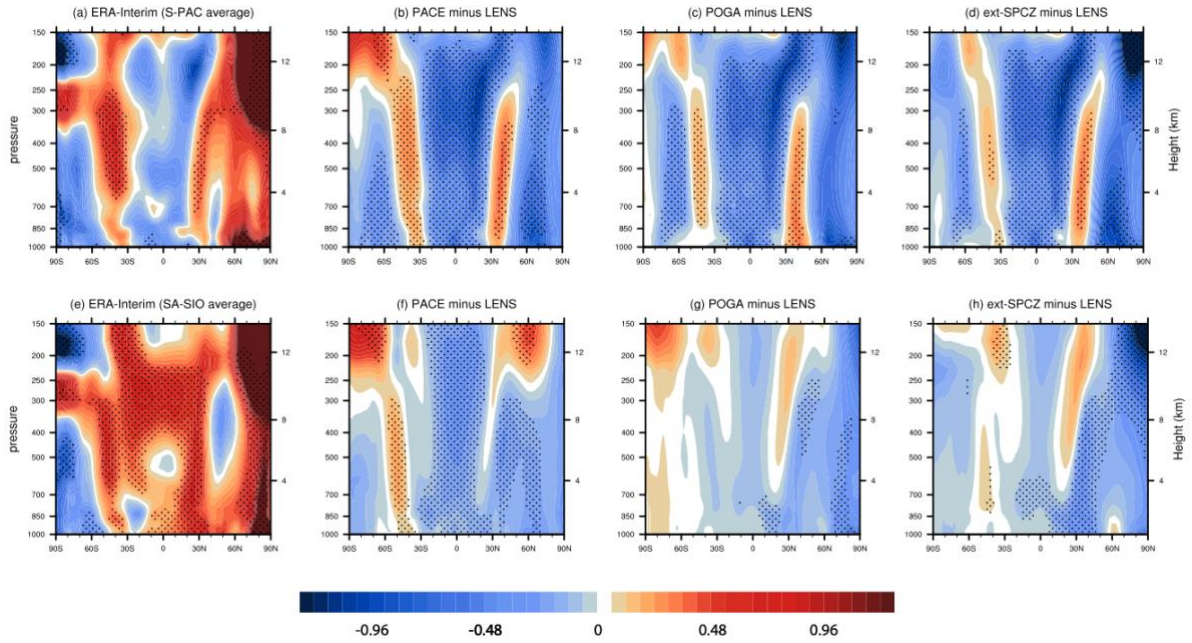

Figure 3.10 Top: Decadal difference (P2-P1) of the South Pacific basin-averaged temperature (K) for (a) ERA-Interim; (b) PAC-C minus LENS; (c) PAC-A minus LENS; (d) extSPCZ-A minus LENS. **Bottom**: Same as the top panels but for the South Atlantic-Indian basin average. Stippling indicates differences are significant at the 95% level based on a t-test.

Over the South Atlantic-Indian region, in contrast to the extensive warming belt in the PAC-C, PAC-A simulates only a very weak warming anomaly in the mid-latitudes (Figure 3.10g), leading to a depressed tropic-to-pole temperature contrast, less baroclinity and eddy generation, and the absence of the poleward displacement of the Atlantic-Indian jet at 50°S. The South Atlantic-Indian temperature contrast and jet displacement in extSPCZ-A lie between PAC-A and the PAC-C, i.e., the warming band in extSPCZ-A is larger than in PAC-A, but much weaker compared to PAC-C, resulting in only a moderate meridional temperature gradient and partial poleward movement of the Indian Ocean jet.

The absence of air temperature gradients across the Atlantic-Indian mid-latitudes in PAC-A could be related to the SST patterns discussed above. In the coupled PAC-C, responding to the tropical Pacific cooling, the Southern Hemisphere subtropical SST and the tropospheric temperature aloft involves a warming anomaly in each basin (i.e., South Pacific, Atlantic and Indian convergence zones at the surface) and prompts an increased meridional temperature gradient at about 50°S. In contrast, the tropospheric temperature warming anomaly at 40°S is considerably less significant in the PAC-A in

the absence of subtropical SST warming anomalies, which further leads to disparities in the latitudinal position of the Atlantic-Indian jet between the PAC-A and PAC-C simulations.

3.5 Summary and Discussions

In Chapter 2, we have suggested that the IPO has made a major contribution to the Southern Hemisphere summertime eddy-driven jet variations over the satellite era, including the strengthening of the South Pacific jet and poleward shift of the South Atlantic-Indian jet. One of the remaining questions, however, is whether tropical Pacific SSTs influence the Southern Hemisphere jet via direct atmospheric teleconnections or by interbasin interactions which first change the SSTs in other basins. In this study, we addressed this question by designing an atmosphere-only PAC-A experiment using CAM5 and comparing it with the fully coupled CESM1 tropical Pacific pacemaker experiments (referred to here as PAC-C). In both frameworks, the tropical Pacific SST anomalies follow the observed trajectory, which allows the PAC-C and PAC-A member ensemble mean (with external forcing excluded, i.e., minus LENS) to estimate the response to the internally-driven tropical Pacific SST variability. Outside of the tropical Pacific, the SST in the PAC-C can freely respond to the tropical Pacific through interbasin interactions, whereas in the uncoupled PAC-A runs, SSTs are constrained to follow the LENS ensemble mean SST. Therefore, the PAC-A minus LENS can isolate the direct atmospheric impact of tropical Pacific SST on Southern Hemisphere eddy-driven jet changes.

We found that in all seasons, the uncoupled PAC-A could capture the observed eddy-driven jet variation in the South Pacific basin, including the equatorward shift in the JJA-SON seasons and strengthening during DJF-MAM. This indicates that the South Pacific eddy-driven jet responds to tropical Pacific SST mainly via atmospheric pathways. Comparisons between PAC-C and PAC-A suggest that the air-sea coupling is notably more important in forcing the South Atlantic-Indian basin to enable the Pacific–South American Rossby wave propagation. A further uncoupled experiment extSPCZ-A was conducted to investigate the relative roles of tropical Pacific and SPCZ convective centres for the above teleconnections. Differences between PAC-A and extSPCZ-A reveal the importance of the SPCZ SST warming in bridging the Pacific–South American Rossby wave pattern and generating a more realistic Amundsen Sea Low position and South Indian jet variations. The basin-averaged meridional temperature gradient in each model experiment is also analysed to explain the jet similarities in the South Pacific basin and disparities in the South Atlantic-Indian basin between PAC-C and PAC-A simulations.

Waugh et al. (2020) suggested that the austral winter-spring trends in the latitude of the Pacific jet are due to internal atmospheric variability based on the fact that the observed trends lie within the CMIP5 ensemble member spread. In this study, using the CESM1 LENS, coupled PAC-C and uncoupled PAC-A simulations, we systematically analysed the impact of internally-driven tropical Pacific SST variability on the westerlies in all seasons, and further clarified which internal process (ie., direct atmospheric pathway or coupling) is predominantly important for different basins. We concluded that tropical Pacific SST influences the South Pacific jet decadal variation mainly via a direct atmospheric pathway in all seasons, but for the South Atlantic-Indian basins, the air-sea coupling is more important, especially in the DJF season.

Despite the Pacific–South American Rossby wave propagation, another possible dynamic pathway for tropical Pacific SST influence on the South Atlantic-Indian jet could be the tropical Pacific and Atlantic inter-basin interactions. For example, in response to the tropical Pacific cooling, the tropical Atlantic evolves a warming SST anomaly in observation (Figure 3.1a), which could further impact the Southern Hemisphere mid-latitude jet by the Hadley Cell circulation changes or via Rossby waves (Simpkins et al. 2014; Li et al. 2015). These potential mechanisms worth to be further addressed in the future.

Transient eddy-mean flow interactions have also been compared in the coupled PAC-C and uncoupled PAC-A simulations to explain the difference in the latitudinal position of the Atlantic-Indian jet between these two simulations. In observations and in PAC-C, the South Atlantic-Indian jet moves poleward in association with increased mid-latitude temperatures at around 45°S (Figure 3.10e-f) which enhances the meridional temperature gradient. By contrast, in PAC-A, in the absence of the mid-latitude SST warming anomalies over the South Atlantic and Indian Ocean (Figure 3.1d), the mid-latitude temperature warming anomaly in the troposphere is missing (Figure 3.10g), leading to a degraded tropic-to-pole temperature contrast. As a result, the PAC-A fails to reproduce the poleward displacement of the Atlantic-Indian jet at 50°S.

Previous studies have found a poleward jet shift can result from imposed temperature anomalies in the subtropical and mid-latitudes (Tandon et al. 2013), however jet shifts themselves can also induce adiabatic warming in the middle troposphere (Lim et al. 2016a). In other words, the warming anomalies shown in observations and in PAC-C (Figure 3.10e-f) include the impact of SST warming from the subtropical South Atlantic-Indian Ocean and any secondary adiabatic heating generated by the poleward-shifted eddy-driven jet. Nevertheless, this positive feedback between the jet shift and middle troposphere warming has little impact on the key conclusion that coupling is required to

reproduce the observed poleward shift in the South Atlantic-Indian jet in response to tropical Pacific SSTs.

Our findings could provide useful references for future air-sea-ice coupling studies. For instance, previous studies (Lefebvre et al. 2004; Holland et al. 2017b) have found that variations in the mid-latitude jet can have a large impact on the Southern Ocean circulation and Antarctic sea ice distribution. Therefore, applying a more realistic zonally asymmetric wind forcing, as suggested in this study, instead of zonal-mean SAM-like winds for ocean sea-ice models, could potentially lead to more accurate sea ice predictions (Goyal et al. 2021), especially over the Amundsen and Ross Sea regions. In addition, the uncoupled PAC-A and coupled PAC-C simulations enable an "apple-to-apple" comparison to identify the tropical Pacific SST influence on global SST and atmospheric teleconnections. Understanding the role of tropical internal variability on the Southern Hemisphere eddy-driven jet is critical to understanding past and future changes in the Southern Ocean circulation and Antarctic sea-ice and ice sheets.

Chapter 4

Impact of tropical Indian and western Pacific SST on the sea ice trend over the western Ross Sea

4 Impact of tropical Indian and western Pacific SST on the sea ice trend over the western Ross Sea

Preface:

The total Antarctic sea ice extent experienced a weak increase over the satellite era despite a warming background. By contrast, most current coupled climate models (e.g., historical experiments in CMIP5 and CMIP6) simulated a decreasing trend over this same time period, resulting in a large disparity from the observations that is not completely understood. Moreover, though teleconnections between each tropical basin SST and Antarctic sea ice variations have been established, no study has quantified the relative impacts of individual tropical basin variability on the Antarctic Sea sea ice expansion in recent few decades. Therefore, in Chapter 4, the same methodology using CESM LENS and tropical pacemaker experiments as in Chapter 2 was employed to quantify the relative roles of each tropical basin SSTs on Antarctic sea ice trends.

4.1 Introduction

Unlike the significant decline of Arctic sea ice extent (SIE), total Antarctic SIE experienced an overall increase in all seasons over the satellite era until the mid-2010s (Parkinson and Cavalieri 2012; Simmonds 2015). However, there are large regional variations in this expansion. For example, the Ross Sea and Indian Ocean sector shows positive sea ice concentration trends in each month during 1979-early 2010s, with the Ross Sea dominating the overall expansion of Antarctic sea ice (Parkinson and Cavalieri 2012; Turner et al. 2016). The sea ice in the Amundsen-Bellingshausen Seas experienced a significant decrease especially in summer and autumn.

As noted in Chapter 1, from the annular perspective, the overall Antarctic sea ice expansion/retreat is primarily impacted by the Southern Annular Mode (SAM), which exhibited a positive trend over 1979-2013, associated with increasing greenhouse gases, ozone depletion and tropical Pacific variability (Swart et al. 2015). In response to the positive SAM, the Southern Ocean sea surface temperature (SST) exhibited a cooling anomaly with sea ice expansion in the initial few years (Lefebvre et al. 2004), but developed into a warming trend with sea ice melting at decadal timescales as the subsurface warm water pumped up due to Ekman suction. (Ferreira et al. 2015; Kostov et al. 2017).

For the sea ice regional variation, different atmospheric and oceanic processes are analysed to explain its local changes (Lefebvre et al. 2004; Lefebvre and Goosse 2008; Goosse and Zunz 2014; Goosse et al. 2018). For example, the Amundsen Sea Low (ASL) is found to be a dominant atmospheric driver of sea ice changes around Amundsen-Bellingshausen Sea. Clem et al. (2017b) suggested that the Western Antarctic Dipole, a see-saw structure of SST and sea-ice, experienced an increase over the Ross Sea in the spring season responding to the deepening of the ASL located at around near 135°W.

The largest contribution to the total multidecadal sea ice expansion over the satellite era comes from the increase in the Ross Sea (Hobbs et al. 2016), and as such, understanding the sea ice increase in this region has received particular attention in the literature. Using an ocean–sea-ice model, Lecomte et al. (2017) suggested that following an external perturbation, sea-ice expansion and surface cooling in the Ross Sea can be sustained or amplified through a positive ocean–sea-ice feedback. However, it remains unclear what initial forcing may have triggered this positive feedback in the real world.

The impact of each tropical basin SST variability on Antarctic sea ice and Southern Ocean SST has been widely investigated, but with a main focus on west Antarctica, motivating our investigation of tropical links to east Antarctica, including the South Indian and Ross Sea sectors, where long-term sea ice trends are positive in all months. Specifically, we aim to assess whether a tropical-to-high latitude teleconnection may have triggered a positive ocean-sea ice feedback in the Ross Sea, which leads to a sustained expansion there.

Earlier studies have demonstrated the disparities between the simulated decreasing trend in the historical experiments of Coupled Model Intercomparison Project phases 5 (CMIP5) and 6 (CMIP6) and the observed sea-ice expansion during 1979-2010s (Roach et al. 2020). Simmonds (2015) and Gagné et al. (2015) suggested the model and observed difference still lies within the bounds of natural variability. Purich et al. (2016a) established that one of the contributors for this discrepancy is that most CMIP5 models underestimate the strengthening of the Southern Hemisphere westerly jets in the summertime and thus fail to simulate surface temperature cooling via Ekman suction. On the other hand, at interannual timescales, Schroeter et al. (2018) argue that the majority of the CMIP5 models display sea ice variations that are too zonally-symmetric as a result of their overestimated SAM impact, and also that the influence of the tropical variability has been underestimated. Meehl et al. (2016) found that ten out of 262 CMIP5 models that simulated a negative IPO phase were able to reproduce the positive Antarctic sea ice extent trends in the early-2000s, suggesting further investigation of the impact of tropical variability on the sea ice could help to identify what processes are missing in the models and what improvements could potentially be made to better capture the observed trend.

Quite a few previous studies have managed to partially reproduce the interannual variations and/or trends in Antarctic sea ice in a hierarchy of model simulations which utilised nudging to observed atmospheric or oceanic variables in the region. For example, Goosse et al. (2009) directly assimilated the near surface temperature around the sea-ice zone into a coupled climate model and found the model could capture the observed small increase in ice area over the period 1980–2000. Similarly, Zhang et al. (2020) nudged the observed Southern Ocean SST anomalies into the CESM1 and suggested that Southern Ocean cooling reduced the simulated Antarctic SIE loss over recent decades but could not alone explain the observed increasing trends. Blanchard-Wrigglesworth et al. (2021) applied the same nudging technique as in Zhang et al. (2020) with nudged winds in addition to SSTs and illustrated that the surface winds could explain the observed SIE interannual variability, and when combined with the observed SSTs, the SIE decadal trend is in better agreement with observations. The importance of salinity is also stressed in Purich et al. (2018), where an additional freshwater flux

was added into the ocean component of a fully coupled model and the observed increasing trend in Antarctic sea ice was captured. These experiments highlight the significant impact of local atmospheric or oceanic circulation on Antarctic sea ice variations.

While previous studies have focused on the role of external forcing in driving local atmospheric and oceanic trends in the Antarctic sea ice region, Chapter 2 and 3 highlighted that the remote impact of tropical SST variability is also a factor. Hence, it follows that tropical SSTs could also directly impact Antarctic sea ice changes. The impact of tropical Pacific SSTs on Antarctic sea ice extent has been examined based on some pacemaker simulations where the tropical Pacific SST anomalies were restored to observations (Purich et al. 2016b; Schneider and Deser 2017): using the CESM tropical Pacific pacemaker simulations, Schneider and Deser (2017) found the internal variabilities generated by tropical Pacific SST could successfully reproduce the ASL deepening and regional sea ice variations around the Amundsen-Bellingshausen Sea. However, the influences of tropical Indian and Atlantic SST variations have not been fully investigated using this pacemaker methodology. Therefore, in this chapter, the same pacemaker framework was applied as in the earlier chapters, but with a primary focus on the role of tropical Indian and Atlantic internally-driven SST variabilities.

Schneider & Deser (2017) stressed the importance of the Southern Ocean vertical temperature gradient in maintaining the zonal-mean surface cooling (their Figure 13). Similar arguments were reached in Lecomte et al. (2017) for the Ross Sea sector based on results from an ocean-ice model. They suggested that if there is an initial sea ice increase (or sea surface freshening, SST cooling), this initial change will be amplified by a positive feedback cycle. For example, if there is a sea ice advancing anomaly in one or a few years, the brine released would be trapped to deeper layers, lead to a stronger vertical stratification, and suppress the sub disparities surface warm and dense water to pump up. This would leave the surface in a freshening and cooling environment, and further induce the surface ice increase. Haumann et al. (2020) also argue that the observed sea ice trends have been instrumental to the vertical structure of the Southern Ocean temperature trends. It is of scientific interest to understand whether fully coupled climate models such as CESM can capture the ocean-sea ice feedbacks suggested by Lecomte et al. (2017). Furthermore, the driver of the initial surface cooling is not addressed by their study.

In this study, we are motivated by the following questions:

1. What is the impact of tropical Indian SST anomalies on multidecadal trends in Antarctic sea ice?

2. What atmospheric and oceanic processes are important in driving the sea ice expansion in the Ross Sea during 1979-2010s?

3. Can fully coupled models reproduce the positive ocean-sea ice feedback and sustained sea ice increase in the Ross Sea?

The rest of the chapter is established as follows. Section 4.2 describes the data and model simulations. The main results and associated mechanism are presented in Section 4.3. We conclude with a brief summary and discussion in Section 4.4.

4.2 Data and Methods

In this study we make use of passive microwave processed sea ice concentration (SIC) data from the National Sea and Ice Data Centre (NSIDC) processed with the National Aeronautics and Space Administration (NASA) team algorithm (Cavalieri et al. 1996). The monthly zonal (U) and meridional (V) winds and sea level pressure (SLP) are from the European Centre for Medium-Range Weather Forecasts Interim reanalysis (ERA-Interim; Dee et al. 2011), which has been identified as one of the best reanalysis data for the Southern Hemisphere high latitudes, specifically over Antarctica (Bromwich et al. 2011; Bracegirdle et al. 2013). The monthly SST data is from the National Oceanic and Atmospheric Administration (NOAA) Extended Reconstruction Sea Surface Temperature, version 3b (ERSSTv3b, Smith et al. 2008). The EN4 ocean temperature and salinity datasets are from the UK Met Office (Good et al. 2013).

As in Chapter 2, we utilise experiments with the fully-coupled CESM version 1, including the 40-member Large Ensemble LENS (LENS, Kay et al. 2015) and 10-member tropical Indian (IND) pacemaker to investigate the impact of tropical Indian and western Pacific SST on sea ice decadal variations (Table 2-1).

The CESM LENS 40 ensemble members use the same model physics and are constrained to the same radiative forcing scenario (Taylor et al. 2012, i.e., historical forcing over 1920-2005 and the Representative Concentration Pathway (RCP) 8.5 (Moss et al. 2010) during 2006-2080, following the Coupled Model Intercomparison Project Phase 5 (CMIP5) design protocol). The only difference between each member is a small perturbation of the initial atmospheric temperature field imposed at the beginning of the simulations at 1920, which develops into 40 different realizations of internal variability. The 40-member LENS ensemble mean (LENS-EM) averages this internal variability and can be used to provide a robust estimate of the external forcing impact on the climate system, as given by CESM1.

As in Chapter 2, the Indian pacemaker experiment uses the same coupled model and nearly identical external forcing to the LENS, however the SST anomalies within the tropical Indian and western Pacific Oceans (from the African coast to 175°E, 15°S-15°N are nudged to follow the observed trajectory while the rest of the model evolves freely (Table 2-1). Through this framework, the Indian pacemaker ensemble mean (IND-EM) combines the responses to external forcing and to observed tropical Indian-western Pacific SST variations. Thus subtracting the LENS-EM from the IND-EM isolates the impact of observed time-varying internally-driven tropical Indian-western Pacific SSTs on the climate system. Similarly, two additional pacemaker ensembles with observed SST anomalies restored in the tropical Pacific and North Atlantic basin were also analysed to compare with the Indian pacemaker.

Here, we focus on the 1979–2013 period for alignment with the years available for the CESM pacemaker ensembles and to compare with previous sea ice multidecadal trend studies (Hobbs et al. 2016; Lecomte et al. 2017).

4.3 Results

4.3.1 Spatial sea ice patterns

The observed 1979-2013 trend of annual-mean Antarctic sea ice concentrations shows an overall increase (Figure 4.1a). However, in addition to the broad expansion, the sea ice also shows zonal asymmetric variations. To better discuss regional changes and following Turner et al. (2016) and Lecomte et al. (2017), we divide the Antarctic into five sectors in this chapter, indicated in Figure 4.1: the Weddell Sea, the South Indian sector, the Adélie, the Ross Sea, and the Amundsen and Bellingshausen Seas. Substantial increases are observed in the western Ross Sea, part of the Weddell Sea and the western South Indian sector. Sea ice retreat is seen in the Amundsen-Bellingshausen region and the outer Weddell Sea, as well as between the South Indian and Adélie sectors (around 90°E). This zonal wavenumber two pattern in sea ice closely aligns with the SLP trend distribution from the ERA-Interim reanalysis, where alternating low/high SLP centres are associated with the expansion/retreat of sea ice. For example, in response to the extensively deepened ASL, the sea ice in the Amundsen-Bellingshausen Sea and outer western Weddell sector experienced a large decrease due to a warm northerly inflow. Conversely, over the western Ross Sea, the sea ice shows a significant increase associated with a cold southerly outflow. Similar sea ice-SLP relations can be found for the South Indian low and the Weddell and South Pacific high centres, consistent with the findings of Raphael (2007), namely that the atmospheric circulation, especially the meridional component, can largely influence regional shifts in sea ice.

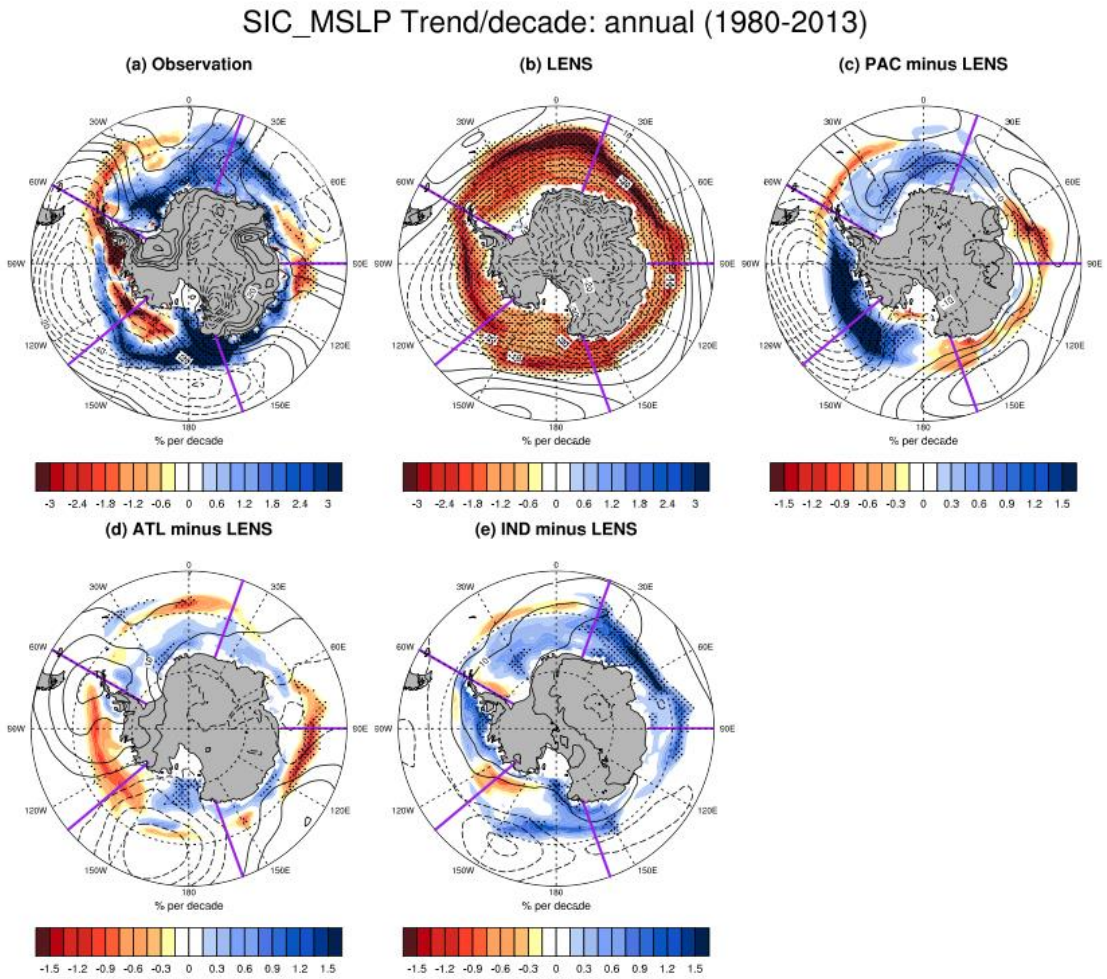

Figure 4.1 Annual-mean trends in sea ice concentration (shading, unit: fraction/decade) and SLP (contours, unit: hPa/decade) in (a) NSIDC observations & ERA-Interim reanalysis; (b) CESM Large Ensemble mean (LENS), indicative of external forcing; (c) tropical Pacific pacemaker minus LENS; (d) North Atlantic pacemaker minus LENS; (e) tropical Indian pacemaker minus LENS. The contour range is -1 hPa to 1 hPa with 0.1 hPa intervals in (a), and -0.5 hPa to 0.5 hPa with 0.05 hPa intervals in (b-e). Stippling indicates differences are significant at the 90% levels, based on a t-test.

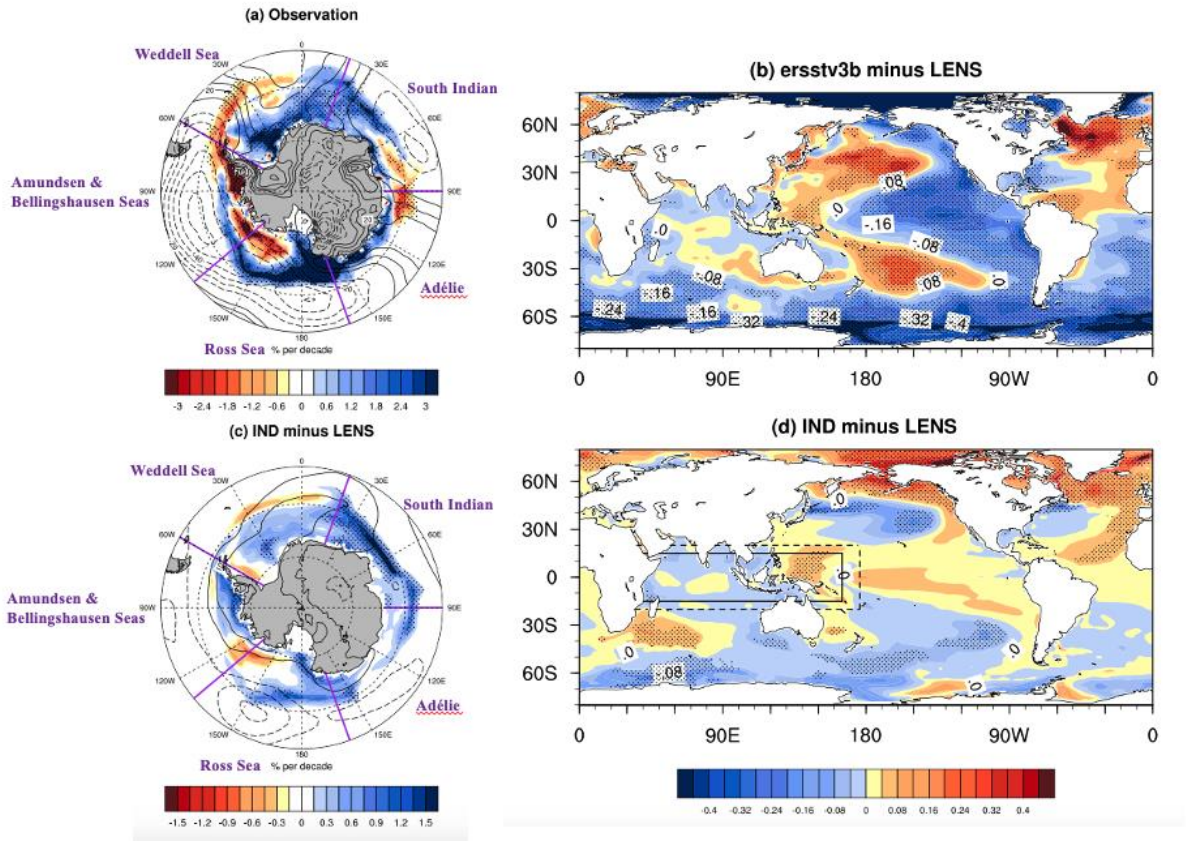

Figure 4.2 Left: Annual-mean trends from 1980-2013 (per decade, hereafter) in sea ice concentration (shading, unit: fraction/decade) and sea level pressure (SLP, contours, unit: hPa/decade) in (a) NSIDC observations & ERA-Interim reanalysis and (c) tropical Indian pacemaker ensemble mean minus LENS ensemble mean (IND minus LENS, hereafter). The contour range is -1 hPa to 1 hPa with 0.1 hPa intervals in panel (a), and -0.5 hPa to 0.5 hPa with 0.05 hPa intervals in panel (c). **Right:** SST trend (K per decade) in (b) ERSSTv3b minus LENS, and (d) IND minus LENS. Stippling indicates trend significant at the 90% level for (a/c) and 95% level for (b/d), based on a t-test. In panel (d), within the solid black lines, the SST anomalies are nudged to the observed anomalies; between the solid and the dashed lines are the buffer belts where the observed SST anomalies are linearly tapered to zero; outside of the dashed lines, the SSTs are free to evolve. The purple lines divide the Antarctic into five sectors: the Weddell Sea, the South Indian sector, the Adélie, the Ross Sea, and the Amundsen and Bellingshausen Seas.

Similar to most CMIP5 and CMIP6 models, the CESM LENS-EM (forced component) and tropical pacemakers (forced component + tropical SST internal variability) both simulated positive SST trends and sea ice declines around Antarctica over 1980-2013. However, when external forcing is removed (by subtracting LENS-EM), the pacemakers can reproduce some regional changes of the observed sea ice trends. As discussed in Schneider and Deser (2017), the Pacific pacemaker (Figure 4.1c, with external forcing removed) largely simulates the deepening of the ASL as in observations, however, it does not lead to a better sea ice reproduction in the Amundsen-Bellingshausen Sea region, with overestimated sea ice expansion around the Amundsen Sea. The north Atlantic pacemaker can capture the observed zonal wave number two distributions of sea ice and SLP, though the SLP centres differ from the reanalysis and the entire Antarctic sea ice shows an overall retreat, even with the externally forced component removed.

While neither the Pacific or Atlantic pacemaker ensembles closely resemble observations, the IND minus LENS reproduces most of the detailed observational features, including the increasing trend in the western Ross Sea, the inner Weddell Sea and the South Indian sector, as well as the decrease in the outer Weddell Sea, though the the magnitude of simulated variations is 2-3 times smaller than the observed (Figure 4.1a). It should be noted that a direct comparison of magnitudes is not possible because the observed trends include both forced and unforced signals, while the IND-EM minus LENS-EM (hereafter, IND minus LENS) trends only include the unforced signal.

There are also some discrepancies, for instance, the model simulates a slight expansion instead of the retreat in the Bellingshausen Sea (60-90°W) and fails to depict the decreasing trend at about 90°E. However, compared the internal variability driven trends in the Pacific and Atlantic pacemaker ensembles, the circumpolar similarity in sea ice trends between IND minus LENS and observations is improved. Consistent results are also found in the SLP field, where the IND minus LENS captures the general low and high pressure centres, although with much weaker magnitude than observed. The high pressure centre in the South Pacific Ocean is also not captured by the model and the ASL centre is shifted west into the the eastern Ross Sea. Overall, the results provide further support for the importance of the zonally asymmetric atmospheric circulation in driving Antarctic sea ice trends.

The seasonality of the sea ice trends in the IND minus LENS is shown in Figure 4.3. In DJF and MAM the simulated sea ice is in good agreement with observations, with expansion everywhere apart from the Amundsen-Bellingshausen Sea retreat. In JJA and SON the observed increasing trends in the Ross Sea and the South Indian Ocean are generally replicated well. However, there are mismatches in the Weddell Sea, Amundsen-Bellingshausen Sea sector and at around 90°E. Overall, for the Ross Sea region, which we focus on for the rest of this chapter, the IND minus LENS results are in accordance with the observed trends in all four seasons, including an east-west dipole structure in DJF and MAM, and a uniform increase in JJA and SON.

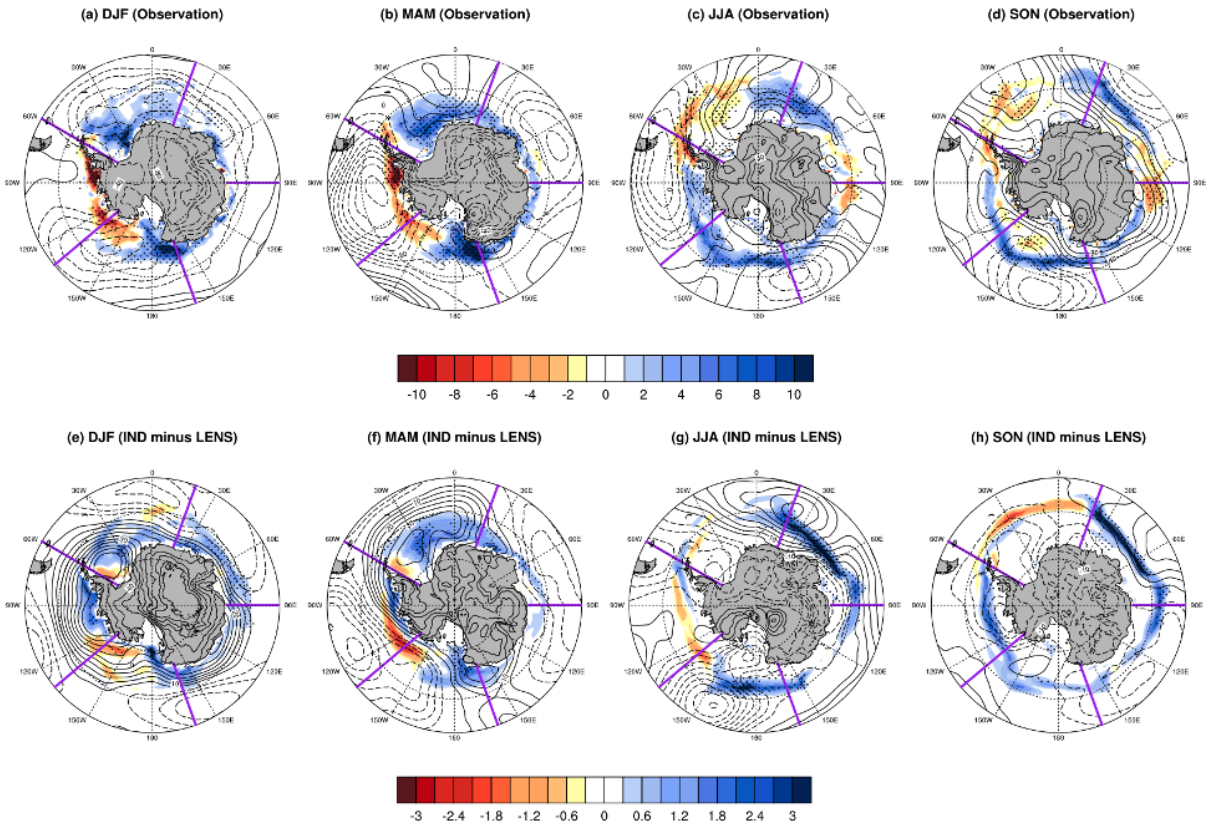

Figure 4.3 Seasonal trends in sea ice concentration (shading, unit: fraction/decade) and SLP (contours, unit: hPa/decade) for 1980-2013 in (a-d) NSIDC observations & ERA-Interim reanalysis and (e-h) IND minus LENS. The contour range is -1 hPa to 1 hPa with 0.1 hPa intervals in (a-d), and -0.5 hPa to 0.5 hPa with 0.05 hPa intervals in (e-f). Stippling indicates trend significant at the 90% level based on a t-test.

4.3.2 Ocean and sea ice trends in the western Ross Sea

As noted above, the western Ross Sea SIC makes the largest contribution to the observed Antarctic sea ice expansion over 1979-2013, hence the rest of this chapter focuses on understanding trends in this region. Given the remarkable alignments between the IND minus LENS and observed sea ice trends in all four seasons, most of the following analyses are conducted from the annual-mean perspective.

Figure 4.4 shows the sea ice time evolution of the Ross Sea section from observations and the Indian pacemaker. The observed annual mean SIC averaged over the western Ross Sea ((150°E-180°, 50-90°S) shows the previously documented increase, the Indian pacemaker ensemble captures most of the observed interannual variability but with a negative sea ice trend (Figure 4.4a). With external component removed, the IND minus LENS shows better alignment with the observation, including the year-to-year variations as well as the long-term trends (Figure 4.4b). This further verifies the

importance of tropical Indian-western Pacific SST internal variability in driving the Ross Sea ice interannual and decadal changes.

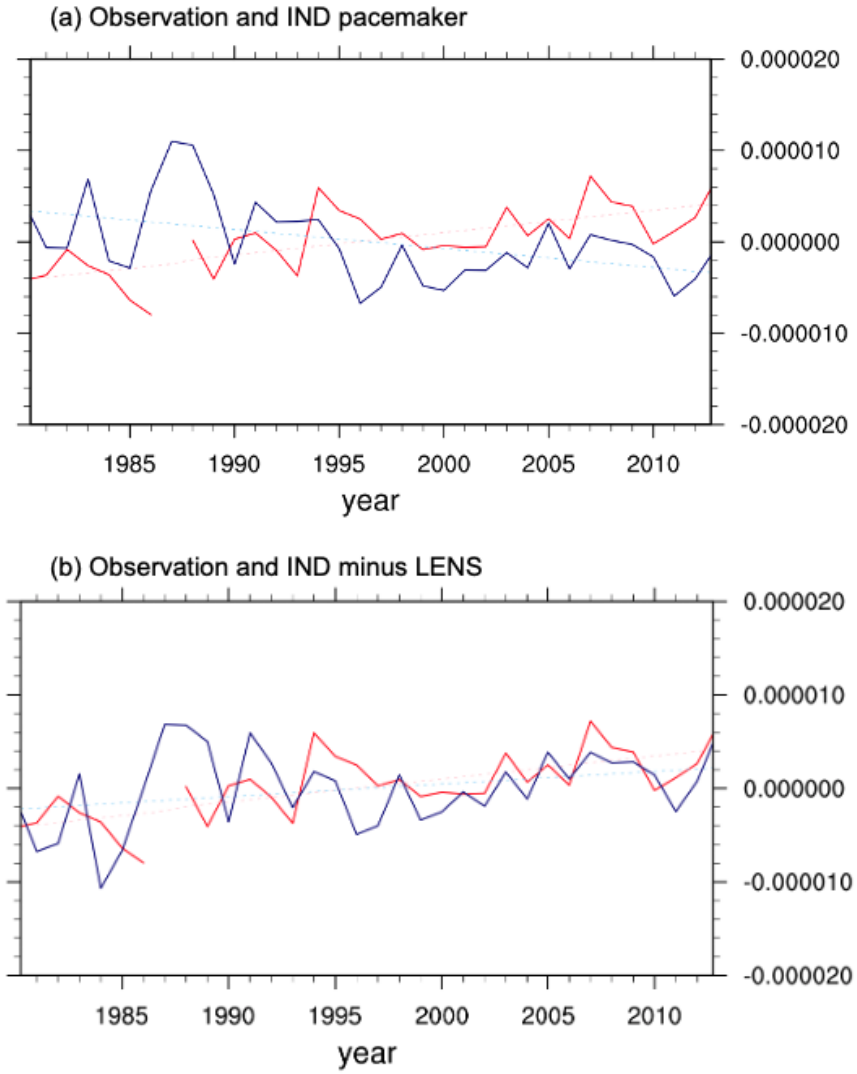

Figure 4.4 Annual-mean Antarctic sea ice concentration anomalies (unit: fraction) during 1980-2013 averaged over the western Ross Sea region (150°E-180°, 50-90°S). Top: Observed (NSIDC, red) with its linear trend (dashed pink), and Indian pacemaker (blue) with its linear trend (dashed blue); Bottom: Same as top plot except the external forcing is removed from the tropical Indian pacemaker (IND minus LENS, blue line). The red line is discontinuous around 1987 because there are two months of missing values for all NSIDC variables in Dec 1987 and Jan 1988 due to satellite retrieval issues.

We turn next to understanding the connection between the tropical SSTs and the sea ice changes in the Ross Sea. The observed SST trends (Figure 4.1b; minus LENS) are largest in the Maritime continent and western Pacific region which is included in nudged region of the tropical Indian pacemaker (from the African coast to 175°E, 15°S-15°N; outlined in black in Figure 4.1d), with insignificant variations in the eastern tropical Indian basin (Figure 4.1b). In response to the internally-

driven variability from this nudged SSTA region, the Southern Ocean SST in both observations and IND minus LENS shows extensive cooling, especially in the South Indian Ocean and the western Ross Sea.

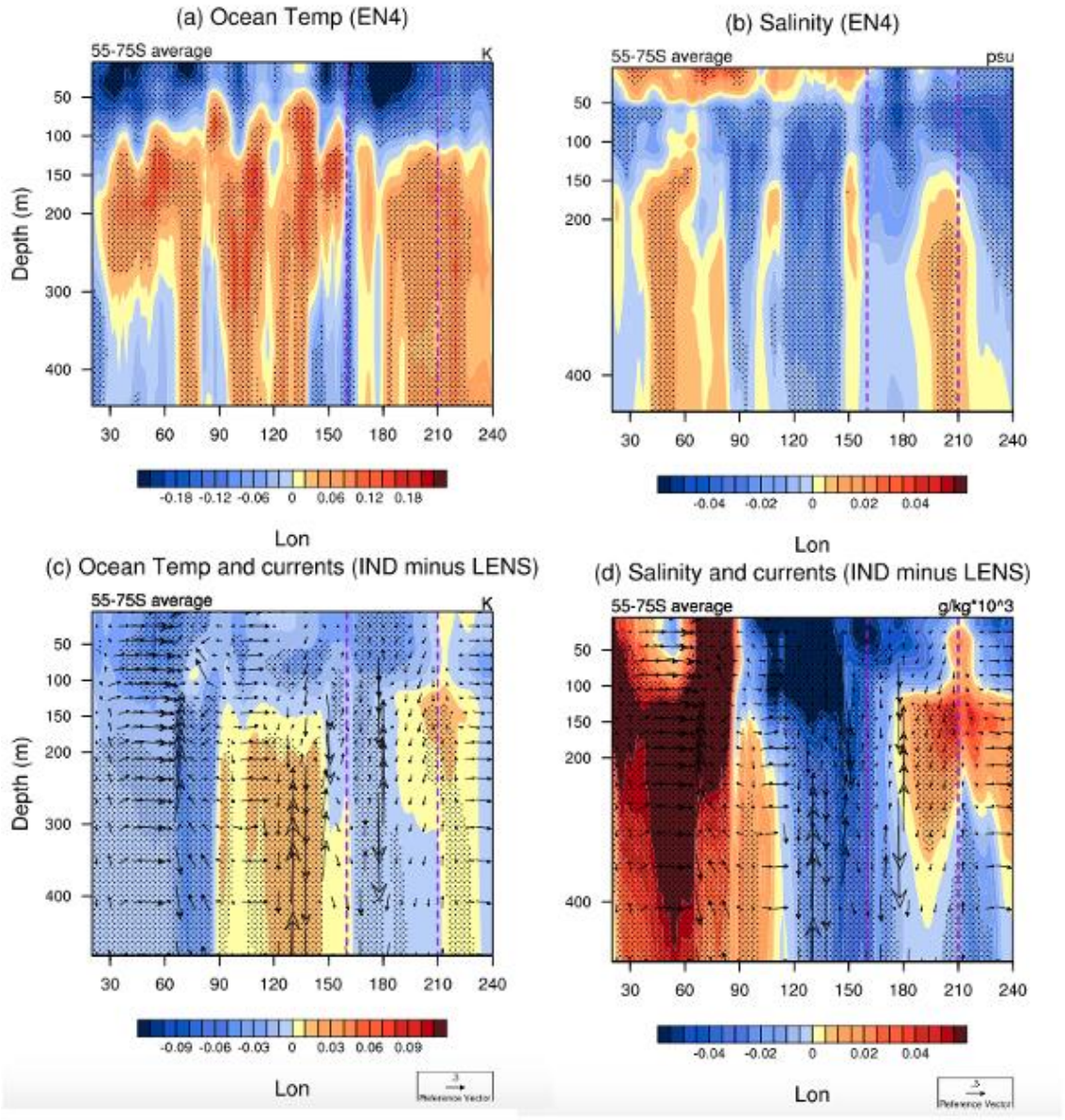

Figure 4.5 Annual-mean trends **in Left:** ocean temperature trend (unit: K/decade) and **Right:** ocean salinity trends (unit: gram/kilogram/decade) from 1980-2013 averaged over 55-75°S for the upper 500 m for (a/c) EN4 reanalysis and (b/d) IND minus LENS. In panel (b/d), the vectors are ocean zonal (U, unit: centimeter/s/decade) and vertical currents (W, unit: centimeter/s/1000000). The dashed purple lines indicate the western Ross Sea region. Stippling indicates trends are significant at the 95% level based on a t-test.

The prominent Southern Ocean cooling trend is further detected below the surface in both reanalysis (Figure 4.5a) and IND minus LENS (Figure 4.5c). The upper 100 m of EN4 reanalysis ocean

temperature averaged over 55-75°S displays a substantial circumpolar cooling trend, with the strongest cooling in the South Indian basin (30-90°E) and the western Ross Sea (180-210°E; Figure 4.5a), which aligns with the observed SST changes (Figure 4.1c). The IND minus LENS shows a close resemblance to the observed cooling trend at the ocean surface (Figure 4.1d) and in the top 100 m (Figure 4.5c).

Another important feature about the western Ross Sea (150-210°E) is that the upper 100 m temperature displays a cooling (Figure 4.5a,c) and freshening (Figure 4.5b,d) trend, however in the subsurface (150-300 m, 180-210°E), warming and increased salinity is exhibited, along with a downwelling trend (Figure 4.5b,d, ocean currents only available for model output). This vertical distribution of ocean temperature and salinity is found in both observations and IND minus LENS, and are consistent with the ice-ocean positive feedback in Lecomte et al. (2017) that explains the sustained sea ice growth in the Ross Sea. In response to the tropical Indian-western Pacific SST anomalies, the western Ross Sea displayed a substantial surface cooling and freshening with subsurface warming and salinity increasing, suppressing the heat content and brine released to deeper layers, producing a fresh and cool environment at the surface, further conducive to the sea ice increase. Our results indicate, for the first time, that a fully coupled model nudged to observed SST anomalies in the tropical western Pacific and Indian Oceans can capture this ice-ocean positive feedback. In addition, an examination of what process triggers the initial increase in sea ice is required and is undertaken in Section 4.3.3.

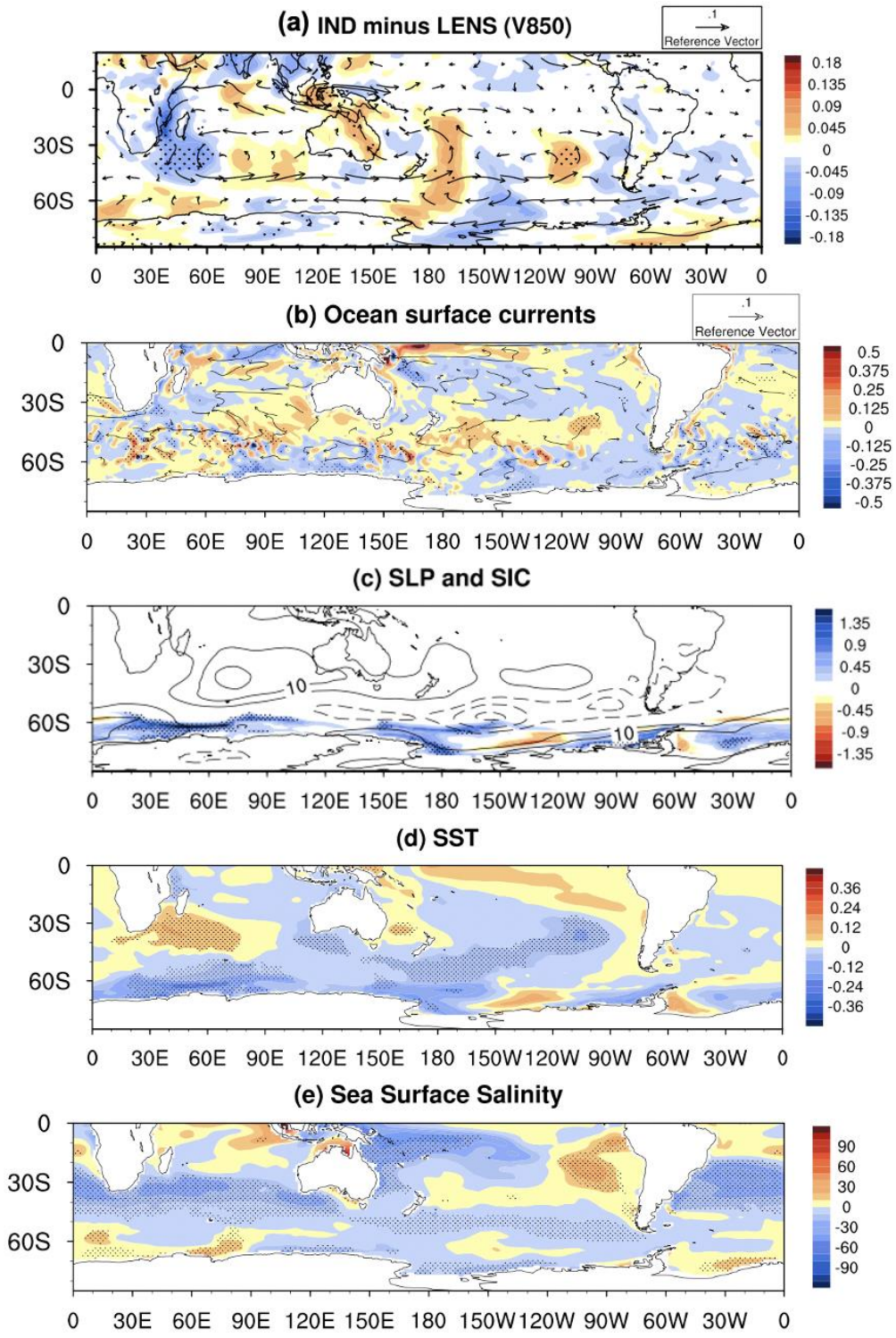

Figure 4.6 Annual-mean trends in near-surface and surface fields for IND minus LENS for (a) 850 hPa winds (vectors; m/s/decade) and the meridional wind speeds (shading); (b) ocean surface currents (vectors, unit: centimeter/s/decade) and its meridional component (shading); (c) sea ice concentration (shading, unit: fraction/decade) and SLP (unit: hPa/decade, the contour range is -0.5 hPa to 0.5 hPa with 0.05 hPa intervals); (d) sea surface temperatures (unit: K/decade) (e) sea surface salinity (unit: gram/kilogram/decade). Stippling indicates trends are significant at the 90% level based on a t-test.

Consistent results associated with the sea ice dipole pattern around the Ross Sea are identified in other atmospheric and oceanic fields in IND minus LENS (Figure 4.6). For instance, the near-surface wind exhibits southerly outflow in the western Ross Sea (Figure 4.6a), which directly drives a northward movement of the ocean surface currents (Figure 4.6b), conveying the polar cold and freshwater equatorward and leading to the sea ice expansion (Figure 4.6c) and SST cooling (Figure 4.6d) around 150°E-180°. The opposite sign is found in the eastern Ross Sea (120-150°W), with simulated northerly winds and ocean currents, warm SST anomalies and sea ice melting. This also corresponds to a region of observed sea ice decline in the inner ice zone (Figure 4.1a), indicating the local circulation changes are essential for reproducing the Ross Sea ice variations (Turner et al. 2016; Holland et al. 2017a).

4.3.3 Atmospheric teleconnections from tropical Indian-western Pacific SST Anomalies

The above consistencies between the observed and simulated tropical SST anomalies SLP, Southern Ocean temperature and salinity, as well as the sea ice indicate that internal variability from tropical Indian and western Pacific SST anomalies could contribute to the observed trends in Antarctic sea ice. Recent work has demonstrated that tropical Indian SST variability could affect the Australian climate (Cai et al. 2011; McKay et al. 2021) and Antarctic sea ice (Meehl et al. 2019b; Purich and England 2019; Wang et al. 2019) via Rossby wave teleconnection. Here, we explore these tropical-polar teleconnections further with a focus on the Ross Sea region.

Increased precipitation is observed in association with the SST warming trend in the Maritime continent and western Pacific Ocean, with the largest positive values along the Equator between 120°-150°E (Figure 4.7a). This precipitation anomaly coincides with an upper troposphere horizontal divergence in the same region (positive geopotential height anomaly at 200 hPa, Figure 4.7c), which induces a Rossby wave propagating from the north-west of Australia to the Ross Sea and leads to a positive SAM-like pattern at 200 hPa, especially over the Ross Sea and South Pacific basin (positive geopotential height anomaly at around 40° S and a negative tendency along 65° S). Consistent with these wave trains, the observed near-surface eddy-driven jet along 60°S is strengthened with a large cyclone sited at the Ross and Amundsen Sea region (Figure 4.7e).

The IND minus LENS reproduces some tropical features in the observations, with a warming SST anomaly, enhanced rainfall, upper-level divergence in the Maritime continent and western Pacific (Figure 4.7b). However, it fails to match the extratropical circulations as in observation. For example, the observed positive SAM-like pattern and the associated westerly wind strengthening is not well

captured by the model, instead, the simulated westerly wind seems to be weakened at 60°S. Though a relatively smaller size of cyclone is captured in the Ross Sea area, leading to a local SST and sea ice dipole distribution as shown in Figure 4.6.

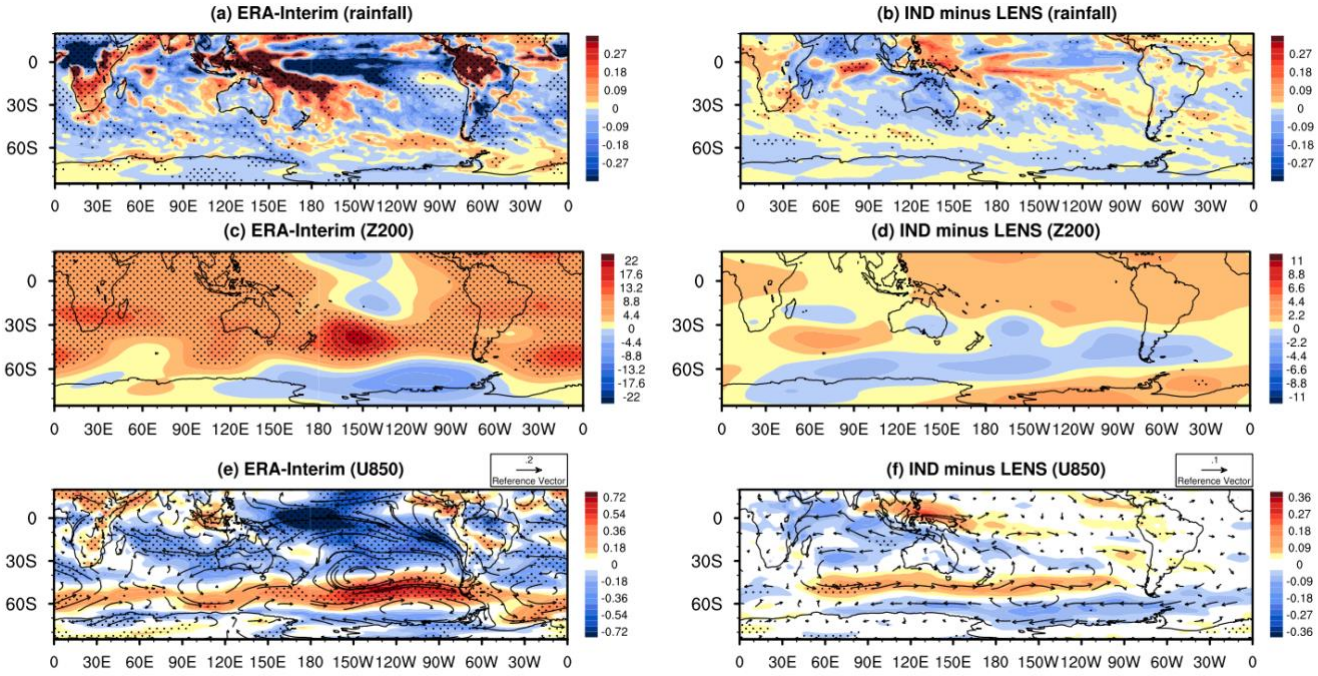

Figure 4.7 Annual-mean trends in Left: ERA-Interim reanalysis and Right: IND minus LENS for (a/b) Rainfall (mm/day/decade); (c/d) 200 hPa geopotential height (unit: m/decade); (e/f) 850 hPa zonal wind (units: m/s/decade). Stippling indicates trends are significant at the 90% level based on a t-test.

Another possible explanation for why IND minus LENS reproduces the observed Antarctic sea ice expansion trend pattern can be related to the two-time scale Southern Ocean SST and sea ice response to the SAM. On interannual timescales the positive SAM is associated with a surface northward Ekman drift, leading to cool SST anomalies and sea ice expansion around Antarctica (Lefebvre et al. 2004). However, at longer timescales, sustained positive SAM and enhanced westerly winds cause upward Ekman pumping of deep warm water from below the mixed layer, inducing a warm SST anomaly and sea ice decline (Ferreira et al. 2015; Kostov et al. 2017). Most CMIP5 models generally capture this two-time scale response to the SAM, and for the CESM1 model used in this study, the transitioning time from the initial fast cooling response to the slow warming response is around 2 years (Figure 4 in Holland et al. 2017b). Therefore, with external-forced positive SAM removed, the weak simulated SAM in IND minus LENS allows the initial SST cooling and sea ice expansion to sustain, postponing the eventual warming and sea ice decline, favouring sea ice expansion over 1980-2013.

4.4 Summary and Discussion

Previous investigations into how tropical variability influences Antarctica via tropical-to-high latitude teleconnections has mainly focused on the roles of the tropical Pacific SST variations in driving the ASL and associated west Antarctic sea ice changes, especially over the Amundsen-Bellingshausen Sea and Weddell Sea. Here, we are principally focused on changes in the Ross Sea, the region of highest sea ice growth during the satellite era. Using the CESM LENS and tropical Indian pacemaker experiments, we identify that internal variability from the tropical Indian/western Pacific SSTs (the SST regression map on the Ross Sea ice interannual variations exhibit the same warming in the tropical Indian/western Pacific, not shown), could explain part of the annual-mean sea ice expansion in the western Ross Sea and South Indian sector (Figure 4.1a,c).

Both atmospheric and oceanic processes are analysed to investigate the mechanisms behind sea ice expansion in the Ross Sea. In observation, the tropical Indian and western Pacific SST variability induces a Rossby wave train propagating southwest, leading to a Ross Sea low located around 180°. As a consequence, at the western flank of the Ross Sea low, the sea ice expands with large SST cooling and freshened salinity (Figure 4.5). The IND minus LENS reproduces some tropical and polar features in the observations but fails to capture the extratropical circulations.

An ocean-ice positive feedback in the western Ross Sea as suggested in Lecomte et al. (2017) is simulated in IND minus LENS . The stable vertical structure of ocean temperature and salinity (with surface cooling and freshening versus subsurface warming and increased salinity) produces a fresh and cool environment at the surface and leads to further sea ice expansion in the western Ross Sea. Through this positive feedback, the initial sea-ice expansion and surface cooling in the western Ross Sea can be sustained and amplified. The identification of surface and subsurface trends in a global coupled climate model that closely resemble observations is one of the key findings of our study, and further demonstrates the importance of this positive ice-ocean feedback (Lecomte et al. 2017) in driving sea ice trends in the Ross Sea.

IND minus LENS fails to capture a strong positive SAM trend as in observation but well reproduces the observed Antarctic sea ice increasing trend. This could be associated with the two-time scale Southern Ocean SST and sea ice response to the positive SAM. With a weak simulated positive SAM, the transitioning time (from the initial SST cooling to the slow SST warming) in IND minus LENS is likely to be postponed, which is in favour of a longer time scale Antarctic sea ice expansion over

1980-2013. Further investigation is needed to tackle this SAM related two-time scale process in future studies.

Though in this study we mainly emphasized the good agreement between the IND minus LENS and observations in the decadal SST and sea ice trend in the western Ross Sea, their alignments on the year-to-year variability are also clear (Figure 4.4). Blanchard-Wrigglesworth et al. (2021) use atmospheric nudging experiments with the CESM1 to observed U/V winds over the Southern Hemisphere high latitudes to suggest that the local atmospheric circulation is a key factor for simulating the year-to-year variability of regional Antarctic sea ice. Our results based on the Indian pacemaker runs take this one step further, indicating that nudging to the observed SST anomaly in the tropical Indian and western Pacific, can also reproduce the interannual variability of the western Ross Sea sea ice, highlighting the importance of tropical Indian and western Pacific variability in driving the local atmospheric circulation and sea ice changes in the region.

Understanding the drivers of the multi-decadal sea ice expansion in the Ross Sea over a period of globally increasing temperatures is critical for constraining future projections of Antarctic sea ice and Southern Ocean circulation: the Ross sea ice expansion contributed most of the total Antarctic sea ice increase during the satellite era. We have related part of the sea ice changes in the western Ross Sea and South Indian sector to intrinsic variability from the tropical Indian-western Pacific SSTs. In addition, we identified that the fully coupled CESM pacemaker simulations capture the ocean-sea ice positive feedbacks as suggested in Goosse and Zunz (2014) and Lecomte et al. (2017). These findings are relevant for future air-sea-ice coupling studies.

Chapter 5

Conclusion

5 Conclusion

5.1 Thesis Summary

The aim of this thesis was to improve our current understanding of the impact of decadal variability of tropical SSTs on the Southern Hemisphere eddy-driven jet and Antarctic sea ice, with a main focus on the dynamical mechanisms. Chapter 2 and 3 were largely motivated by the fact that previous work mainly emphasized the role of external forcing (such as increasing greenhouse gases and stratospheric ozone depletion) in driving the decadal changes of Southern Hemisphere eddy-driven circulation, the influence of natural intrinsic variability, however, had been less investigated. Similarly, Chapter 4 developed due to the deficient understanding of the impact of tropical Indian-western Pacific Ocean SST variability on Antarctic sea ice decadal changes. Besides, earlier studies of tropical-Antarctic teleconnections have mainly focused on western Antarctica, motivating our investigation of tropical links to east Antarctica, especially in the Ross Sea sectors, which makes the largest contribution to the total multidecadal sea ice expansion during the satellite era.

This section will provide a summary and conclusion of Chapters 2-4, followed by some discussion on the thesis limitations and which motivates future work.

5.1.1 Role of tropical variability

In this chapter, using a hierarchy of fully-coupled CESM Large Ensemble (LENS) and Pacemaker experiments, we separated the relative impacts of external forcing and tropical internal variability on decadal variations of the SH eddy-driven jet during austral summer. The response to each tropical basin SSTs was examined individually by restoring the observed SSTs in three tropical regions separately: the tropical central and eastern Pacific, the tropical Indian and western Pacific, and the tropical and North Atlantic.

We found that both external forcing and internal tropical Pacific SST variability were important in driving a positive Southern Annular Mode (SAM) phase and poleward migration of the eddy-driven jet in austral summer from the late 20th Century (1980-1999) to early 21st Century (2000-2013). Tropical Pacific SST variability, associated with the negative phase of Interdecadal Pacific Oscillation (IPO), acted to shift the jet poleward over the South Indian and Southwest Pacific and

intensify the jet in the Southeast Pacific basin, while external forcing drove a significant poleward jet shift in the South Atlantic basin. In comparison, the tropical & North Atlantic SST and Indian Ocean SST made a weak and sometimes offsetting contribution. The zonal asymmetric movement of the eddy-driven jet was highlighted in our study instead of the zonal-mean perspective which was generally a focus in previous work. Furthermore, our results showed, for the first time, that tropical Pacific SSTs were comparable in their influence on the eddy-driven jet to external forcings.

A dynamical mechanism by which external forcing and tropical Pacific SSTAs induced eddy-driven circulation variations was proposed. From a zonal mean perspective, we found that poleward migration of the eddy-driven jet could be explained by changes in the transient eddy momentum flux convergence (EMFC) belt. Under the external forcing influence, the mid-latitude EMFC shows a significant poleward migration around 55°S, leading to the southward migration of the eddy-driven jet by ~1° of latitude. In addition to the external forcing component, the importance of tropical Pacific SST was also demonstrated. During the negative phase of the IPO the meridional temperature gradient between the subtropics and the middle latitudes is further increased, resulting in faster speed eddies generated in the higher latitudes, thus leading to the poleward migration of EMFC and eddy-driven jet. In addition, the subtropical EMFD and associated subtropical wave-breaking critical latitude displaces poleward for slower eddies during negative IPO, pushing the mid-latitude EMFC and eddy-driven jet further poleward. This analysis established that the mechanism by which the IPO influences the mid-latitude circulation is somewhat distinct from that operating on interannual timescales.

5.1.2 Role of coupled feedbacks

While Chapter 2 established the importance of tropical Pacific SSTs to the zonal mean movement of the Southern Hemisphere eddy-driven jet, important asymmetries were also noted i.e., the South Atlantic-Indian jet underwent a poleward movement while the South Pacific jet experienced an intensification. The tropical Pacific SST coupled pacemaker experiment reproduced this asymmetric response, however a dynamical mechanism was only examined for the zonal mean change. In addition, though the strength of the coupled pacemaker framework used in Chapter 2 is that it allows coupled feedbacks, it fails to separate out the direct atmospheric teleconnections. Hence another outstanding question arises: Do tropical Pacific SSTs impact the jet variation via direct atmospheric pathway or by inducing SST changes in other basins first due to air-sea coupling?

To tackle these questions we designed an atmosphere-only experiment (PAC-A) using CAM5 to allow a direct comparison with the fully coupled tropical Pacific pacemaker. The major difference

between PAC-A and the Pacific pacemaker is that outside of the tropical Pacific, the SSTs in the Pacific pacemaker can respond freely to the tropical Pacific due to the coupling, whereas in the uncoupled PAC-A, the SSTs are prescribed to the large ensemble (LENS) ensemble mean time-varying SST. Therefore, the PAC-A (with external forcing removed) could isolate the direct atmospheric impact of observed internally-driven tropical Pacific SSTs on the SH eddy-driven jet trends.

We found that the observed summertime South Pacific jet intensification was reproduced in both coupled and uncoupled experiments, indicating that tropical Pacific SST impacts the South Pacific jet mainly via direct atmospheric teleconnections. Furthermore, expanding the nudged SST region down to 35°S to include the South Pacific Convergence Zone (SPCZ) had little additional impact. By contrast, only the coupled pacemaker captured the summertime poleward shift of the South Atlantic-Indian jet; without coupling the Rossby wave train of the Pacific-South American (PSA) pattern was restricted to the Pacific basin. The absence of mid-latitude tropospheric warming in the uncoupled experiments was suggested as a potential explanation for the different results. A recent study (Waugh et al. 2020) indicates the difference between the South Pacific jet and South Indian-Atlantic jet movements is mainly caused by internal variability, and our results here further established that the tropical Pacific SST decadal variability can explain this asymmetric change, causing the South Pacific jet changes via direct atmospheric Rossby waves while impacting the South Atlantic-Indian jet through air-sea coupling.

5.1.3 Impact of tropical Indian-western Pacific SST on Ross Sea ice

The total Antarctic sea ice extent experienced a weak increase over the satellite era despite a warming background (Parkinson and Cavalieri 2012; Simmonds 2015). By contrast, most current coupled climate models (e.g., historical experiments in CMIP5 and CMIP6) simulated a decreasing trend over this same time period, resulting in a large disparity from the observations that is not completely understood. An early study (Lecomte et al. 2017) based on ocean-ice models suggest that a positive ocean vertical temperature gradient and a positive ocean–sea ice feedback is important to reproduce the sea ice expansion and surface cooling in the Ross Sea region. However no study had determined whether fully coupled climate models such as the CESM1 could capture this ocean-sea ice feedback, which is important for better understanding the sea ice trend difference between the coupled model and observations.

this ocean-sea ice feedback, which is important for better understanding the sea ice trend difference between the coupled model and observations.

Moreover, though teleconnections between each tropical basin SST and Antarctic sea ice variations have been established, no study had quantified the relative impacts of individual tropical basin variability on the decadal Antarctic Sea sea ice expansion in recent few decades. Therefore, in Chapter 4, the same methodology using CESM LENS and tropical pacemaker experiments as in Chapter 2 was employed to quantify the relative roles of each tropical basin SSTs on Antarctic sea ice trends.

We found the Indian pacemaker showed overall circumpolar similarity in sea ice trends with observations, especially over the Ross Sea region, along with an east-west dipole structure in DJF and MAM, and a uniform increase in JJA and SON. In other words, the internal variability from the tropical Indian-western Pacific SSTs could explain at least half of the annual-mean sea ice expansion in the western Ross Sea and South Indian sector during 1980-2013.

Both atmospheric and oceanic processes were analysed to investigate the mechanisms behind sea ice trends in the Ross Sea. In response to internal variability from the tropical Indian-western Pacific SST anomalies, the western Ross Sea and South Indian Ocean upper 100 m displayed a substantial cooling and freshening in the Indian pacemaker experiment. By contrast, the Ross Sea subsurface warmed and salinity increased in both an ocean reanalysis and the Indian pacemaker ensemble, with a downwelling trend seen in the Indian pacemaker, building a stable stratification. This vertical distribution of ocean temperature and salinity suppresses the heat content and brine released to deeper layers, producing a fresh and cool environment at the surface, further conducive to the sea ice increase. The identification of surface and subsurface temperature and salinity trends that closely resemble observations is simulated in a coupled pacemaker simulations was one of the key findings of our study, and further demonstrated the importance of this positive ocean-sea ice feedback (Goosse and Zunz 2014; Lecomte et al. 2017) in driving sea ice trends in the Ross Sea.

5.2 Future Perspective

This thesis highlighted the importance of tropical SST internal variability in driving decadal changes in Southern Hemisphere mid-latitude circulation and sea ice. In particular, the tropical Pacific decadal variability associated with the IPO transitioning to the negative phase in the late 1990s has been identified as a dominant internal driver of the poleward jet movement. However,

to the negative IPO and a slowdown in global mean surface temperature in the early 2000s. On the other hand, Liguori et al. (2020) suggested only 0-15% of the IPO might be externally forced, with two out of five Earth System Model large ensembles (ESM-LE) showing no externally forced impact on the IPO (their Figure 4). Despite the unpredictable nature of future volcanic aerosol forcing and their role in decadal variability of future climate (Liguori et al. 2020), this thesis has shown the importance of including both the competing roles of increasing GHGs and ozone recovery as well as tropical internal variability in Southern Hemisphere mid-latitude and Antarctic decadal predictions (Meehl et al. 2014; Fyfe et al. 2016; Smith et al. 2016).

Though the methodology employed in this thesis (CESM LENS and pacemakers) has been used to distinguish the internal SST variability and external forcing, the residual SSTs (pacemaker minus LENS) could still include an externally forced component since linearity is assumed when using LENS to remove the externally forced component following numerous other studies (Solomon and Polvani 2016; Schneider and Deser 2017; Holland et al. 2019). Furthermore, the CESM LENS ensemble mean is only one model's expression of the external forcing and there is some sensitivity regarding the number of LENS ensemble members used to estimate this forced component (Chapter 2). As we know there are significant differences between models (in coupling between tropics and high latitudes, as well as in the representation and coupling with stratospheric ozone). So without collaborating results from other models there remains some uncertainty in the results presented. Hence it would be important for future work to repeat these LENS and pacemaker experiments with other models to test the robustness of the results.

Another limitation with our experimental design is the model resolution of the CESM1 with 1° atmosphere x 1° ocean. While this is typical of current CMIP-class models, there has been extensive literature documenting the benefits of higher horizontal resolution in an atmospheric model for better simulating atmospheric dynamics, and we could assume that for future works, a higher horizontal resolution will produce better simulations of midlatitude mesoscale storms, and thus improved representations of storm tracks (Hertwig et al. 2015), as well as the jet variations via eddy-mean flow interactions. However, Priestley et al. (2020) argued that in CMIP6, the impact of higher resolution on Southern Hemisphere storm tracks is less apparent and some improvements in simulating these storm tracks are more likely to be a result of improved model physics. For example, Meehl et al. (2019c) explored the effects of model resolution and physics on the Southern Hemisphere storm tracks in two versions of the CESM1. Comparing the two high-resolution CESM1.3 (0.25˚ atmosphere x 1˚ ocean), CESM1.1 (0.25˚ atmosphere x 0.1˚ ocean) with the low resolution CESM1.1 (1˚ atmosphere x 1˚ ocean, which is used throughout this thesis), they found that the increased atmosphere and ocean resolution generally improved the simulation of the Southern Hemisphere 850

hPa eddy kinetic energy (EKE) distribution in winter. However, the high-resolution experiment (0.25˚ atmosphere x 0.1˚ ocean) with an older generation of model physics simulated a degraded EKE compared to observation and the low-resolution runs (0.25˚ atmosphere x 1˚ ocean) with improved physics. This indicates a need to combine both improved physics and higher resolution to produce a better simulation of Southern Hemisphere mid-latitude circulations for future studies.

Previous studies (Lefebvre et al. 2004; Holland et al. 2017b) have found that variations in the mid-latitude jet can have a large impact on the Southern Ocean circulation and Antarctic sea ice distribution. In the past, ocean-only model studies have tended to focus on the response of the Southern Ocean and the Antarctic margin to the forced component of the westerly changes (i.e., the jet annular shift, Lovenduski and Gruber 2005; Hazel and Stewart 2019; Stewart et al. 2020). Based on this thesis, it is clear that there are also some zonal asymmetric varitions of the eddy-driven jet on decadal timescales that are induced by tropical SST internal variability. Both the externally-forced and tropical internally-driven SST forced westerly variations should be considered for near-term Southern Ocean and Antarctic climate projections, given the comparable impacts of external forcing and internal variability on the summertime jet changes over the past 40-50 years. Incorporating a zonally asymmetric westerly wind forcing, as suggested in our study, instead of zonal-mean SAM-like winds for ocean sea-ice models, could potentially lead to an improved understanding of regional ocean circulation and sea ice changes in the future (Stewart et al. 2020).

Recent studies have highlighted the role of tropical SST variations in driving the drastic sea ice retreat event during austral spring in 2016 (Turner et al. 2017). In particular, Wang et al. (2019), Purich and England (2019) and Meehl et al. (2019b) found that tropical Indian Ocean SST likely contributed to the Antarctic sea ice decline in austral spring 2016 via SAM and zonal wave number three teleconnections. Furthermore, Meehl et al. (2019b) suggested the negative decadal trend of wind stress curl with negative IPO persistently pushes the Southern Ocean subsurface warmer water to move upward to the surface via Ekman suction, and a transition to the positive IPO around 2014–2016 suddenly produced warm SSTs that completed a warming of the upper 600 m. Future studies could employ the same CESM LENS and tropical pacemaker experiments as used in Chapter 4 and extend these pacemaker simulations from 2013 to 2020 to distinguish the relative contributions of individual tropical basin SST for the 2016 event.

Overall, using a novel hierarchy of CESM LENS and pacemaker experiments, this thesis has highlighted the importance of tropical SST internal decadal variability in driving the zonal asymmetric changes of Southern Hemisphere eddy-driven jet as well as the regional variations of

Antarctic sea ice. Some limitations of the climate model simulations employed in this study and associated future works have also been identified. This thesis has improved our current understanding of the mechanisms of decadal changes in the Southern Hemisphere extratropical circulation and Antarctic climate, leading to better insights for constraining future projections of Southern Hemisphere westerly winds, precipitation, Southern Ocean circulation, and Antarctic sea ice changes.

References

Adames, Á. F., and J. M. Wallace, 2017: On the tropical atmospheric signature of El Niño. *Journal of the Atmospheric Sciences*, **74,** 1923-1939.
Arblaster, J. M., and G. A. Meehl, 2006: Contributions of external forcings to southern annular mode trends. *Journal of climate*, **19,** 2896-2905.
Ashok, K., Z. Guan, N. Saji, and T. Yamagata, 2004: Individual and combined influences of ENSO and the Indian Ocean dipole on the Indian summer monsoon. *Journal of Climate*, **17,** 3141-3155.
Banerjee, A., J. C. Fyfe, L. M. Polvani, D. Waugh, and K.-L. Chang, 2020: A pause in Southern Hemisphere circulation trends due to the Montreal Protocol. *Nature*, **579,** 544-548.
Barnes, E. A., and L. Polvani, 2013: Response of the Midlatitude Jets, and of Their Variability, to Increased Greenhouse Gases in the CMIP5 Models. *Journal of Climate*, **26,** 7117-7135.
Barnes, E. A., D. L. Hartmann, D. M. Frierson, and J. Kidston, 2010: Effect of latitude on the persistence of eddy-driven jets. *Geophys. Res. Lett.*, **37**(11).
Blanchard-Wrigglesworth, E., L. A. Roach, A. Donohoe, and Q. Ding, 2021: Impact of winds and Southern Ocean SSTs on Antarctic sea ice trends and variability. *Journal of Climate*, **34,** 949-965.
Bracegirdle, T. J., E. Shuckburgh, J. B. Sallee, Z. Wang, A. J. Meijers, N. Bruneau, T. Phillips, and L. J. Wilcox, 2013: Assessment of surface winds over the Atlantic, Indian, and Pacific Ocean sectors of the Southern Ocean in CMIP5 models: Historical bias, forcing response, and state dependence. *Journal of Geophysical Research: Atmospheres*, **118,** 547-562.
Bromwich, D. H., J. P. Nicolas, and A. J. Monaghan, 2011: An assessment of precipitation changes over Antarctica and the Southern Ocean since 1989 in contemporary global reanalyses. *Journal of Climate*, **24,** 4189-4209.
Butler, A. H., D. W. J. Thompson, and R. Heikes, 2010: The Steady-State Atmospheric Circulation Response to Climate Change–like Thermal Forcings in a Simple General Circulation Model. *Journal of Climate*, **23,** 3474-3496.
Cai, W., P. Van Rensch, T. Cowan, and H. H. Hendon, 2011: Teleconnection pathways of ENSO and the IOD and the mechanisms for impacts on Australian rainfall. *Journal of Climate*, **24,** 3910-3923.
Cai, W., and Coauthors, 2019: Pantropical climate interactions. *Science*, **363,** eaav4236.
Cavalieri, D., C. Parkinson, P. Gloersen, and H. Zwally, 1996: Sea ice concentrations from Nimbus-7 SMMR and DMSP SSM/I-SSMIS passive microwave data. *Boulder, Colorado USA: NASA DAAC at the National Snow and Ice Data Center*, **25**.
Ceppi, P., and D. L. Hartmann, 2013: On the speed of the eddy-driven jet and the width of the Hadley cell in the Southern Hemisphere. *Journal of Climate*, **26,** 3450-3465.
Ceppi, P., and D. L. Hartmann, 2015: Connections Between Clouds, Radiation, and Midlatitude Dynamics: a Review. *Current Climate Change Reports*, **1,** 94-102.
Ceppi, P., Y. T. Hwang, D. M. Frierson, and D. L. Hartmann, 2012: Southern Hemisphere jet latitude biases in CMIP5 models linked to shortwave cloud forcing. *Geophys. Res. Lett.*, **39**(19).
Chen, G., and I. M. Held, 2007: Phase speed spectra and the recent poleward shift of Southern Hemisphere surface westerlies. *Geophys. Res. Lett.*, **34**(21).
Chen, G., J. Lu, and D. M. Frierson, 2008: Phase speed spectra and the latitude of surface westerlies: Interannual variability and global warming trend. *Journal of Climate*, **21,** 5942-5959.
Chipperfield, M. P., and Coauthors, 2017: Detecting recovery of the stratospheric ozone layer. *Nature*, **549,** 211-218.
Chung, E.-S., A. Timmermann, B. J. Soden, K.-J. Ha, L. Shi, and V. O. John, 2019: Reconciling opposing Walker circulation trends in observations and model projections. *Nature Climate Change*, **9,** 405.
Ciasto, L. M., and D. W. Thompson, 2008: Observations of large-scale ocean–atmosphere interaction in the Southern Hemisphere. *Journal of Climate*, **21,** 1244-1259.

Ciasto, L. M., and M. H. England, 2011: Observed ENSO teleconnections to Southern Ocean SST anomalies diagnosed from a surface mixed layer heat budget. *Geophys. Res. Lett.*, **38**(9).
Cionni, I., and Coauthors, 2011: Ozone database in support of CMIP5 simulations: results and corresponding radiative forcing. *Atmospheric Chemistry and Physics*, **11,** 11267-11292.
Clem, K. R., J. A. Renwick, and J. McGregor, 2017a: Relationship between eastern tropical Pacific cooling and recent trends in the Southern Hemisphere zonal-mean circulation. *Clim. Dyn.*, **49,** 113-129.
——, 2017b: Large-scale forcing of the Amundsen Sea Low and its influence on sea ice and West Antarctic temperature. *Journal of Climate*, **30,** 8405-8424.
Clem, K. R., B. R. Lintner, A. J. Broccoli, and J. R. Miller, 2019: Role of the South Pacific Convergence Zone in West Antarctic Decadal Climate Variability. *Geophys. Res. Lett.*
Dee, D. P., and Coauthors, 2011: The ERA-Interim reanalysis: Configuration and performance of the data assimilation system. *Quarterly Journal of the royal meteorological society*, **137,** 553-597.
Deser, C., and A. S. Phillips, 2009: Atmospheric Circulation Trends, 1950–2000: The Relative Roles of Sea Surface Temperature Forcing and Direct Atmospheric Radiative Forcing. *Journal of Climate*, **22,** 396-413.
Ding, Q., E. J. Steig, D. S. Battisti, and M. Küttel, 2011: Winter warming in West Antarctica caused by central tropical Pacific warming. *Nature Geoscience*, **4,** 398.
England, M. H., and Coauthors, 2014: Recent intensification of wind-driven circulation in the Pacific and the ongoing warming hiatus. *Nature Climate Change*, **4,** 222-227.
Eyring, V., and Coauthors, 2013: Long-term ozone changes and associated climate impacts in CMIP5 simulations. *Journal of Geophysical Research: Atmospheres*, **118,** 5029-5060.
Ferreira, D., J. Marshall, C. M. Bitz, S. Solomon, and A. Plumb, 2015: Antarctic Ocean and sea ice response to ozone depletion: A two-time-scale problem. *Journal of Climate*, **28,** 1206-1226.
Fogt, R. L., D. H. Bromwich, and K. M. Hines, 2011: Understanding the SAM influence on the South Pacific ENSO teleconnection. *Clim. Dyn.*, **36,** 1555-1576.
Fyfe, J. C., and Coauthors, 2016: Making sense of the early-2000s warming slowdown. *Nature Climate Change*, **6,** 224.
Gagné, M. È., N. Gillett, and J. Fyfe, 2015: Observed and simulated changes in Antarctic sea ice extent over the past 50 years. *Geophys. Res. Lett.*, **42,** 90-95.
Gillett, Z., H. Hendon, J. Arblaster, and E.-P. Lim, 2021: Tropical and Extratropical Influences on the Variability of the Southern Hemisphere Wintertime Subtropical Jet. *Journal of Climate*, **34,** 4009-4022.
Gong, D., and S. Wang, 1999: Definition of Antarctic oscillation index. *Geophys. Res. Lett.*, **26,** 459-462.
Gong, T., S. B. Feldstein, and D. Luo, 2013: A simple GCM study on the relationship between ENSO and the southern annular mode. *Journal of the Atmospheric Sciences*, **70,** 1821-1832.
Good, S. A., M. J. Martin, and N. A. Rayner, 2013: EN4: Quality controlled ocean temperature and salinity profiles and monthly objective analyses with uncertainty estimates. *Journal of Geophysical Research: Oceans*, **118,** 6704-6716.
Goosse, H., and V. Zunz, 2014: Decadal trends in the Antarctic sea ice extent ultimately controlled by ice-ocean feedback. *The Cryosphere*, **8,** 453.
Goosse, H., W. Lefebvre, A. de Montety, E. Crespin, and A. H. Orsi, 2009: Consistent past half-century trends in the atmosphere, the sea ice and the ocean at high southern latitudes. *Clim. Dyn.*, **33,** 999-1016.
Goosse, H., and Coauthors, 2018: Quantifying climate feedbacks in polar regions. *Nature communications*, **9,** 1-13.
Goyal, R., A. Sen Gupta, M. Jucker, and M. H. England, 2021: Historical and projected changes in the Southern Hemisphere surface westerlies. *Geophys. Res. Lett.*, **48,** e2020GL090849.
Haumann, F. A., N. Gruber, and M. Münnich, 2020: Sea-ice induced Southern Ocean subsurface warming and surface cooling in a warming climate. *AGU Advances*, **1,** e2019AV000132.

Hazel, J. E., and A. L. Stewart, 2019: Are the near-Antarctic easterly winds weakening in response to enhancement of the Southern Annular Mode? *Journal of Climate*, **32,** 1895-1918.
Hendon, H. H., E.-P. Lim, and H. Nguyen, 2014: Seasonal Variations of Subtropical Precipitation Associated with the Southern Annular Mode. *Journal of Climate*, **27,** 3446-3460.
Hertwig, E., J.-S. von Storch, D. Handorf, K. Dethloff, I. Fast, and T. Krismer, 2015: Effect of horizontal resolution on ECHAM6-AMIP performance. *Clim. Dyn.*, **45,** 185-211.
Hobbs, W. R., R. Massom, S. Stammerjohn, P. Reid, G. Williams, and W. Meier, 2016: A review of recent changes in Southern Ocean sea ice, their drivers and forcings. *Global and Planetary Change*, **143,** 228-250.
Holland, M. M., L. Landrum, M. Raphael, and S. Stammerjohn, 2017a: Springtime winds drive Ross Sea ice variability and change in the following autumn. *Nature communications*, **8,** 1-8.
Holland, M. M., L. Landrum, Y. Kostov, and J. Marshall, 2017b: Sensitivity of Antarctic sea ice to the Southern Annular Mode in coupled climate models. *Clim. Dyn.*, **49,** 1813-1831.
Holland, P. R., 2014: The seasonality of Antarctic sea ice trends. *Geophys. Res. Lett.*, **41,** 4230-4237.
Holland, P. R., T. J. Bracegirdle, P. Dutrieux, A. Jenkins, and E. J. Steig, 2019: West Antarctic ice loss influenced by internal climate variability and anthropogenic forcing. *Nature Geoscience*, **12,** 718-724.
Hurrell, J. W., and Coauthors, 2013: The community earth system model: a framework for collaborative research. *Bulletin of the American Meteorological Society*, **94,** 1339-1360.
Irving, D., and I. Simmonds, 2016: A New Method for Identifying the Pacific–South American Pattern and Its Influence on Regional Climate Variability. *Journal of Climate*, **29,** 6109-6125.
Karoly, D. J., 1989: Southern hemisphere circulation features associated with El Niño-Southern Oscillation events. *Journal of Climate*, **2,** 1239-1252.
Kay, J. E., C. Wall, V. Yettella, B. Medeiros, C. Hannay, P. Caldwell, and C. Bitz, 2016: Global climate impacts of fixing the Southern Ocean shortwave radiation bias in the Community Earth System Model (CESM). *Journal of Climate*, **29,** 4617-4636.
Kay, J. E., and Coauthors, 2015: The Community Earth System Model (CESM) Large Ensemble Project: A Community Resource for Studying Climate Change in the Presence of Internal Climate Variability. *Bulletin of the American Meteorological Society*, **96,** 1333-1349.
Keppler, L., and P. Landschützer, 2019: Regional wind variability modulates the Southern Ocean carbon sink. *Scientific reports*, **9,** 1-10.
Kimura, N., 2004: Sea ice motion in response to surface wind and ocean current in the Southern Ocean. *Journal of the Meteorological Society of Japan. Ser. II*, **82,** 1223-1231.
Koch, P., H. Wernli, and H. C. Davies, 2006: An event-based jet-stream climatology and typology. *International Journal of Climatology*, **26,** 283-301.
Kosaka, Y., and S.-P. Xie, 2013: Recent global-warming hiatus tied to equatorial Pacific surface cooling. *Nature*, **501,** 403.
Kostov, Y., J. Marshall, U. Hausmann, K. C. Armour, D. Ferreira, and M. M. Holland, 2017: Fast and slow responses of Southern Ocean sea surface temperature to SAM in coupled climate models. *Clim. Dyn.*, **48,** 1595-1609.
Kuo, H., 1956: Forced and free meridional circulations in the atmosphere. *Journal of Atmospheric Sciences*, **13,** 561-568.
Kusahara, K., P. Reid, G. D. Williams, R. Massom, and H. Hasumi, 2018: An ocean-sea ice model study of the unprecedented Antarctic sea ice minimum in 2016. *Environmental Research Letters*, **13,** 084020.
L'Heureux, M. L., and D. W. Thompson, 2006a: Observed relationships between the El Niño–Southern Oscillation and the extratropical zonal-mean circulation. *Journal of Climate*, **19,** 276-287.
L'Heureux, M. L., and D. W. J. Thompson, 2006b: Observed Relationships between the El Niño–Southern Oscillation and the Extratropical Zonal-Mean Circulation. *Journal of Climate*, **19,** 276-287.

Lecomte, O., H. Goosse, T. Fichefet, C. De Lavergne, A. Barthélemy, and V. Zunz, 2017: Vertical ocean heat redistribution sustaining sea-ice concentration trends in the Ross Sea. *Nature communications*, **8,** 1-8.
Lee, S., and S. B. Feldstein, 2013: Detecting ozone-and greenhouse gas–driven wind trends with observational data. *Science*, **339,** 563-567.
Lefebvre, W., and H. Goosse, 2008: An analysis of the atmospheric processes driving the large-scale winter sea ice variability in the Southern Ocean. *Journal of Geophysical Research: Oceans*, **113**.
Lefebvre, W., H. Goosse, R. Timmermann, and T. Fichefet, 2004: Influence of the Southern Annular Mode on the sea ice–ocean system. *Journal of Geophysical Research: Oceans*, **109** (C9).
Li, X., E. P. Gerber, D. M. Holland, and C. Yoo, 2015: A Rossby wave bridge from the tropical Atlantic to West Antarctica. *Journal of Climate*, **28,** 2256-2273.
Li, X., S.-P. Xie, S. T. Gille, and C. Yoo, 2016: Atlantic-induced pan-tropical climate change over the past three decades. *Nature Climate Change*, **6,** 275.
Liguori, G., S. McGregor, J. M. Arblaster, M. S. Singh, and G. A. Meehl, 2020: A joint role for forced and internally-driven variability in the decadal modulation of global warming. *Nature communications*, **11,** 1-7.
Lim, E.-P., and H. H. Hendon, 2015: Understanding and predicting the strong Southern Annular Mode and its impact on the record wet east Australian spring 2010. *Clim. Dyn.*, **44,** 2807-2824.
Lim, E.-P., H. H. Hendon, P. Hope, C. Chung, F. Delage, and M. J. McPhaden, 2019: Continuation of tropical Pacific Ocean temperature trend may weaken extreme El Niño and its linkage to the Southern Annular Mode. *Scientific reports*, **9,** 1-15.
Lim, E.-P., H. H. Hendon, J. M. Arblaster, C. Chung, A. F. Moise, P. Hope, G. Young, and M. Zhao, 2016a: Interaction of the recent 50 year SST trend and La Niña 2010: amplification of the Southern Annular Mode and Australian springtime rainfall. *Clim. Dyn.*, **47,** 2273-2291.
Lim, E. P., H. H. Hendon, J. M. Arblaster, F. Delage, H. Nguyen, S. K. Min, and M. C. Wheeler, 2016b: The impact of the Southern Annular Mode on future changes in Southern Hemisphere rainfall. *Geophys. Res. Lett.*, **43,** 7160-7167.
Lopez, H., S. Dong, S. K. Lee, and E. Campos, 2016: Remote influence of Interdecadal Pacific Oscillation on the South Atlantic meridional overturning circulation variability. *Geophys. Res. Lett.*, **43,** 8250-8258.
Lovenduski, N. S., and N. Gruber, 2005: Impact of the Southern Annular Mode on Southern Ocean circulation and biology. *Geophys. Res. Lett.*, **32**(11).
Lu, J., G. Chen, and D. M. Frierson, 2008: Response of the zonal mean atmospheric circulation to El Niño versus global warming. *Journal of Climate*, **21,** 5835-5851.
Ludescher, J., N. Yuan, and A. Bunde, 2019: Detecting the statistical significance of the trends in the Antarctic sea ice extent: an indication for a turning point. *Clim. Dyn.*, **53,** 237-244.
Luo, J.-J., G. Wang, and D. Dommenget, 2018: May common model biases reduce CMIP5's ability to simulate the recent Pacific La Niña-like cooling? *Clim. Dyn.*, **50,** 1335-1351.
Mantsis, D. F., S. Sherwood, R. Allen, and L. Shi, 2017: Natural variations of tropical width and recent trends. *Geophys. Res. Lett.*, **44,** 3825-3832.
Marsh, D. R., M. J. Mills, D. E. Kinnison, J.-F. Lamarque, N. Calvo, and L. M. Polvani, 2013: Climate change from 1850 to 2005 simulated in CESM1 (WACCM). *Journal of climate*, **26,** 7372-7391.
McGregor, S., M. F. Stuecker, J. B. Kajtar, M. H. England, and M. Collins, 2018: Model tropical Atlantic biases underpin diminished Pacific decadal variability. *Nature Climate Change*, **8,** 493.
McGregor, S., A. Timmermann, M. F. Stuecker, M. H. England, M. Merrifield, F.-F. Jin, and Y. Chikamoto, 2014: Recent Walker circulation strengthening and Pacific cooling amplified by Atlantic warming. *Nature Climate Change*, **4,** 888.
McKay, R. C., J. M. Arblaster, P. Hope, and E.-P. Lim, 2021: Exploring atmospheric circulation leading to three anomalous Australian spring heat events. *Clim. Dyn.***,** 1-18.

Meehl, G., and Coauthors, 2019a: Mutually Interactive Decadal-timescale Processes Connecting the Tropical Atlantic and Pacific. *AGU Fall Meeting 2019*, AGU.
Meehl, G. A., H. Teng, and J. M. Arblaster, 2014: Climate model simulations of the observed early-2000s hiatus of global warming. *Nature Climate Change*, **4,** 898.
Meehl, G. A., J. M. Arblaster, C. M. Bitz, C. T. Y. Chung, and H. Teng, 2016: Antarctic sea-ice expansion between 2000 and 2014 driven by tropical Pacific decadal climate variability. *Nature Geoscience*, **9,** 590.
Meehl, G. A., J. M. Arblaster, C. T. Chung, M. M. Holland, A. DuVivier, L. Thompson, D. Yang, and C. M. Bitz, 2019b: Sustained ocean changes contributed to sudden Antarctic sea ice retreat in late 2016. *Nature communications*, **10,** 14.
Meehl, G. A., and Coauthors, 2019c: Effects of model resolution, physics, and coupling on Southern Hemisphere storm tracks in CESM1. 3. *Geophys. Res. Lett.*, **46,** 12408-12416.
Moss, R. H., and Coauthors, 2010: The next generation of scenarios for climate change research and assessment. *Nature*, **463,** 747.
Nie, Y., Y. Zhang, G. Chen, X. Q. Yang, and D. A. Burrows, 2014: Quantifying barotropic and baroclinic eddy feedbacks in the persistence of the Southern Annular Mode. *Geophys. Res. Lett.*, **41,** 8636-8644.
Nuncio, M., and X. Yuan, 2015: The influence of the Indian Ocean dipole on Antarctic sea ice. *Journal of Climate*, **28,** 2682-2690.
Parkinson, C. L., and D. J. Cavalieri, 2012: Antarctic sea ice variability and trends, 1979–2010. *The Cryosphere*, **6,** 871-880.
Polvani, L. M., D. W. Waugh, G. J. Correa, and S.-W. Son, 2011: Stratospheric ozone depletion: The main driver of twentieth-century atmospheric circulation changes in the Southern Hemisphere. *Journal of Climate*, **24,** 795-812.
Priestley, M. D., D. Ackerley, J. L. Catto, K. I. Hodges, R. E. McDonald, and R. W. Lee, 2020: An overview of the extratropical storm tracks in CMIP6 historical simulations. *Journal of Climate*, **33,** 6315-6343.
Purich, A., and M. H. England, 2019: Tropical teleconnections to Antarctic sea ice during austral spring 2016 in coupled pacemaker experiments. *Geophys*. Res. Lett., **46(**12), 6848-6858

Purich, A., T. Cowan, S.-K. Min, and W. Cai, 2013: Autumn precipitation trends over Southern Hemisphere midlatitudes as simulated by CMIP5 models. *Journal of Climate*, **26,** 8341-8356.
Purich, A., W. Cai, M. H. England, and T. Cowan, 2016a: Evidence for link between modelled trends in Antarctic sea ice and underestimated westerly wind changes. *Nature Communications*, **7,** 10409.
Purich, A., M. H. England, W. Cai, A. Sullivan, and P. J. Durack, 2018: Impacts of broad-scale surface freshening of the Southern Ocean in a coupled climate model. *Journal of Climate*, **31,** 2613-2632.
Purich, A., and Coauthors, 2016b: Tropical Pacific SST drivers of recent Antarctic sea ice trends. *Journal of Climate*, **29,** 8931-8948.
Randel, W. J., and I. M. Held, 1991: Phase speed spectra of transient eddy fluxes and critical layer absorption. *Journal of the atmospheric sciences*, **48,** 688-697.
Raphael, M. N., 2007: The influence of atmospheric zonal wave three on Antarctic sea ice variability. *Journal of Geophysical Research: Atmospheres*, **112** (D12).
Rayner, N., D. E. Parker, E. Horton, C. K. Folland, L. V. Alexander, D. Rowell, E. Kent, and A. Kaplan, 2003: Global analyses of sea surface temperature, sea ice, and night marine air temperature since the late nineteenth century. *Journal of Geophysical Research: Atmospheres*, **108** (D14).
Roach, L. A., and Coauthors, 2020: Antarctic Sea Ice Area in CMIP6. *Geophys. Res. Lett.***,** e2019GL086729.
Rodrigues, R. R., E. J. Campos, and R. Haarsma, 2015: The impact of ENSO on the South Atlantic subtropical dipole mode. *Journal of Climate*, **28,** 2691-2705.

Schneider, D. P., and C. Deser, 2017: Tropically driven and externally forced patterns of Antarctic sea ice change: reconciling observed and modeled trends. *Clim. Dyn.*, **50**(11), 4599-4618.
Schneider, D. P., C. Deser, and T. Fan, 2015: Comparing the Impacts of Tropical SST Variability and Polar Stratospheric Ozone Loss on the Southern Ocean Westerly Winds. *Journal of Climate*, **28,** 9350-9372.
Schroeter, S., W. Hobbs, N. Bindoff, R. Massom, and R. Matear, 2018: Drivers of Antarctic sea ice volume change in CMIP5 models. *Journal of Geophysical Research: Oceans*, **123,** 7914-7938.
Seager, R., N. Harnik, Y. Kushnir, W. Robinson, and J. Miller, 2003: Mechanisms of hemispherically symmetric climate variability. *Journal of Climate*, **16,** 2960-2978.
Simmonds, I., 2015: Comparing and contrasting the behaviour of Arctic and Antarctic sea ice over the 35 year period 1979-2013. *Annals of Glaciology*, **56,** 18-28.
Simpkins, G. R., L. M. Ciasto, D. W. Thompson, and M. H. England, 2012: Seasonal relationships between large-scale climate variability and Antarctic sea ice concentration. *Journal of Climate*, **25,** 5451-5469.
Simpkins, G. R., S. McGregor, A. S. Taschetto, L. M. Ciasto, and M. H. England, 2014: Tropical connections to climatic change in the extratropical Southern Hemisphere: The role of Atlantic SST trends. *Journal of Climate*, **27,** 4923-4936.
Simpson, I. R., and L. M. Polvani, 2016: Revisiting the relationship between jet position, forced response, and annular mode variability in the southern midlatitudes. *Geophys. Res. Lett.*, **43,** 2896-2903.
Simpson, I. R., C. Deser, K. A. McKinnon, and E. A. Barnes, 2018: Modeled and Observed Multidecadal Variability in the North Atlantic Jet Stream and Its Connection to Sea Surface Temperatures. *Journal of Climate*, **31,** 8313-8338.
Simpson, I. R., and Coauthors, 2020: An evaluation of the large-scale atmospheric circulation and its variability in CESM2 and other CMIP models. *Journal of Geophysical Research: Atmospheres*, **125,** e2020JD032835.
Smith, D. M., and Coauthors, 2016: Role of volcanic and anthropogenic aerosols in the recent global surface warming slowdown. *Nature Climate Change*, **6,** 936-940.
Smith, T. M., R. W. Reynolds, T. C. Peterson, and J. Lawrimore, 2008: Improvements to NOAA's historical merged land–ocean surface temperature analysis (1880–2006). *Journal of Climate*, **21,** 2283-2296.
Solomon, A., and L. M. Polvani, 2016: Highly Significant Responses to Anthropogenic Forcings of the Midlatitude Jet in the Southern Hemisphere. *Journal of Climate*, **29,** 3463-3470.
Stammerjohn, S. E., D. Martinson, R. Smith, X. Yuan, and D. Rind, 2008: Trends in Antarctic annual sea ice retreat and advance and their relation to El Niño–Southern Oscillation and Southern Annular Mode variability. *Journal of Geophysical Research: Oceans*, **113** (C3).
Stewart, K. D., A. M. Hogg, M. H. England, and D. W. Waugh, 2020: Response of the Southern Ocean overturning circulation to extreme Southern Annular Mode conditions. *Geophys. Res. Lett.*, **47,** e2020GL091103.
Stuecker, M. F., C. M. Bitz, and K. C. Armour, 2017: Conditions leading to the unprecedented low Antarctic sea ice extent during the 2016 austral spring season. *Geophys. Res. Lett.*, **44,** 9008-9019.
Swart, N. C., and J. C. Fyfe, 2012: Observed and simulated changes in the Southern Hemisphere surface westerly wind-stress. *Geophys. Res. Lett.*, **39,** 6.
Swart, N. C., J. C. Fyfe, N. Gillett, and G. J. Marshall, 2015: Comparing Trends in the Southern Annular Mode and Surface Westerly Jet. *Journal of Climate*, **28,** 8840-8859.
Tandon, N. F., E. P. Gerber, A. H. Sobel, and L. M. Polvani, 2013: Understanding Hadley cell expansion versus contraction: Insights from simplified models and implications for recent observations. *Journal of Climate*, **26,** 4304-4321.
Taylor, K. E., R. J. Stouffer, and G. A. Meehl, 2012: An overview of CMIP5 and the experiment design. *Bulletin of the American Meteorological Society*, **93,** 485-498.
Thompson, D. W., and S. Solomon, 2002: Interpretation of recent Southern Hemisphere climate change. *Science*, **296,** 895-899.

Turner, J., J. S. Hosking, G. J. Marshall, T. Phillips, and T. J. Bracegirdle, 2016: Antarctic sea ice increase consistent with intrinsic variability of the Amundsen Sea Low. *Clim. Dyn.*, **46,** 2391-2402.
Turner, J., T. Phillips, G. J. Marshall, J. S. Hosking, J. O. Pope, T. J. Bracegirdle, and P. Deb, 2017: Unprecedented springtime retreat of Antarctic sea ice in 2016. *Geophys. Res. Lett.*, **44,** 6868-6875.
Vallis, G., 2006: Atmospheric and oceanic fluid dynamics: fundamentals and large-scale circulation, 2006. Cambridge: Cambridge University Press.
Vallis, G. K., E. P. Gerber, P. J. Kushner, and B. A. Cash, 2004: A mechanism and simple dynamical model of the North Atlantic Oscillation and annular modes. *Journal of the atmospheric sciences*, **61,** 264-280.
Wang, C., L. Zhang, S.-K. Lee, L. Wu, and C. R. Mechoso, 2014: A global perspective on CMIP5 climate model biases. *Nature Climate Change*, **4,** 201.
Wang, G., H. H. Hendon, J. M. Arblaster, E.-P. Lim, S. Abhik, and P. van Rensch, 2019: Compounding tropical and stratospheric forcing of the record low Antarctic sea-ice in 2016. *Nature communications*, **10,** 13.
Waugh, D. W., A. Banerjee, J. C. Fyfe, and L. M. Polvani, 2020: Contrasting recent trends in Southern Hemisphere Westerlies across different ocean basins. *Geophys. Res. Lett.***,** e2020GL088890.
Yu, J.-Y., H. Paek, E. S. Saltzman, and T. Lee, 2015: The early 1990s change in ENSO–PSA–SAM relationships and its impact on Southern Hemisphere climate. *Journal of Climate*, **28,** 9393-9408.
Yuan, X., 2004: ENSO-related impacts on Antarctic sea ice: a synthesis of phenomenon and mechanisms. *Antarctic Science*, **16,** 415-425.
Zhang, L., W. Han, K. B. Karnauskas, G. A. Meehl, A. Hu, N. Rosenbloom, and T. Shinoda, 2019: Indian Ocean Warming Trend Reduces Pacific Warming Response to Anthropogenic Greenhouse Gases: An Interbasin Thermostat Mechanism. *Geophys. Res. Lett.*, **46**(19), 10882-10890.
Zhang, X., C. Deser, and L. Sun, 2020: Is there a tropical response to recent observed Southern Ocean cooling? *Geophys. Res. Lett.***,** e2020GL091235.